Univerza v Mariboru

Fakulteta za kemijo in kemijsko tehnologijo

Maja Pori

RAZVOJ NOVIH KOVINSKIH MATRIC Z IONSKO IN KOVALENTNO VEZANIMI TRDNIMI SNOVMI

Diplomsko delo

Maribor,september 2013

Univerza v Mariboru

Fakulteta za kemijo in kemijsko tehnologijo

Diplomsko delo univerzitetnega študijskega programa

Razvoj novih kovinskih matric z ionsko in kovalentno vezanimi trdnimi snovmi

Študent: Maja Pori

Študijski program: univerzitetni študijski program

Predvideni strokovni naslov: diplomirana inž. kem. tehnologije (UN)

Mentor: Red.prof.Dr.Andreja Goršek, univ.inž.kem.teh

Komentor: Doc.Dr.Darja Pečar, univ.inž.kem.teh

IZJAVA

Izjavljam, da sem diplomsko delo izdelal sam, prispevki drugih so posebej označeni. Pregledal sem literaturo iz področja diplomskega dela po naslednjih elementih:

Viri:	Chemical abstracts
Gesla:	MMC, PVD process, InduClad, Wear
Časovno obdobje.	Od leta 1984 do leta 2011
Število referenc:	70
Število prebranih člankov:	51
Število prebranih knjig:	19

Maribor, avgust 2013

---

podpis študenta(ke)

Univerza v Mariboru

FAKULTETA ZA KEMIJO IN KEMIJSKO TEHNOLOGIJO

Številka: K-669
Datum: 26.07.2013

Na osnovi 330. člena Statuta Univerze v Mariboru (Ur. l. RS, št. 46/2012)

izdajam

SKLEP O DIPLOMSKEM DELU

Maja Pori, študent-ka univerzitetnega študijskega programa KEMIJSKA TEHNOLOGIJA, lahko izdela diplomsko delo pri predmetu Gradiva.

Mentor-ica: red. prof. dr. Andreja Goršek
Somentor-ica: doc. dr. Darja Pečar

Naslov diplomskega dela:

RAZVOJ NOVIH KOVINSKIH MATRIC Z IONSKO IN KOVALENTNO VEZANIMI TRDNIMI SNOVMI

Naslov diplomskega dela v angleškem jeziku:

DEVELOPMENT OF NEW FE-BASE MMC WITH IONIC AND COVALENT BONDED HARD PARTICLES

Diplomsko delo je potrebno izdelati skladno z »Navodili za izdelavo diplomskega dela« in ga oddati v treh izvodih ter en izvod elektronske verzije do 26.07.2014 v referatu za študentske zadeve Fakultete za kemijo in kemijsko tehnologijo.

Pravni pouk: Zoper ta sklep je možna pritožba na senat članice v roku 3 delovnih dni.

DEKAN:
red. prof. dr. Željko Knez

Obvestiti:
- kandidata -ko,
- mentorja,
- somentorja,
- odložiti v arhiv

UNIVERZA V MARIBORU FAKULTETA ZA KEMIJO IN KEMIJSKO TEHNOLOGIJO 3

FAKULTETA ZA KEMIJO IN KEMIJSKO TEHNOLOGIJO

Razvoj novih kovinskih matric z ionsko in kovalentno vezanimi trdnimi snovmi

Povzetek:

Obraba je glavni krivec za potrato materialov in izgubo njihovih mehanskih lastnosti. Vsako zmanjšanje obrabe materiala lahko vodi do velikih prihrankov. Glavna motivacija te diplomske naloge je razvoj novih kovinskih kompozitov na osnovi Fe. Ti kompoziti so sestavljeni iz kovinske matrice s fino razpršenimi trdimi delci v njeni mikrostrukturi. Cene zlitin na osnovi Ni and Co so visoke, prav tako imajo te zlitine toksičen in kancerogen efekt. Trde zlitine na osnovi Fe predstavljajo ekonomsko in ekološko alternativo. Potreba po optimizaciji se lahko pojavi z ozirom na trde delce, ki so vstavljeni v kovinsko matrico. Kot spojina za trdi delec je bil uporabljen kovinsko vezan WC. Zaloge le tega na tržišču so omejene, sočasno naraščajo cene te spojine na tržišču. Poleg cene kot pomanjkljivost lahko omenimo raztopitev WC v materialih, ki temeljijo na Fe. V želji, da bi se izognili visokim cenam in omejili raztopitev WC, predstavljajo novi trdi ionsko vezani (SiO_2, AlZrO) in kovalentno vezani (SiC) trdi delci zanimivo alternativo. Vzroke, zakaj ti trdi delci niso bili uporabljeni že prej, lahko pripisujemo njihovim lastnostim vezave, ki omejuje vezavo teh trdih delcev v kovinsko matrico. Za izboljšanje njihove vezave je na površino teh delcev nanesena ovojnica s PVD procesom. V primeru ionsko vezanih delcev ta ovojnica spodbuja vezavo delcev v kovinsko matrico, v primeru kovalentno vezanih delcev pa nanesena ovojnica služi kot ovira za raztopitev trdih delcev v materialih, ki temeljijo na Fe. Kovinski kompoziti z vezanimi trdimi delci so proizvedeni s procesom InduClad. V ospredju raziskav so stičišča med trdimi delci in ovojnico, ter ovojnico in kovinsko matrico. Raziskave so bile opravljene z elektronskim in optičnim mikroskopom. Nadalje je raziskana mikrostruktura in obraba proti trdim abrazivom kovinskih kompozitov. Za primerjavo med mikrostrukturo in obrabo delcev so bili vzorci raziskani po standardu ASTM G65. Rezultati so pokazali, da nanos ovojnice na ionsko vezane trde delce (SiO_2 , AlZrO) izboljša vezavo delcev v kovinsko matrico in posledično zmanjša obrabo kovinskih kompozitov. Nanos ovojnice na kovalentno vezane delce skoraj popolnoma prepreči raztopitev delcev v kovinskih matricah.

Ključne besede: Obraba, zlitine na osnovi Fe, PVD proces, InduClad proces, WC, AlZrO, SiO_2, SiC

UDK: 669.112.2:669.15(043.2)

DEVELOPMENT OF NEW FE-BASE MMC WITH IONIC AND COVALENT BONDED HARD PARTICLES

Abstract:

Wear is the main cause of material wastages and and loss of mechanical performance. Any reduction of wear can result in considerable savings. The main focus of the diploma thesis is the development of Fe-base MMC. These kind of composite materials are made of a metallic binder matrix with embedded HPs, finely distributed in the microstructure. Fe-base hardfacing alloys represent an economical and ecological alternative to Co- and Ni-base hardfacing alloys, since the prices of Ni- and Co-hardfacing alloys are high, futhermore, they can have toxic and carcinogenic effect. The need for optimatization of MMC can appear also with regard to the HPs embedded into the MM. Conventionally, metallic powders and metallic bonded HP like FTC is used for the production of composite materials. The disadvantages by using FTC can be found in high costs (50kg/EUR) and the FTC-dissolution in Fe-base materials, resulting in the formation of the brittle carbide close to the stoichiometry (Fe3W3)C. Therefore, it makes sense to regard new HP, to produce new MMC with covalent bonded (SiC) and ionic bonded (SiO_2, AlZrO) HPs. The reasons, why this HPs were not used prior can be traced back in their bonding behaviour, counteracting the formation of stable phases as a result of reactions between the HP and the MM. To fulfil a good embedding of the HP, an additionally coating, produced with the PVD process is required. In the case of thermal sensitive HPs, a barrier coating protects HP against dissolution. In the case of the ionic bonded HPs the coating enchance the particle embedding and improves the adhesive bonding of the HPs in the MM by formating of more stable phases with the HPs as well as with the MM, respectively. The MMC were produced with the InduClad process. In foreground of the investigations are the interfaces between the HP, the MM and the coatings produced with the PVD process. The interfaces were investigated by means of OM and SEM. Futhermore, the microstructure and the wear resistance of the produced MMC on the construction steel was investigated. The samples were investigated by means of ASTM 65, to compere the microstructure with the wear resistance of the produced MMCs. According to the results, the deposited coating on the ionic bonded HPs (SiO_2, AlZrO) improves the embedding of those HP in the MM. The deposited coating on the covalent bonded HPs (SiC) almost completely reduces the dissolution of HP in the MM. Consequelntly the wear resistance is improved.

Key words: Wear, Fe-base MMC, PVD process, InduClad process, FTC, AlZrO, SiO_2, SiC

UDK: 669.112.2:669.15(043.2)

Content

Nomenclature 5

1 Introduction 9

1.0.1 Aim and way 10

2 Theoretical background 12

2.1 Wear resistant materials 12

2.1.1 Hardfacing alloys 12

2.1.2 Hard phases 13

2.1.3 Metal matrix 13

2.1.4 Fe-base materials 14

2.1.5 Hard coatings 15

2.2 Coating of tools 16

2.2.1 Build-up welding 16

2.2.2 InduClad 17

2.3 Ceramic/metal joining 18

2.3.1 Reactive brazing 18

2.3.2 Spreading and wetting 18

2.4 Physical vapour deposition 19

2.4.1 Vacuum deposition 19

2.4.2 Sputtering 20

2.4.3 Ion plating 21

3 Materials and experimental techniques 22

3.1 Ceramic materials 22

3.1.1 Silicium carbide 22

3.1.2 Tungsten carbide 23

3.1.3 Zirconia Toughened Alumina 23
3.1.4 Silicium dioxide 24
3.2 Coating materials 24
3.2.1 Titanium 24
3.2.2 Titanium carbide 25
3.2.3 Titanium nitrid 25
3.2.4 Aluminium 25
3.3 Matrix materials 25
3.3.1 X220CrVMo13-4 26
3.3.2 X200CrNiBMo10-4-3-3 26
3.4 Sample nomenclature 26
3.5 Deposition of thin and thick coatings 26
3.5.1 Thin coatings on hard particles 26
3.5.2 Build-up welding 27
3.6 Microscopy and metallurgy 27
3.6.1 Sample preparation 27
3.6.2 Light optical microscope 28
3.6.3 Scanning electron microscopy 28
3.7 Mechanical and tribological investigations 28
3.7.1 Abrasion test 28
3.7.2 Hardness measurements 29

4 Results 30
4.1 Microstructure of the mixture of the X220CrVMo13-4 and X200CrNiBMo10-4-3-3 steels densified by InduClad 30
4.2 Deposition of thin film on hard particle surface via sputtering process 30
4.2.1 Deposition of a thin film on AlZrO HP 31
4.2.2 Deposition of thins film on SiC HP 31
4.2.3 Deposition of thin films on SiO_2 HP 32
4.2.4 Deposition of thin films on FTC HP 32
4.3 The microstructure of MMCs produced by InduClad process 33
4.3.1 Microstructure of the MMC with coated AlZrO HP produced by InduClad process 33

4.3.2 Microstructure of the MMC with coated SiC HP produced by InduClad process 34
4.3.3 Microstructure of MMC with coated SiO_2 HP produced by InduClad process 35
4.3.4 Microstructure of the MMC with coated FTC HP produced by InduClad process 35
4.4 Hardness measurements of the HP 36
4.5 Abrasion test 36

5 Discussion 38
5.1 Deposition of thin and thick coatings 38
5.2 Microstructure of the MM 39
5.3 Microstructure of the samples produced by InduClad process 40
5.3.1 Microstructure of the MMC with coated AlZrO hard HP produced by InduClad process 41
5.3.2 Microstructure of the MMC with coated SiC hard HP produced by InduClad process 42
5.3.3 Microstructure of the MMC with coated SiO_2 HP produced by InduClad process 45
5.4 Microstructure of the MMC with coated FTC HP produced by InduClad process 46
5.5 Tribological properties of the new developed Fe-base MMC 47
5.6 Conclusions and outlook 48

A Tables 51

B Pictures 57

Literature 89

Nomenclature

Symbols

$\cos\theta$	Contact angle	[°]
ΔG	Free gibs energy	[kJ]
T_l	Liquidus temperature	[K]
T_{PVD}	Physical vapour deposition process temperature	[K]
T_s	Solidus temperature	[K]
γ_{sv}	Solid/vapour surface tension	[Nm^{-1}]
γ_{sl}	Solid/liquid surface tension	[Nm^{-1}]
γ_{lv}	Liquid/vapour surface tension	[Nm^{-1}]
α_{th}	Coefficient of thermal expansion	[K^{-1}]
W_a	Work of adhesion	[kJ]

Acronyms

AlZrO	Aluminium Zirconia Oxid
bbc	Body-centered cubic
CVD	Chemical vapor deposition
FRD	Federal Republic of Germany
hex	Hexagonal
HIP	HotIsostatic Pressing
fcc	Face-centered cubic
HP	Hard particle
MM	Metal matrix
MMC	Metal matrix composite
OM	Optical microscopy
PM	Powder metallurgy
PVD	Physical vapour deposition
SLPS	Supersolid liquid phase sintering

Elements

Al	Aluminium
Ar	Argon
B	Boron
C	Carbon
Co	Cobalt
Cr	Chromium
Fe	Iron
Hf	Hafnium
Mo	Molybdenum
Mn	Manganese
Nb	Niobium
Ni	Nickel
Si	Silicon
Ta	Tantalum
Ti	Titanium
V	Vanadium
Zr	Zirconium
W	Tungsten

Compounds

AlN	Aluminium nitride
BN	Boron nitride
FTC	Fused tungsten carbide
NbO_2	Niobium oxide
TiC	Titanium carbide
TiN	Titanium nitride
TiO_2	Titanium oxide
SiC	Silicium carbide
SiO_2	Silicium oxide
WC	Tungsten carbide

Chapter 1

Introduction

Wear is the main cause of material wastages and loss of mechanical performance. Any reduction in wear can result in considerable savings. It is estimated that 30 % of the production in the industry goes for replacing worn out products with new ones. In FDR the financial damage in the year 2009 due to wear and friction is estimated at 120 billion. A big part (50 %) of those costs is associated with abrasive wear [1, 2].

Transformation, separation and joining processes of materials may cause wear due to contact force and relative movements between the material and machine tool [3]. The interactions result in a steady material loss of the components and a limited machine running time. On this account hardfacing of low-alloyed steels with wear resistant coatings based on the thermal spraying process or plasma-transferred arc was established. As the coatings Fe-, Co- or Ni-base hardfacing alloys are commonly used. They posses high hardness and toughness [2].

During the transport or processing of the minerals or rocks wear is caused due to rough abrasion. Powder metallugical (PM) alloys could be established, which are reinforced with hard particles (HP). Also here hardfacing alloys are used, for supporting and carrying the hard phases. The concept based on metallic powder mixed with HP is described as metal matrix composites (MMC) [3]. Investigations are dealing with the development of new hardfacing alloys and MMCs. The motivation can be found in high prices of raw materials and in toxic and carcinogenic effect of Ni- and Co-base alloys [4]. If wear appears at low temperatures (between RT and 600 °C), Fe-base hardfacing alloys and metal matrix (MM) represent an economic and ecologic alternative to Ni- and Co-base hardfacing alloys [3]. Fe-base alloys posses martensitic hardenability, which increases the wear resistance of the material due to a high hardness [5]. As a disadvantage of Fe-base alloys the high processing temperature can be mentioned. In addition

the HP require expensive alloying elements like Cr, Mo and V for bonding. The increased processing temperatures during compression of MMC can lead to decomposition of the hard phases due to formation of termodinamical stable phases [3]. The need for optimatization of MMC can appear also with regard to HP embedded into the MM. As HP metallic bonded fused tugsten carbide (FTC) is normally used. It is an eutectic mixture of WC and W_2C with a high hardness (2300 HV) and a simultaneously high fracture toughness [6]. As a disadvantage, the dissolution of metastable FTC in Fe and Ni base materials can be mentioned. FTC tend to dissolve due to high melting temperature and strong diffusion of C in Fe. The result of the FTC-dissolution is the formation of the brittle M_6C structure, which features low hardness and fracture toughness, decreasing the wear resistance of the material. The disadvantage can be not only be found in the dissolution of FTC, but also the prices are rather high (30-55 EURO/kg) [6, 7]. To avoid high costs and reduce the dissolution of FTC and WC, new ionic bonded (AlZrO, SiO_2) and covalent bonded particles (SiC) are an interesting alternative. The reasons why this HPs were not prior to this used can be traced back in their bonding behaviour, limiting the embedding in the MM and influencing their mechanical and finally the wear properties. To fulfil a good embedding of the HP in the MM, an additional coating surrounding the HP is required. The coatings can be produced via PVD or CDV process. In the case of thermally sensitive particles (SiC) the coating protects the hard particles against dissolution and acts like diffusion barrier coating. In the case of ionic bonded hard particles the coating enchance the particle embedding and improves the adhesive bonding of the particles in the MM by formating of more stable phases at the interface, respectively.

1.0.1. Aim and way

This research topic is dealing with development of novel Fe-based MMCs using high covalent bonded SiC or low price ionic bonded (SiO_2 and AlZrO) HP. These HP were coated by means of PECVD process at the University of applied science Lausitz, to achieve a embedding character of the ionic bonded HPs and a counteracting of the dissolution of SiC-ceramic. The interface between the HP and the coatings as well as between the coating and MM schould be investigated by means of OM and SEM. The phase tranformations due to diffusion reactions are in the foreground. Futhermore, an interest of this thesis is to investigate the microstructure and the wear resistance of the produced MMC coatings on construction steel. The coatings were produced with the InduClad process. To compare the wear resistance with the microstructure

of the Fe-based MMCs, the samples were investigated by means of ASTM G65.

Chapter 2

Theoretical background

In this work, the main interest is to observe the bonding behaviour between the coating, the ionic or covalent bonded HP and the MM. The coatings were produced by PECVD-process. The basics and the effects of this process on the coatings morphology will be described, consecutively. The investigated materials are Fe-based MMCs with AlZrO, SiC and SiO_2 as HP. The MMCs were produced by means of InduClad process. The properties of Fe-base MMCs and the process InduClad will be also described. Futher the main parameters in direct brazing of ceramics to metals will be reviewed with primary emphasis on those influencing wetting of solid ceramics by liquid filler materials.

2.1. Wear resistant materials

2.1.1. Hardfacing alloys

Hardfacing alloys describe materials, where primary or eutectic alloy hard phases are solidified in a MM. This materials feature high wear resistance and high resistance to fracture. On this account the materials can be used in applications where wear resistance to abrasion is essential. At temperatures lower than 600 °C Fe-base matrices are to be given performance. At temperatures higher than 600 °C Ni- and Co-base matrices are used. Nitrides, borides and carbides of the transition materials can be suited as HP, attaching well to the surrounding MM [8, 9].

2.1.2. Hard phases

Under the concept of hard phases all oxides, nonmetallic, anorganic and high-fusing materials are gathered. The biggest difference between the ceramic and metalic materials is based on coefficient of electrical resistance. The metallic metarials have a negative coefficient and the ceramic materials have a positive one [3, 9]. Metallic hard phases are carbides, borides and nitrides of the transition metals with the M_aX_b structure. The nonmetallic hard phases are borides, nitrides and carbides of Al, Si and B and oxides of Al, Zr, and Be for example [3, 9]. While the embedding of the ionic and covalent hard phases in a MM is limited, the embedding of the metallic hard phases is better due to the coherent interface formation between the metallic hard phase and the MM [10].

2.1.3. Metal matrix

The MM of the hardfacing alloys has a function of a carrier and protector of the HP and also as a binder phase. The factories demand wear resistance, toughness and strenght from a material. To fulfill this requirements, Fe-, Co- and Ni-base systems are used. In this work the Fe-base system is of main interest.

Ni-base alloys

Ni-base hardfacing alloys possess a fcc lattice over the complete temperature range, for which case the Ni-base alloys can be used as technical alloys for high temperature applications.
In principle it can be distinguished between three Ni-B-Si, Ni-Cr-B-Si, Ni-Co-B-Si alloying types. The alloying elements Si, Cr and B significantly determine the material properties like hardness, wear and corrosion resistance. Additionaly elements Fe and C are present (0.02 - 0.07 %) due to melting metallurgical fundamentals. The hardness of pure Ni is 90 HV0.05 and it is increased by the solid solution hardening (Cr, Ni, Mo, W, V, Ti, Al, T) and precipitation hardening (B $\rightarrow$ Ni_3B) to 400 - 750 HV0.05 [3].

Co-base alloys

Co-base hardfacing alloys are materials for wear, corrosion and erosion protection at high temperatures. The alloys can be used in a temperature range between 700 °C and 1000 °C, above the operating temperature of Ni-base alloys.

The Co-base materials can be divided into two major groups, Co-Cr-W-C (stellite 6 alloy) and Co-Cr-W/Mo-Ni/Fe-C with S + B modification. The alloying element Cr is responsible for solid solution hardening and increases the corrosion resistance. Futhermore, if enough C is present Cr-rich carbides of types $Cr_{23}C_6$, Cr_7C_3, Cr_3C_2 can be present, which improve the wear resistance significantly. Elements like W and Mo increase the volumen fraction of the hard phases and thus also the wear resistance and hardness of the Co-base hardfacing alloys.
Co-base hardfacing alloys are used for coating of cutting dies and extruder screws and for coating the inside of pumps [3].

2.1.4. Fe-base materials

Wear resistant Fe-base alloys are extensively used as hardfacing materials due to their excellent abrasive wear resistance. The wear resistance results from a high volumen fraction of primary carbides and a simultaneouly high matrix toughness [3]. They tend to replace the Ni- and Co-base hard alloys under 600 °C due to a favourable component cost to service life ratio. In addition, they have the advantage of the precipitation and solid solution hardening. They can be also hardnened martensitically [9]. Nowadays the FeCrC system is commonly employed. The C hardens the matrix and forms Cr-rich carbides, which improve the wear resistance to abrasion. The Fe-base materials are used as tool steels, cast parts or as deposits on the substrate materials and can be used to a temperature of 900 °C [10]. Following, cast irons and tool steels, two special groups of Fe-base alloys, should be described more in datails.

Cast irons

Cast iron is a low-cost, high strengt and wear resistant material that can be easily casted into a wide variety of useful and complex shapes [11]. Typically cast irons contain of 2 - 4 mass.-% C and of 0.3 - 1.5 mass.- % of Si. There are different structures of cast iron, depending on the cooling rate from the molten state. If the cooling rate of a material is sufficiently rapid during the solidification, the metal will solidify with C combined with the element Fe as iron carbide (cementite). Cementite is brittle and hard and dominates the structure of white iron. Slow cooling rates promote graphitization due to the decomposition of cementite into ferrite + graphite or graphite + pearlite/ferrite. Graphite dominates the structure of grey cast iron. The white cast iron is britle, hard and cannot be easily machined. The C is mostly bonded into a carbide, which makes the material wear resistant and extremely hard. The grey iron is softer

and has a microstructure of graphite and transformed-austenite or cementite. The machinability of grey cast iron is good, the graphit acts like a chip breaker and solid lubricant.
Alloying elements like Cr, Ni and Mo, and, occasionally Co and Al are added to cast iron to increase the wear and corrosion resistance and to increase the resistance against oxidation for high temperature service [12].

Tool steels

Tool steels have been developed specifically for tooling applications. They are known for their hardness, resistance to abrasion and resistance to deformation at elevated temperatures. In the market today there are three classes of tool steels available: Cold work tool steel, hot work tool steel and high speed tool steel. [3]. Cold work steels are essentially high carbon steels with low alloy addition of W, Mn, Cr and Mo. Among the most useful feature, placing this group in their own class of tool steels is their low temperatures heat treatment. According to their chemical composition and their structure they can be divided into three groups; tough, hard and carbid rich cold work steels. The C-content in the tough cold work tool steels (51CrV5, 60MnSiCr4, C60W3) is about 0.4 - 1.5 mass.- %. Cold work steel tools can be used as materials for trimming tools, rotary slitter knives, gripping jaws and etc. The C-content of the hard cold work steels (100Cr6, C105W1, 90MnCrV8) is 0.7 - 1.5 mass.- %. The structure consists of martensite and carbides. The carbide rich cold work tool steels have a high C-content to 4.5 mass.- % and form Cr-, Mo- and V-rich carbides of type MC, M_2C, M_6C and M_7C_3. The ledeburitic cold work tool steels (X22OCrVMo13-4, X155CrVMo12-1) and plastic mould steels (X190CrVMo20-4) are representatives of the carbide rich cold work steels [3].

2.1.5. Hard coatings

The protection of materials by hard coatings is one of the most important means of improving the component performance. The knowledge about microstructure, properties, application behaviour and constitution can be used to optimize the coatings.
There are thre different zones of the coating, each having different properties. At first there is a substrate interface, where the reaction of the substrate with the layer and the adherence takes place. Second there is the layer material, where the hardness, strenght, internal strenght, thermal conductivity and stability are influenced by the microstructure and chemical composition.

The last zone is the layer surface, where is an influence of the enviroment [13].
Hard materials for coatings can be divided in three groups depending on the dominating atomic binding structure. The metallic hard coating materials (TiN, CrN, VC, TiC) exhibit a fcc structure and good adhesion on metallic substrate in contrast to the other two groups. Ionic bonded hard materials (SiO_2, Al_2O_3) show a good thermal stability and a low interaction tendency to the substrate as well as to the surrounding enviroment. Materials such as diamond, cubic BN and AlN belong to the covalent hard coating materials and generally exhibit a high hardness and a good temperature strenght [14]. If properties such as hardness, toughness and good adhesion at the interface have to be achieved, multiphase coatings can be a good solution. In multilayers, every layer has a special obligation, for example the inner layer can provide good adherence to the substrate, the intermediate layer is responsible for hardness and strenght, the outer layer reduces friction and adhesion [13].

2.2. Coating of tools

The hardfacing alloys can be placed on the substrate material by means of build up welding, hot isostatic pressing (HIP), liquid phase sintering and thermal spraying. The alloys are commonly fabricated by means of build-up welding process, which is described in detail in the following chapter. In the last 10 years at the chair of materials technology of the Ruhr University Bochum has developed different surface and coating technologies. Weber, Berns, Wewers and Saltykova investigated the development of wear resistant steel composites with in situ hard particles via supersolid liquid phase sintering (SLPS) [15, 16, 17, 18, 19, 20]. The properties and structure of the MMC produced via radial-axial ring rolling can be gathered by Moll and Schütte [21, 22]. Futhermore, Röttger investigated the thermal spraying of the Fe-base MMC on austenitic and construction steel substrates [23].

2.2.1. Build-up welding

Build-up welding is a fabrication route, where the coating is applied on a substrate by a molten phase. A bonding between the coating and the substrate material is created, when both materials are partially or completely molten. Build-up welded coating technique in comparison with other coating techniques features a higher thickness (up to 10µm and 15µm in one layer) and a higher adhesion to the substrate [24].

The welding process can be divided into groups according to the chemical composition of the filler material, the energy source (flames, arc, radial energy) or the feed (wire, stick). All this processes have in common that the filler material is supplied to the heat source, molten and then applied on the surface of the substrate material.
A feature of the build-up welded coatings is a strong bond to the substrate. High temperatures are required to achieve a strong bond due to the partially melting of the substrate, resulting in a high level of dulition between the substrate material and the coating material. The dulition causes changes in the chemical composition of the deposited weld due to admixture of the base material and the substrate material. On this account, the potential of the coating properties can be reached when a second or third layer is deposited on the prior deposited layer [3]. Protective coatings by means of build-up welding can be used locally to protect edges of a tool for example or for large areas. Some coatings are designed to withstand surface attacks in terms of corrosion, wear and combined loads of corrosion and wear [24].

2.2.2. InduClad

To improve the wear resistance of materials, processes mentioned already in chapter 2.2 are employed to deposit a coating on the surface of the material. In the case of a conventionally build up welding process, the admixture of materials is 30 vol.- % and the energie input is not controlled. To neglect the influence of the surface material on the coating material and to decrease the process energy, the chair of the materials tehnology of the Ruhr University Bochum has developed a new coating process named Inductive Cladding (InduClad). In this work this process was used to deposit coatings on the surface of low-alloyed steels and is thus briefly described [6].
The bulk powder package was compressed to a green body, fixed on the substrate material and molten [3]. The heat for melting of the powder mixture is produced by means of induction heating, which is a combination of two scientific laws, the Faraday Law and the Joule Effect law. A magnetic field is generated, when a AC current is formed in a generator and is send trought an inductor into a second coil. When an electrical conductive material (in this work the substrate material) is pushed in a time-varying magnetic fied, an alterning current is induced in a conductive material (Faraday law), the alterning current can be also named eddy current. The substrate material offers resistance to eddy current and due to the Joule effect, the energy is dissipated by generating an induction heat. A Joule heating of the base material can melt

the powder particles from below due to thermal conduction. Direct heating of the particles can not occure due to the small diameter of the particles in conscleration of the the skin effect [25]. The thickness of the produced coatings by InduClad is approximately 10 - 12 µm. Besides, also MMCs can be deposited on a substrate material with this process. The oxidation of the bulk powder or the deposited coating is minimized due to the short cooling and heating time. The admixture of the base material is minor (less then 200 µm) and on this account also sensitive hard particles can be used [3].

2.3. Ceramic/metal joining

A firmly bond between the HP and the MM can be achieved, if thermodynamically stable phases are build at the interface region [3]. Since the reactions at the interface between the MM and HP are similar to those between the braze and ceramic, the active brazing process is described in following chapter in details.

2.3.1. Reactive brazing

Reactive alloy bonded (active) brazing is a joining process, where at least one component must be a ceramic. The process eliminates the need for a traditional ceramic metallization prior to the brazing process, as the active component promotes wetting on a ceramic surface.
The active brazing alloy consists of two groups of alloys Cu-X and Ag-Cu-X, where X represents active elements like Ti, Zr, Hf and Ti-Zr alloys. Active alloys can contain also additions of Ni, Be, Cr, V and Co, which improve the wetting of the ceramics.
Active elements promote good wetting of the ceramic surface and estimate the need of metallization. They posses a high reactivity resulting in the formation of stable phases (oxids/ carbides/ nitrides/ borides) to metals at the respectively interfaces [26]. Due to the negative Gibbs free energy, distribution of thermodynamical stable phases and the formation energy at ceramic/metal interface is reduced. Therefore the wettability of metals to the ceramic substrate is improved [27].

2.3.2. Spreading and wetting

The understanding of spreading and wetting is important to determine the optimal brazing conditions. When a liquid is placed on a surface, there are three systems of reference: the liquid,

the vapor and the surface. The relation between the various surface tensions and the contact angle is given by the Youngs equation (see equation 2.1):

$$\gamma_{sv} = \gamma_{sl} + \gamma_{lv} \cos\theta \tag{2.1}$$

The angle cos θ is a rate of wettability. A shematic of a liquid drop can be observed on the figure B. 1. Wetting is a process, when a liquid spreads over a solid substate material and the contact angle is between 0° and 90°. The wetting can be done physically or chemically. The physical wetting occures, when reversible Van der Waals forces occur at the interface, chemical wetting is present when chemical reaction between solid and liquid take place, resulting in a metallurgical strong bonds. A liquid is non-wetting, when the contact angle is larger than 90°. Spreading means that the contact angle is 0° and the liquid drop spreads across the solid [28, 26].

2.4. Physical vapour deposition

Before bonding of the ionic and covalent HP in the MM takes place, a reaction layer was deposited on the surface of the HP via sputtering process. On this account the physical vapour deposition (PVD) will be described more exactly in this chapter.

PVD is a vapor deposition method used to deposit films by the condensation of the desired film onto the workpiece surface. It is used to deposit films, elements, alloys or compounds. In the first stage the target consists of the material which should be deposited is bombarded with the energy source. The vapourized atoms are then moved from the target to the substrate to be coated. If the coatings consist of oxides, nitrides or carbides, the target consist of the metal. The atoms of metal react then with the appropriate gas (O_2, N_2,..) during the transport towards the substrate material [29].

The PVD-technique is used for a wide field of coating applications e.g working industry, biomedical applications, electrical and optical components [30]. Variants of PVD include sputtering, vacuum and ion plating deposition.

2.4.1. Vacuum deposition

The substrate and the source are placed in a vacuum chamber. Vacuum is needed to reduce the elastic hits between the atoms, respectively. Instead of vacuum also atmosphere and reac-

tive gases can be used to introduce plasmas. The pressure in which vacuum deposition takes place is between 10^{-5} and 10^{-9} Torr. Considering the evaporation source, e-beam and resistive evaporation can be mentioned. In the case of resistive evaporation cheap resistance heat wires and metal foils are used to produce Joule heating. They are usually made of refractory metals W, Mo, Ta with a low partially pressure. The substrates are mounted at a appreciable distance from the evapouration source to reduce a radiant heating of the substrate. Vacuum deposition can be used to produce coatings for tribological applications (hard coatings, erosion resistant coatings, solid film lubricants), as diffusion barriers (vapour permeation barrier), for automative applications (lamp reflectors and trim application) and many more applications [29].

2.4.2. Sputtering

Sputtering deposition is a widely used technique for the erosion of surfaces and depositing of thin films. The target and the substrate are plane-parallel plates and serve as cathode and anode for the gas discharge that produces Ar-plasma. The target electrode is always a cathode and it is made out of the material to be deposited. A high purity target is needed, typically the size of the substrate or larger. An inert gas (typically Ar) is converted to a plasma and acts as a source for ions. The negatively charged cathode attracts Ar^+ ions and is thus bombarded by constant flux of Ar^+ ions. This bombardement ejects atoms from the target surface, which are converted into a vapor by physical state. The vaporized coating atoms hit the surface of the substrate material with energy large enough to get stuck, but not to eject substrate atoms. As more and more atoms coalesce on the substrate, they begin to bind to each other forming an atomic layer. The components of a sputtering can be observed in figure B. 2 [31].
Sputtering is conventionally used for etching, analytical techniques and thin-film deposition [29]. Basic sputtering techniques are DC sputtering, RF sputter deposition and magnetron sputter deposition.

Magneton sputtering process

The magnetron sputtering process uses the principle of applying a magnetic field to a target surface. This magnetic field causes travelling electrons along magnetic flux lines due to the Lorentz force instead of beeing attracted towards the substrate. The electrons travell a longer distance and there is more hits between the electrones and process gas. On this account ionisation efficiency of the plasma is incerased. More ions mean more ejected atoms from the

target and therefore an increased efficiency of the sputtering process. The faster ejection rate minimizes impurities [32].

Reactive sputtering process

This sputtering process is used to deposit metal and also ceramic thin films, when a reactive gas is introduced with inert Ar to form a plasma. The atoms of the reactive gas become activated and react with their sputtering atoms to form compound thin films (such as SiO_2, AlN, TiC). The most widely used gases are N_2 (producing nitrides) and O_2 (producing oxides) [33]. The reactive gas reacts with the the ejected target material. This is the so-called tagret poisoning, reducing the thin film growth. Reactive sputtering process is used to produce thin film compunds films of controlled stochiometry and composition at high deposition rates and high-purity films [34].

2.4.3. Ion plating

Ion plating can be also called ion assisted deposition or ion vapor deposition. The process takes advantages from concurrent or periodic bombardement depositing film by atomic-size energetic particles. The surface is cleaned with positive ion bombardement, which controlls and modifies also the substrate surface. The depositing material can be vaporized by evaporation, sputtering and arc vaporization. The particles used for bombardement are ions of an inert or active gas or in some cases also ions of the condensing film material. The ion plating can be done in plasma enviroment, where the ions for bombardement are taken out of plasma or in vacuum enviroment, where ions for bombardement are formed in an ion gun. The high energy of the ion collosion with the surface heats it and therefore chemical reaction and interfacial diffusion can occure. Ion plating is mostly used for tool steel coating, to deposit hard coatings of compounds materials and for optical coatings with a high densities. The deposition energy is high, so the adhesion of the ion plated coatings is better than in evapourated coatings [29].

Chapter 3

Materials and experimental techniques

3.1. Ceramic materials

In this thesis the expensive and conventional HP FTC is replaced by cheaper ionic bonded SiO_2 and AlZrO and covalent bonded SiC, which feature good mechanical and tribological properties. The applications, structure, mechanical and physical properties of those HP are described in details in the following section.

3.1.1. Silicium carbide

Silicium carbide (SiC) is an advanced non-oxid ceramic material for applications with extreme chemical and high-temperature environments. The wear and corrosion resistance of SiC is high. SiC has some attractive properties like low density (3.2 g/cm^3), high melting point (2200 ˚C) and a high hardness (3500 HV0.05). The mechanical and physical properties can be gathered at table A. 3. SiC exsists at various crystalline forms, cubic and non-cubic. At low temperatures it exsist as β-SiC and at high temperatures as α-SiC modification. The transformation from α − β occurs at 2373 K, but this temperature depends also from the presence of impurities, the atmosphere and the external pressure [35]. SiC is composed of tetrahedrons of C and Si atoms with strong sp^3 bonds. The bonding between carbon and silicium is mainly covalent. But because of the large difference in electronegativity of the C and Si atoms, the SiC has also a partially ionic character of about 20 %.

SiC can not be attacked by any acids or alkalis up to 800 ˚C. It forms a protective silicion oxid layer on the surface, thus this material can be used up to 1600 ˚C.

The applications can be found in devices and machines, where a high temperature is present like gas turbines, engines and wear or cutting applications [36, 37].

3.1.2. Tungsten carbide

Tungsten carbide (WC) is one of the most important transition metal carbides, produced in severl thousand tons per year [38]. According to the C-content two structures of fcc WC exsist ($WC_{0,55}$ and $WC_{0,45}$). The transformation from cubic α-WC to hexagonal β-WC occurs below 2500 ˚C. The carbide posseses a high hardness (2000 HV0.05) and a moderate fracture toughness (2-3 $MPam^{-0,5}$) [3].

WC is used as a hard component in cuting tools, wire drawing dies, drills and other wear resistant materials. For this purpose they are embedded in a binder matrix with a low melting point like Fe, Co or Ni [38].

Commercially tungsten fused carbide (FTC) is normally used. FTC posseses a higher hardness then the monolitic WC (2200 HV0.05) and a higher fracture toughness (6 - 7 $MPam^{-0,5}$). It is an eutectic mixture consisting of 20 - 27 mass.-% of WC and 73 - 80 mass.-% of W_2C [39].

The main disadvantage of WC and FTC is the formation of the brittle η phase of type $(TM_6)C$ (T= Ti, Zr, Hf, Nb, Ta, Mo, F; M= Mn, Fe, Co, Ni) or κ- carbide with the structure T_3MC (T= F; M= Mn, Fe, Co, NI) [3]. The mechanical and physical properties of FTC can be gathered from table A. 3.

3.1.3. Zirconia Toughened Alumina

Zirconia Toughned Aluminia (ZTA) is an eutectic mixture of Al_2O_3 and ZrO_2. The eutectic point of the binary system exists at the temperature of 1870 ˚C with 38 at.-% of ZrO_2. ZTA features a high hardness (1450-1800 HV0.05), great mechanical properties of Al_2O_3 and high fracture toughness of ZrO_2. The mechanical and physical properties are listed in table A. 3. ZTA is used in the medical industry for joint replacement and rehabilitation. Futhermore, it is used in load-bearing applications, as the corrosion and strenght resistance enables the material to withstand heavy loads. Cuting tools can be manufactured from ZTA, which are then used in metal-cutting applications [40].

3.1.4. Silicium dioxide

The compound SiO_2 is formed from Si and O atmos. Silicon can be easily found in the nature, since oxygen and silicon are one of the most abundant elements on earth. The most common form which can be found in the nature is silica sand, which is dominant composed of quartz. Quartz posseses a high hardness of 1200 HV0.05 and a high melting point (1713 ˚C). The density of SiO_2 is 2.2 g/cm^3. The mechanical and physical properties can be found in table A. 3.
SiO_2 shows tetrahedral coordination with 4 oxygen atoms surrounding the central Si atom. It can exsist in an amorphous form or in a variety of crystalline forms. The various forms of crystaline silica are α quartz, β cristobaline and tridymite, which are stable at different temperatures. The most common form of silica is the thermodynamically stable α-quartz, the other forms are metastable. It is widely used because of its availabilty, cleaning efficiency and low costs. The major use of this material is for the glass manufacture, for high technological applications in the electronic industry and for buildings and constructions [41].

3.2. Coating materials

The deposition of the coating materials was performed at the University of applied science Lausitz by means of magnetron sputtering. The materials which were ejected from the target and deposited on the surface of the HP as a thin film are described in this chapter.

3.2.1. Titanium

Titanium (Ti) is a strong transition material with outstanding physical properties. The two most beneficial properties are a good corrosion resistance and a high weight-to-strenght ratio. Ti belongs to the group of light metals due to the low density (4.51 g/cm^3). The melting point of Ti is at 1680 ˚C and the thermal expansion coefficient of Ti is rather low ($\alpha = 8.5*10^{-6}$ K^{-1})
The physical and mechanical properties of Ti are listned in table A. 4.
Pure Ti is allotrope, which changes its crystallographic structure from hexagonal α form into a body-centered cubic lattice β form at 882 ˚C. The Ti-targets feature a high degree of purity (99.5 %). On this account the contamination with companion elements durring the sputtering process can be neglected [33, 42].

3.2.2. Titanium carbide

Titan carbide (TiC) possesses a high hardness of 3200 HV0.05, a good corrosion resistance in acid and soap medium, a high melting point (1680 °C) and a low friction coefficient. In table A. 4 the characteristic values of TiC are shown. TiC has a fcc structure. When the content of C falls, the resulting hardness is continously decreased to 1900 HV0.05, reaching the stoichiometry of $TiC_{0.65}$. It is mainly used for preparation of cermets and added to Co - WC to improve the wear resistance [43].

3.2.3. Titanium nitrid

TiN is a compound with a high melting point (2950 °C) and a low density (5.769 g/cm^3). It is experiencing an increased attention in the tool industries, because of its advantages like a high chemical inertness, good adhesion to the substrates, hard surfaces to reduce abrasive wear, a high productivity at low costs and a high hardness (1800 HV0.05). In table A. 4 the main physical and mechanical properties of TiN are listned.

TiN crystalizes in a fcc structure with a mainly metallic bonding. The colour of TiN varies with the Ti to N ratio. With increasing N content the colour changes from Ti gray to ligh yellow (Ti_2N) to golden (TiN) to brown to bronz and finally to red (TiN_{1+x}). It can be used as a coating for cutters and for decorative coatings. It is an excellent diffusion barrier for Si and therefore it is widely used in the field of microelektronic applications [33].

3.2.4. Aluminium

Aluminium is a silvery-white metal with a low density of (2.7g/cm^3). The melting point is at T= 660.3 °C. The hardness of pure Al is low (21 - 48 HV0.05). The product of corrosion is Al_2O_3, which protects the surface from futher oxidation and enviromental influences [44]. The mechanical and physical properties are listned in table A. 4.

3.3. Matrix materials

In this work a mixture of 30 mass.-% of X220CrVMo13-4 and 70 mass.-% of X200CrNiBMo10-4-3-3 was used as Fe-base MM. The properties and structure of those two steels are described in details in this chapter.

3.3.1. X220CrVMo13-4

The used gas-atomized steel powder X220CrVMo13-4 is a ledeburitic cold work tool steel [45]. It belongs to the group of secondary hardnened steels. Its microstructure is formed by tempered martensite of 18 vol.-%, Fe-Cr rich M_7C_3 carbid and 4 vol.-% V-rich MC-carbide in heat treated condition. After the heat treatment the achieved hardness is between 58 to 64 HRC. The chemical composition of this steel is listed in table A. 6. The material can be used for cutting tools, cold pressing tools and and for shearing knives [3].

3.3.2. X200CrNiBMo10-4-3-3

The X200CrNiBMo10-4-3-3 steel possesses a high proportion of hard phases a low solidus temperature. The chemical composition of this steel is given in table A. 5. Borides of type M_2B, $M_3(C,B)$ and $M_{23}(C,B)_6$ are present in the steel X200CrNiBMo10-4-3-3 due to a high proportion of the metalloids carbon and boron. They can solidify primarly from the melt (M_2B) or they react eutectically with the residual melt at low temperatures to γ- Fe and $M_3(C,B)$. In addition, the element C forms with the element Cr to Fe-Cr-rich carbide of type M_7C_3 [6].

3.4. Sample nomenclature

The elements, which form the HP are included in the brackets, (Al-Zr-O) for AlZrO, (Si-C) for SiC, (Si-O) for SiO_2 and (F-C) for FTC. Behind the HP abbreviations the coating material name is placed with the time needed for coating the HP. The samples, where the HP is embedded into the MM have are abbreviation IC.

3.5. Deposition of thin and thick coatings

3.5.1. Thin coatings on hard particles

The HP were coated with the magnetron sputtering device of type BS30 at the University of applied science Lausitz. The HP SiO_2, SiC, AlZrO and FTC were used as substrate material for the coating. The HP exsist in two grain sizes: F80 (the size of the grains are between 150 µm to 212 µm) and F18 (the size of the grains are less than 2.5 mm).
The sputtering parameters are shown in tables A. 1 and A. 2. Sputtering device BS30 consist

of a vacuum chamber (hight: 500 mm high, volumen: 35 l, diameter: 300 mm), a source for the magnetron sputtering (DC-power supplier), which can provide 2.5 kW of power and a sample holder (see picture B. 44). A vibration plate was put into a vaccum chamber due to the recilculation of the particles. Vaccum is produced with a solid vane rotary vaccum pump Triviac D16 B and the turbomolekular pump turbovac 361. A heating coil for heating the samples is placed between the pump and the sample holder. Additionally, a high voltage supply for glowing processes up to 3 kV can be found within the vacuum chamber. The glowing process removes the watter and oxide coatings and other residues on the surface of the HP prior to sputtering. Before the ion etching process the samples were cleaned in a ultrasonic bath with isopropanol and dried for 4 hours in a furnace. The TiC and TiN thin films were produced with reactive sputtering process. The used gas mixture consisted of 50 .-% of N_2 and 50 -% of Ar.

3.5.2. Build-up welding

For the green body production, the powder mixture consisting of HP and steel powder was homogenized, compressed with a pressure from 1.4 to 3.4 MPa and then hardened by drying. The ratio between the binder and the mass of the powder was set to be 1/200.
The green body with a low moisture content was fixed on a previous cleaned construction steel substrate, where a 60 kW generator created an alternating electromagnetic field in the construction steel substrat. The substrate temperature was increased by Joule heating. Due to heat convection, heat radiation and heat conduction the powder particles started to melt. The temperature on the substrate surface was measured and the work of induction could be determined. The powder bulk was molten, while the inductor with a speed of 20 mm/min and a distance of 5 mm trevelled above the powder bulk.

3.6. Microscopy and metallurgy

3.6.1. Sample preparation

The sample preparation was conducted by applying a standart metallographic method. At first the samples were manually grinded with diamond discs from 54 µm to 15 µm with water as lubricant. This step flatens the surfaces flat and removes the surface imperfections. In the next step the samples were polished in a rotating maschine with diamond suspension fluids from 6 µm to 0.25 µm. Between every polishing step samples were cleaned in a ultrasonic bath and at

the end atched with Nital.

3.6.2. Light optical microscope

At first, analyzes of the samples were done using a BX60M light optical microscope (OM) (Olympus GmbH, Germany) with magnification of max 1000X, being able to use bright contrast, interface contrast and polarized light. The light optical microscope was used to investigate the microstructure of the produced samples.

3.6.3. Scanning electron microscopy

LEO-1530 VP scanning electron microscope (SEM) was employed when a higher magnification and a greater depth of focus was required. The chemical composition of the structural constituents was examined by energy-dispersive X-ray spectrometry (EDX) using the EDAX system. The EDX measurements were carried out with acceleration voltage of 10 keV to 20 keV and a working distance of 9 - 11 mm.

3.7. Mechanical and tribological investigations

3.7.1. Abrasion test

The abrasion wear resistance of the produced samples was evalutated by means of "Dry Sand Rubber Wheel Test", according to ASTM G - 65 standart procedure.
On figure B. 5 the experimental set-up and the position of the sample is shown.
Quartz sand (grain size between 100 μm and 300 μm) was introduced between the loaded specimen and the rotating steel wheel in order to subject the specimen to constant wear. The specimen with known weight was pressed with a constant force of 100 N against the Hardox500 disc. The constant sand flow rate was 300 g/min and a speed of 1 m/s between the surface of the steel wheel and the specimens surface as abrasive. After 10 minutes of the abrasive test the specific mass loss was determined as the difference between the mass of the specimen after and prior the wear test. The wear intensity can be calculated with the equation 3.1 on the basis of the wear distance (s) and the weight loss $\Delta m = m_0 - m_e$, where m_0 is the original mass and m_e is the mass after wear test.

$$i = \Delta m / v \cdot t \qquad (3.1)$$

3.7.2. Hardness measurements

The hardness and the E-modul of the hard particles were evaluating by performing nanoidention using a identation tester NHTX S/N: 01-03142 from CSM-instruments. It consist of a x-y-z cross table, a scanning force microscope, a diamond identor B-K77 with a face angle of 65.3°, microscope for positioning and filming the deformations and a mikro scratcher.
The Berkovich identor was pressed with a load of 100 mN into the surface of the sample and the depth of the penetration is then used to measure the resistance of the material. The identation hardness can be determined, if we devide the load with the area of impression. According to DIN EN ISO 12577 the thickness of the coatings should be greater than 10 µm, to avoid the influence of the substate material [46]. The nanoidentation measurements were performed at 5 different places in respectively phases. Poisson ratio 0.3 was used to determine the Youngs modules.

Chapter 4

Results

4.1. Microstructure of the mixture of the X220CrVMo13-4 and X200CrNiBMo10-4-3-3 steels densified by InduClad

The microstructure of the MM, which consist of the mixture of the X220CrVMo13-4 and X200CrNiBMo10-4-3-3 steel powders can be observed in figures B. 6 and B. 7. In figure B. 6 the microstructure of the X200CrNiBMo10-4-3-3 steels can be observed, consisting of a Mo-rich hard phases of type M_3(C,B), Fe-rich carboborides of type M_3(B,C) and Fe-rich borides of type M_2B. Despite of the high Cr-content of about 10 mass .-%, Cr-rich carbides of type M_7C_3 did not solidify from the melt due to the high solubilty of the element Cr in Fe-rich carboborides. The particles from the X220CrVMo13-4 steel are not completely molten (figure B. 7).

4.2. Deposition of thin film on hard particle surface via sputtering process

The SiC, AlZrO, FTC and SiO_2 HP were coated with different coating materials via magnetron sputtering process at the University of applied science Lausitz. To evaluate the coatings produced by PVD, the coated particles were first investigated in as-received condition.

4.2.1. Deposition of a thin film on AlZrO HP

In figure B. 8 the eutectic structure of AlZrO HP can be seen, consisting of Y-stabilized ZrO_2 (bright phase) and of Al_2O_3 (dark phase). In the first part the AlZrO HP coated with Ti-layer are investigated, shown in figure B. 9. Areas with a bright Ti-layer firmly bonded to the AlZrO HP can be observed. However, the Ti-layer is not continious. Areas with a good layer formation and areas with layer delimination are exchanging. White spots of Ti on the AlZrO HP surfaces can be noticed (1). The black lines on the surface can represent cavities or embedding material (2). The thickness of the Ti-layer is not steady (3 - 16 µm), which can be attributed to the uneven surface of the AlZrO HP. In figure B. 10 the microstructure of a homogeneneous Ti-layer with craks is shown

AlZrO HP were also coated with a V-Ti-multilayer, whose microstructure is shown in figure B. 11. On the surface of the Ti-V-multilayer features irregularities in form of small couples. The thickness of the Ti-V-multilayer is about 2.5 µm (figure B. 12). Linescan measurements were performed at the interface AlZrO particle - Ti-V-multilayer - embedding material (picture B. 12). According to the gathered results a low amount of elements Zr and Al and a higher amount of the element O diffuse into the Ti-V-multilayer. Two clear peaks, belonging to elements Ti and V were measured. Element O can be measured across the whole layer. First an inner Ti-rich layer is placed, followed by an outer V-rich layer. A small amount of Si can also be measured.

4.2.2. Deposition of thins film on SiC HP

SiC HP were coated with Ti-TiN-TiC, Ti-TiN-TiC-Ti, Ti-TiN-TiC-Ti and Ti-TiN-TiC-Ti-TiN-multilayers.

The SiC HPs stayed after the PVD process almost entirely uncoated (figure B. 13). Cracks and cavities are present on the SiC - surfaces. Cracks and cavities are mostly occuring during the grinding or polishing process of the samples. Some places, where the layer is firmly bonded to the SiC HP can be found. The thickness of those layers is about 2 µm, determined by the processing time (figure B. 14). A wider view of the multilayers can be observed due the fracture of the embedding material (figures B. 15 and B. 16). The microscopic view of the Ti-TiN-TiC-Ti-multilayer reveals defects in form of craks and spalling. SiC HP are partially coated by a Ti-TiN-Ti-TiC-Ti-TiN-multilayer (figure B. 18). On the surface of the Ti-TiN-Ti-TiC-Ti-TiN-multilayer bright, small HP can be observed. According to the gathered EDX results, this

are HP consist of TiN (table A. 8). The microstructure of a Ti-TiN-Al-Ti-TiN-multilayer on a surface of a SiC HP is shown in figure B. 18. At the edges of the SiC HP cracks can observed.

4.2.3. Deposition of thin films on SiO_2 HP

The microstructure of the (Si-O)$Ti_{120}V_{120}$ sample can be observed in figure B. 19. The Ti-V-multilayer surrounding the SiO_2 HP is continious and provides a good adherence to the SiO_2 HP. According to the EDX measurements the Ti-V-multilayer mainly consists of the elements Ti, V, Si and O (table A. 8). The thickness of the Ti-V-multilayers is not constant and varies between 2 µm and 12 µm. Linescan measurement was performed at the interface SiC - Ti-V-multilayer - embedding material (figure B. 20). The mentioned interface features a radically change in the concentartion of the elements, respectively. A large amount of the elements Si and O diffuse into the Ti-V-multilayer. The inner Ti-rich layer and outer V-rich layer are totally mixed. The weight percentage of Ti in the multilayer is much higher than that of V, althought they posses nearly a close atomic mass.

The Ti layer surrounding the SiO_2 HP is continuous and firmly bonded to the SiO_2 HP (figure B. 21). In comparison with the Ti-V-multilayer, here produced Ti-layer has a more constant thickess of 4 µm. Few cracks can be observed on the HP surfaces.

4.2.4. Deposition of thin films on FTC HP

The Ti-TiN-Ti-multilayers surrounding the FTC HP have a constant thickness of about 4 µm and are firmly bonded to the FTC HP. On the surfaces of the FTC HP some break outs can be seen, they could appear during the preparation of the sample (figure B. 22). The distribution of elements across a Ti-TiN-Ti-multilayer, a part of a FTC HP and embedding material was measured with EDX-analysis (figure B. 23). A high amount of W diffused into the multilayer, which consist mainly of the elements Ti and N. The weight percentage of N in the layer is low due its low atomic mass. Element O was also measured in the multilayer, althought the FTC HP is not a oxide compound (table A. 8). The Ti-TiN-multilayer surrounding the FTC hard HP is thinner (about 2 µm) than the Ti-TiN-Ti-multilayer (figure B. 24). Also this multilayer provides a good adherence to the FTC HP. On the figure B. 25 the microstructure of the completely coated FTC HP with a Ti-TiN-Ti-multilayer is shown.

4.3. The microstructure of MMCs produced by InduClad process

Low alloyed steel substrates were coated with a powder mixture of 10 mass.-% of respectively HP and a mixture of the steel powder X220CrVMo13-4 and X200CrNiBMo10-4-3-3 with the InduClad process for the wear investigations.

4.3.1. Microstructure of the MMC with coated AlZrO HP produced by InduClad process

The microstructure of the IC(Al-Zr-O)Ti_{180} sample is shown in figure B. 26. Instead of a Ti-layer a gap is often present at the AlZrO - MM interface. According to the EDX measurements in this gap the element Ti is not present and has totally diffused into the MM. The gap consists mainly of the elements Zr, Al and O (table A. 8). The presence of the Ti-layer at the MM - AlZrO interface could be determined with EDX measurement. Beside the elements Ti also Zr, Al and O and a minor amount of elements from the MM can be found in the layer (table A. 8). EDX-linescan measurement was performed at the interface AlZrO HP - (Ti-layer) - MM (figure B. 27). Two zones were formed at the MM - AlZrO interface. At first a Ti-rich zone with the elements Ti, Zr, Al and O and secondly a Fe-rich zone with the elements Ni, Cr and Fe. The element Mo showed no diffusion from the MM into the respectively zones. Microcracking can be observed in the MM.

The AlZrO HP coated by a Ti-V-multilayer are firmly embedded into the MM. In comparison with to the sample IC(Al-Zr-O)Ti_{180} less gaps are present at the MM - AlZrO interface (figure B. 28). At higher magnification, weak adherence of the T-V-multilayer to the MM can be observed (figure B. 29). EDX-linescan measurements were performed at the interface between AlZrO HP, Ti-V-multilayer and a part of the MM (figure B. 30). The concentration of the elements Zr, O and Al decreases and the concentation of Cr, Fe, Ni increases in the direction of the layer simultaneously. The element Mo did not diffuse from the MM into the respectively interfaces.

4.3.2. Microstructure of the MMC with coated SiC HP produced by InduClad process

The structure of the IC(Si-C)$Ti_{120}TiN_{60}Al_{60}Ti_{60}TiN_{60}$ sample is shown in figure B. 31. Cracks are formed in the diffusion zones and in the MM (6). Gaps are present at the MM - SiC interface (3) and on the surface of the SiC HP (2). The SiC HP is almost completely surrounded by diffusion zones. The formation of diffusion zones is a result of the reactions between the MM and uncoated or partial coated SiC HP. EDX-linescan measurements across the diffusion zone were performed in order to investigate the distribution of the respectively elements in the MMC-microstructure (figure B. 32). The diffusion zone consist of two zones. In the first zone the graphite and the Fe-rich silicides can be observed finely dispersed. The second zone consists of the same but more coarse phases. Beside the diffusion zone, also pores and spheres of the MM can be observed at the MM - SiC interface (figure B. 33), preventing a firmly bond between the MM and the Ti-TiN-Al-Ti-TiN-multilayer. Linescan measurements were performed at the interface between the SiC HP, Ti-TiN-Ti-TiN-multilayer and MM (figure B. 34). According to the gathered results the interface between SiC and MM consists of two zones. The first zone of the interface between MM - SiC consist of high amouts of elements Si and O, the second part is Fe-rich, consisting mainly from elements Ti, Fe and N. Due to the high amount of O, which was measured, it seems that the Ti-TiN-Al-Ti-TiN-multilayer has oxidized during the InduClad process.

The structure of the IC(Si-C)$Ti_{30}TiN_{120}TiC_{60}$ sample is shown in figure B. 35. The Ti-TiN-TiC-multilayer provides low adherent properties. Spheres of the unmolten MM prevent a firmly bond between the MM and the Ti-TiN-TiC-multilayer (figure B. 36). In figure B. 37 the Ti-Ti-TiC-multilayer with furrows on the surface can be observed under a higherer magnification. According to the EDX mesurements the respectively layer consist mostly of elements Si, Ti, N and O (table A. 8).

The microstructure of the SiC HP surrounded by a Ti-TiN-TiC-Ti-multilayer, embedded into the MM is given on the figure B. 38. The coated HP SiC is firmly embedded into the MM. The SiC HP partially reacted with the MM, resulting in the formation of a diffusion zone (1). The diffusion zone can be observed at areas, which stayed uncoated. The Ti-TiN-TiN-Ti-multilayer prevented the reaction between the MM and the SiC. The layer has low adherence to the MM (figure B. 39).

4.3.3. Microstructure of MMC with coated SiO_2 HP produced by InduClad process

The microstructure of the sample IC(Si-O)$Ti_{120}V_{120}$ is shown in figure B. 40. The SiO_2 HP mostly broke out (1) and big gaps are present at the interface MM - SiO_2 (2) (figure B. 41). According to the EDX measurements, the gap at the interface SiO_2 - MM consists mainly of the elements O, Si and Fe (table A. 8). A small amount of V was measured. Element Ti completely diffused into the MM. Some areas with a good layer formation can be found at the interface SiO_2 - MM (figure B. 42). The presence of the elements Ti and V at the interace SiO_2 - MM could be determined by EDX - mesurement (table A. 8).

The microstructure of the sample IC(Si-O)V_{180} can be observed in figure B. 43. The SiO_2 HP are firmly embedded into the MM. Near the interface MM - SiO_2 HP microcracking in the MM can be observed. The microscopic view at higher magnification reveals a coating with good adherence to the MM and simultaneously to the SiO_2 HP. The EDX-investigations confirm the presence of the elements V at the SiO_2 - MM interface (table A. 8).

The SiO_2 HP coated with a Al-Ti-multilayer are firmly embedded into the MM (figure B. 44). Spheres (2) of the MM can be gathered near the interface SiO_2 - MM (1). The EDX - measurements confirmed the presence of the elements Ti and Al at the interface MM - SiO_2 (table A. 8). On the other side of the SiO_2 HP Ti completely diffused into the MM and just a Al-layer (3) is present at the MM - SiO_2 interface. The presence of the element Al was determined with EDX measurements (table A. 8).

The SiO_2 - MM interface shows a partial formed reaction layer (figure B. 45). EDX-linescan measurements were performed across the reaction layer (B. 46). According to the gathered EDX results, Si and O diffuse from the SiO_2 HP into the SiO_2 - MM interface. It seems that elemet O formes Ti- and Al-rich oxides. The Ti-Al multilayer is formed at the X and Y cordinates of the SiO_2 - MM interface.

4.3.4. Microstructure of the MMC with coated FTC HP produced by InduClad process

The microstructure of the samples IC(F-C)$Ti_{120}TiN_{60}Ti_{60}$ is shown in figure B. 47. At the interface MM - FTC HP gaps (3), broke outs (1) and diffusion zones (2) can be observed. However, no craks or pores are present in the MM. The FTC HP are firmly embedded into

the MM. In figure B. 48 the weak adherence of the Ti-TiN-Ti-multilayer to the MM can be seen. The Ti-TiN-Ti-multilayer has a constant thickness of about 2 µm. According to EDX-measurements, the interface FTC HP - MM consist mostly of the element W. The elements Ti and N diffused strongly into the MM. It seems that the Ti-TiN-Ti-multilayer oxidized during the InduClad process due to the high amount of the element O measured at the interface FTC HP - MM (table A. 8).

The microstructure of the sample IC(F-C)$Ti_{120}TiN_{60}$ is shown in figure B. 50. In the MM pores (1) and big break outs of the MM (2) can be observed. The FTC HP coated with Ti-TiN-Ti-multilayer are firmlier embedded into the MM than the FTC HP coated by Ti-TiN-multilayer. Near the MM - FTC HP interface microcracking in the MM occured (2) (figure B. 51). The FTC HP are partially surrounded by a diffusion zone (figure B. 52). EDX-linescan measurements were performed at the interface FTC HP - (Ti-TiN-multilayer) - MM (figure B. 49). According to the gathered results, the interface FTC HP - MM consist of two zones, a Fe-rich zone with the elements Fe, Ni and W and a Ti-rich zone with W, Ti and N elements measured.

4.4. Hardness measurements of the HP

The hardness and Young's modulus of respectively HP obtained with nanoidentation measurements are shown in table A. 7. The highest hardness and Young's modulus were obtained at the SiC HP. The average meaured hardness and E-modul of the SiC HP is 3500 HV0.05 and 450 GPa. The corresponding diffusion zones of the SiC HP possess a considerably lower hardness and E-moduls (about 550 HV0.05 and 150 Gpa). The average measured hardness and Young's modulus of the AlZrO HP were also high (2200 HV0.05 and 300Gpa). The hardness and the E-moduls of the FTC HP are similar to the hardness and E-moduls of the AlZrO HP (2000 HV0.05 and 450 GPa). The lowest average hardness and Young's modulus were measured at the SiO_2 HP (1200 HV0.05 and 100 GPa).

4.5. Abrasion test

Beside the InduClad produced samples reinforced with different HP, the wear resistance of the MM without HP additions was investigated according to ASTM 65. The main interest of the wear investigations is the influence of the sputtered coating on the bonding behaviour between MM and the HP and consequently on the wear resistance. The HP content in the MMC is

about 10 vol.-%. For the determination of the wear rate the mass loss during the experiment. The results can be observed in figure B. 53.

The wear resistance of the coating consisting of X200CrNiBMo10-4-3-3 steel with wear rate of 272 mg/km is higher than the wear resistance of the coating consisting of mixture of X220CrVMo13-4 and X200CrNiBMo10-4-3-3 steels with a wear rate of 290 mg/km. The highest wear resistance of the MMC was obtained by the samples, where coated AlZrO HP were embedded into the MM. Coating the AlZrO HP with a Ti-layer and a V-Ti-multilayer improved the wear resistance significantly. The wear rate of the sample IC(Al-Zr-O)Ti_{180} is 105 mg/km, of the sample IC(Al-Zr-O)$Ti_{180}V_{180}$ 107 mg/km and of the sample with uncoated AlZrO embedded in MM has a wear rate of 193 mg/km. Also the wear resistance of SiC-base MMC is high. The highest wear resistance was obtained at sample IC(Si-C)Ti_{120} $TiN_{60}Al_{60}Ti_{60}$ TiN_{60} with a wear rate of 88 mg/km. The wear resistance of the sample with uncoated FTC embedded was the same as the wear resistance of the sample IC(F-C)$Ti_{120}TiN_{60}$ sample (wear rate 186 mg/km). The wear resistance of the IC(Ti-C)$Ti_{120}TiN_{60}Ti_{60}$ sample was lower (wear rate 255 mg/km). The wear rates of MMCs with SiO_2 HP embedded are higher than the wear rates of the pure MM. The lowest wear resistance was obtained by the sample IC(Si-O)$Ti_{120}Al_{60}$ and by the sample IC(Si-O)V_{180} sample with wear rates 318 mg/km and 316 mg/km.

Chapter 5

Discussion

5.1. Deposition of thin and thick coatings

On the surface of the HP SiO_2, AlZrO, FTC and SiC metalurgical-technological adaptations are required. The metastable character of the thermal sensitive HP (FTC, SiC) leads to the complete dissolution of the HP in the MM. In the case of the ionic bonded HP (AlZrO, SiO_2) the worse embedding behaviour can be described by their stable behaviour. Embedding behaviour and a counteracting of the dissolution can be achieved by a additional coating on the surface of the HP by a PVD a process.

On the AlZrO HP a Ti-layer and a Ti-V-multilayer was deposited. Due to the continious circulation of the AlZrO HP with leaning, rotation and vibration, the AlZrO HP were completely coated by Ti-layer and Ti-V-multilayer. In the Ti-layer crack can be observed (B. 10). The mechanical hits between the AlZrO HP during the circulation could cause the formation of the craks. Futhermore, the hits could occure during the transport of the HP. After the PVD process the surface of the Ti-V-multilayer features unevenness in form of small couples B. 11. This is a sign for a low T/T_{PVD} ratio and for a porous coating consequenlty [47]. Hence, increasing the PVD process temperature can improve the adhesion strenght of the coating material on the hard HP. If the HP were sputtered homogeneously, can be observed at the cross sections of the samples. On the AlZrO HP of the sample IC(Al-Zr-O)$Ti_{180}Al_{180}$ a partial thick coating can be observed (figure B. 9). It seems, that the HP were not continiously turned during the PVD process.

The Ti-TiN-TiC-multilayer was not completely deposited on the surface of the SiC HP (figure

B. 18). The uncomplete covering of the SiC HP can be traced back to the cleaning of the HP. During the cleaning or drying of the sample dirt can still remain on the surface of the SiC HP and counteract the deposition of the layer on the surface of the SiC HP. The edges of the SiC HP feature increased cracks (figure B. 18). The demages indicates the exceed of strenght due to the surface pressure. Multilayers coatings structures are commonly assumed to have cracking resistance superior to the single layer coatings [48], even thought in the microstructure of the Ti-TiN-TiC-Ti-multilayer cracks can still be observed (figure B. 15). The coefficient of thermal expansion of SiC HP (α_{th} = 5,68·10^{-6} K^{-1}) is lower than the coefficient of thermal expansion of Ti-layer (α_{th} = 8.5·10^{-6}) K^{-1} and TiN-layer (α_{th} = 9.4·10^{-6} K^{-1}). The different coefficients of thermal expansion cause intrinsic stresses during the cooling or heating [47]. During PVD process this stresses can cause crack propagation in the coating material. The cross sections of the SiO_2 HP can be observed in figures B. 19 and B. 21. The Ti-V-multilayer and the Ti-layer feature a firmly bonding to the SiO_2 HP. The Ti-layer is more constant in its thickness is in comparison with the Ti-V-multilayer. In figure B. 25 completely coated FTC HP can be observed. The cross sections of the FTC HP revealed homogeneous Ti- TiN and Ti-TiN-Ti-multilayers with a constant thickness of about 2-3 µm (figures B. 22 and B. 24).

5.2. Microstructure of the MM

In the industry the Ni- and Co-base hardfacing alloys like Ni-B-Si, Ni-Cr-B-Si and Co-Cr-W-C are normally used for the coating of cheap substrate materials. They possess excellent tribological, chemical and mechanical properties and can be used in high temperature applications. Disadvantages are the high alloying cost of the Ni- and Co-base hardfacing alloys. On this account the use of Fe-base materials was established at low temperature applications. This group of materials posses higher hardness and toughness than the Ni- and Co-base materials.

In this work Fe-base alloys of type X200CrNiBMo10-4-3-3 and X220CrVMo13-4 were used for coating the substrate material.

The microstructure of the mixture of the X200CrNiBMo10-4-3-3 and X220CrVMo13-4 steels can be observed in figures B. 6 and B. 7. The processing temperature during the InduClad process is lower then the solidus (T_s) and as well the liquidus temperature (T_l) of the X220CrVMo13-4 steel. On this account the HP of the X220CrVMo13-4 steel were not completely molten during the InduClad process, for which reason the cores of gas atomised steel powder can be recognized in the coating microstructure (figure B. 7).

The solubility of the element B in the MM is low and thus the element B contributes strongly to the formation of stable phases. Elements B and Fe form together hard phases of the type M_2B and M_3B. According to the stochiometry of the borides (M/B ratio; M_2B=2, M_3B=3) already a low B-content can lead to the formation of high amounts of the hard phases. The hardness of the hard phase M_2B is between 1500 HV0.05 and 1800 HV0.05 and improves the wear resistance of the MM. Borides of type M_2B are stable only if the the ratio B/(B+C) is higher than 0.85. Element Cr can stabilise the the phase M_2B by transforming the tetragonal lattice of Fe-rich phase M_2B into a orthorhombic lattice. It can be gathered from the literature, that this transformations increase the hardness and fracture toughness [49]. Beside the M_2B phase also Fe-rich carboborides of type $M_3(C,B)$ are formed. Despite of the high Cr-content of about 10 wt .-% in the steel X200CrNiBMo10-4-3-3, Cr-rich carbides of type M_7C_3 do not solidify from the melt due to the high solubility of Cr in Fe-rich carboborides. In the microstructure of the MM also a high amount of Mo-rich borides of type M_3B_2 can be observed.
Beside the elements B, Fe and Mo bonded with C, the MM features also alloying elements Si, Ni and Cu. The element Ni dissolves in the MM and stabilizes the austenitic lattice. Element Cu increases the solubility of the element B in austenite and is thereby increasing the fracture toughness of the Fe-C-B alloys. Element Si increases the activity of C the steel and promotes the formation of the hard phase of type $M_3(C,B)$. Simultaneously the element Si increases the toughness and elasticity moduls of the Fe-C-B alloys [6].

5.3. Microstructure of the samples produced by InduClad process

The focus of the investigations is the bonding of cheap and technological interesting HP (AlZrO, FTC, SiC and SiO_2) in the mixture of X200CrNiBMo10-4-3-3 and X220CrVMo13-4 steel powders. In section 2.3 the bonding between the MM and the ceramic substrate was already described. For a firmly bonding between the ceramic substrate and the MM the formation of termodinamically stable phases is required. On this account the diffusion mechanism at the respectively interfaces must be discussed in following chapters.

5.3.1. Microstructure of the MMC with coated AlZrO hard HP produced by InduClad process

In active metal brazing element Ti is added to the braze alloy to promote reaction and wetting with a ceramic substrate. The addition of the element Ti to several braze alloy compositions results in increased reactivity and considerable improvement in wetting behaviour. The ceramic is wet by the formation of an intermetallic interfacial reaction product [50]. The element Ti forms stable phases with elements O, C, N, which posses a high thermodinamical stability. The formation of stable phases at the interface MM - AlZrO HP improves the bonding between the MM and the AlZrO HP. On the surface of the AlZrO HP a reactive Ti-layer was deposited by magnetron sputtering process. The main task of this Ti-layer is to improve the adhesion bonding of the AlZrO HP to the the MM. The Ti-coated AlZrO HP and a mixture of X200CrNiBMo10-4-3-3 and X220CrVMo13-4 steels was densified to a MMC by the InduClad process.

The microstructure of the MMC produced with InduClad is shown in figures B. 26 and B. 28. After polishing and grinding the AlZrO HP stayed firmly fixed in the MM (figure B. 26). Closed the AlZrO HP microcracking can be observed in the microstructure of the MM (figure B. 27). The crack fomation can be described by the spontaneoulsly transformation of the tetragonal ZrO_2 structure into the monolitic structure during cooling. The volumetric strain associated with the transformation generates large tensile residual stresses, which promotes crack propaganation in the MM [51]. In comparison with the sample IC(Al-Zr-O)Ti_{180}, the AlZrO HP coated with a Ti-V-multilayer are more firmly embedded into the MM. No crack or pores can be observed in the MM due to similar coefficients of thermal expansion of the MM (12.2 - 13.7·10^{-6} K^{-1}) and the AlZrO HP (9·10^{-6} K^{-1}).

Interface AlZrO - Ti-layer - MM

Figure B. 27 clarifies the measurements of the concentration of the elements at the interface AlZrO - Ti-layer - MM. The interface AlZrO - Ti-layer features a distinctly diffusion of elements Zr, Al and O from the AlZrO partices. Since AlZrO is a eutectic mixture of Al_2O_3 and ZrO_2, the reactions of both compounds with the Ti-layer are taken into account. According to the thermodynamical considerations, the Ti-layer can reacts the compounds Al_2O_3 and ZrO_2 and form TiO_2 oxides [52]. From the literature it can be asserted, that at the interface Al_2O_3-Ti-layer the formation of stable phases TiAl and Ti_3Al are possible [53]. Since the measured

concentration of the element Ti at the interface AlZrO HP - Ti-layer is high, it seems that high amounts of Ti-rich phases were formed at the interface AlZrO - Ti-layer. The formed Ti-rich phases possess a high termodinamical stability. Consequently the adherence of the Ti-layer to the AlZrO HP is good. The values for the ΔG of the Ti-rich phases are shown in tables A. 9 and A. 10.

The interface MM - Ti-layer features a distinctly diffusion of alloying elements Fe, Ni and C from the MM. In the work of Berns the formation of in situ TiC at the interface MM - Ti-layer was already described [8]. The TiC phase is formed according to the reaction $Ti + xC \rightarrow TiC_x$. The substoichiometric phase TiC grows with the increasing diffusion of C. According to table A. 10 the termodinamical stability of the phase TiC is high. Consequently the formation of the TiC phase at the interface Ti-layer - MM leads to a great bond of the coated AlZrO HP in the MM.

Interface AlZrO - Ti-V-multilayer - MM

The formation of stable phases at the interface AlZrO HP - Ti-V-multilayer - MM by diffusion was investigated by EDX-measurements (figure B. 30). The interface AlZrO HP - MM features a distinctly diffusion of elements Al, Zr and O from the MM and elements Fe, C and Ni from the AlZrO HP. The measured concentration of the elements V and Ti was high, confirming that a high amount of Ti- and V-rich phases are formed at the interface AlZrO HP - MM. Beside the Ti- and V-rich oxides also the formation of TiAl and Ti_3Al phases is possible at the interface AlZrO - MM. The mentioned phases possess a high thermodinamical stability. The values of ΔG for the Ti-rich phases are gathered in tables A. 9 and A. 10. According to the EDX-results a high concentration of C diffuses into the Ti-V-multilayer. TiC and VC phases are formed. At the equilibrium VC and TiC have complete solubility in each other [54]. This two groups of monocarbides can form a continious series of the solid solutions due to the similarity of the lattice parameters and isomorphisem of TiC and VC [55]. VC diffuses in the direction of the TiC surface and incorporates in the TiC lattice. According to Cherkashenko the formed phase $(Ti,V)X_{1-x}$ has a higher termodinamical stability than the monocarbides TiC and VC [56].

5.3.2. Microstructure of the MMC with coated SiC hard HP produced by InduClad process

The SiC HP are firmly embedded into the MM due to the formation of stable phases at the interface SiC HP - MM (figures B. 31, B. 35, B. 38). The high amount of pores in the MM occured during the InduClad process due to the fast heating and futher cooling of the samples (figure B. 31). At the interface MM - SiC HP big pores are formed (figure B. 33). During the preparation of the samples these pores can occure due to the high amount of graphite and Fe-rich silicides of type M_3Si, M_6Si_3 at the interface. The mentioned phases are brittle and can easily break out from the interface SiC HP - MM during the preparation method. Beside the pores, also spheres of the MM are gathered at the interface SiC HP - MM (figure B. 36). The SiC HP possess a higher specific heat capacity (C_p= 1.36 J/gK) and conductivity than the MM [3]. During the quick compressing process the heat of the MM can be derived into the SiC HP. This leads to a insufficient melting of the MM. In figure B. 38 the formation of cracks in the MM is shown. The crack propaganation in MM is connected with the difference in the coefficients of thermal expansion between the MM (α_{th}=12.2-13.7·10^{-6} 1/K) and the SiC (α_{th}=3-6·10^{-6} 1/K). Futhermore, the crack propagation can occure due to the locally formed compressive stresses during the cooling of the sample. The crack can be formed also in the SiC HP (figure B. 39). The crack propagation in SiC HP can be attributed to the low fracture toughness of the SiC HP and to the shrinking of the MM during the cooling of the sample.
The Ti-TiN-Ti-TiN-multilayer is not surrounding the SiC HP continiously (figure B. 39). On one hand the uncomplete coatings can be attributed to an insufficient circulation during the PVD process, on the other hard to the interactions with steel HP during the homogenization process.

Interfaces SiC HP - MM

To avoid the strong dissolution of SiC HP in the MM, the steel was alloyed with the element Ti in the work of Terry [57]. The high Ti-content should counteract the formation of the diffusion zones due to the formation of TiC diffusion barriers. In this work Ti-TiN -Al -Ti-TiN-, Ti-TiN-TiC-, Ti-TiN-TiC-Ti- and Ti-TiN-TiC-Ti-TiN-multilayers were deposited on the surface of the SiC HP to avoid dissolution.
In figure B. 31 strong decomposition of the SiC HP resulting in formation of a wide diffusion zones can be observed. The Ti -TiN-Al-Ti-TiN-multilayer did not avoid the dissolution of SiC

HP. On the surface of the Al-layer a thin Al_2O_3 oxide coating is formed, which prevents the formation of the Al_2O_3 phase. During the heating the Al-layer is liquified. Due to the volumen increas of Al-layer, the Al_30_3 oxide coating is damaged and the liquid Al flows in the MM. Due to the missing Al-layer at the interface SiC HP - MM , the SiC HP get in contact with the liquid steel melt and react to Fe-silicides according to the reaction $SiC + 2Fe \rightarrow Fe_2Si + C$. The increased dissolution of the SiC HP simultaneouly increases also the Si-content in the MM, leading to the formation of silicides of type FeSi, Fe_3Si and Fe_5Si_3. The element Si increases the activity of the element C in the MM, which promotes the graphite formation. Futhermore, the increased concentrations of the element Si in the MM leads to bonding of Ni-rich mixed silicides of type MSi (M: Ni, Fe), Fe-rich mixed silicides of type M_3 (M:Fe, NI) and iron silicides of type Fe_5Si_3 [58].

The formed Fe-Si-C-rich diffusion zone at the interface MM - SiC (figure B. 32) has a multiphase structure. The phases become more coare in the direction to the MM. The multilayers Ti-TiN-TiC and Ti-TiN-TiC-Ti almost completey reduced the formation of diffusion zones and provided for a firmly embedding of the SiC HP in the MM (figure B. 35, B. 38). In the diffusion zones crack can be observed (figure B. 31). The cracks propagate spontaneously due to the high amount of Fe-rich silicides and graphite in the diffuison zones. The silicides and graphite show a considerably lower temperature strain than the surrounding MM.

Interfaces SiC - Ti-TiN-Al-Ti-TiN-multilayer - MM

For the firmly embedding of the SiC HP into the MM the formation of stable phases at the interface SiC HP - MM is required. From the obained EDX-measurements (figure B. 34) it is clear, that a high amount of C diffuses from the SiC HP and the MM into the interface, resulting in formation of TiC phase. The element N is accumulated in the octahedral vacancies of the TiC lattice, forming a intersitial compound Ti(C,N) [59]. According to Kim and Kang, the thermodinamical stability of the Ti(C,N) phase is higher than the stability of monocarbides TiN and TiC [60]. With the EDX-measurements also a lower concentration of Ti and Al were measured in the interface MM - SiC HP, thus the formation of TiAl and Ti_3Al phases is possible at the interface SiC HP - MM. The formed Ti-rich phases at the interface SiC HP - MM possess a high termodynamical stability (table A. 10), resulting in firmly embedding of the SiC HP in the MM. With the EDX-measurements a high concentration of element O was measured at the interface MM - SiC HP. After or during the deposition process it seems that the Ti-TiN-Al-Ti-TiN-multilayer reacted with the atmosphere. It can be gathered from the literature, that the

bonding of the oxidised surfaces to the MM is weak [61, 62]. The existence of the oxides at the interface Ti - TiN Ti-TiN-Al-Ti-TiN-multilayer - MM is problematical, since they prevent the in situ reactions between the MM and the Ti-TiN-Al-Ti-TiN-multilayer. On this account the adherence of the Ti-TiN-Al-Ti-TiN-multilayer to the MM is weak.

5.3.3. Microstructure of the MMC with coated SiO_2 HP produced by InduClad process

The coated SiO_2 HP and a mixture of X220CrVMo13-4 and X200CrNiBMo10-4-3-3 steel powders were densified to a MMC by the InduClad process. A firmly bonding of the coated SiO_2 into the MM was not accomplished. The SiO_2 HP mostly broke out of the MM or big gaps are present at the interface MM - SiO_2 HP (figure B. 40). Beside the gaps also microcracking can be observed at the interface SiO_2 HP - MM (figure B. 43) The worse embedding behaviour can be traced back to the differences in the coefficient of thermal expansion of SiO_2 HP (α_{th} = $9 \cdot 10^{-6}$ K^{-1}) and the MM (α_{th} = 12.2 - $13.7 \cdot 10^{-6}$ K^{-1}). In the MM the cracks propagation can be attributed to the large tensile stresses formed during the cooling and the thermal-physical properties of the HP. In comparison with the MM, the SiO_2 HP possess higher values for heat conductivity (Cp = 750 J/kgK). During the densification process the heat is derived in the SiO_2 HP from the surrounding MM. The result is a insufficient melting of the MM at the interface SiO_2 - MM interface (figure B. 44).

Interfaces SiO_2 - Ti-Al-multilayer - MM

To investigate the phase transformations at the interfaces SiO_2 - Ti-Al-multilayer - MM, a EDX-linescan was performed (figure B. 46). At the interface SiO_2 - Ti-Al-multilayer a higher amount of elements Al, O and Ti, Si and C was measured. The reactions at the interface Al/SiO_2 were already described by Roberts and Dobson [63]. The Al reacts with SiO_2 according to the reaction $4Al + 3SiO_2 \rightarrow 2Al_2O_3$ to aluminium oxide. Beside Al_2O_3, TiO_2 phase could be formed at the interface SiO_2 - Ti-Al-multilayer. Both oxides posses a higher thermodinamical stability than SiO_2 (table A. 9, A. 10), which enable a firmly bonding of SiO_2 HP in the MM.

At the interface Ti-Al-multilayer - MM a high amount of Al and C is measured with EDX-linescan measurements. In MM dissolved C reacts with Al-layer according to the reaction $4Al + 3C \rightarrow Al_4C_3$ to aluminium carbide. The formed carbides at the interface SiO_2 HP - MM possess a high thermodynamical stability, resulting in firmly bonding of the SiO_2 HP in the

MM.

5.4. Microstructure of the MMC with coated FTC HP produced by InduClad process

The coated FTC HP and a mixture of X220CrVMo13-4 and X200CrNiBMo10-4-3-3 steel powders were densified to a MMC by InduClad process. The FTC HP show very good bonding behaviour with the MM due to the formation of the stable η-phase (M_6C) at the interface MM - FTC HP (figure B. 47 and B. 50). The M_6C carbides solidify primary or eutectitcally from the melt and cause break outs (figure B. 50). Futhermore, the formation of M_6C carbides can be disadvantageous due to the lower hardness and simutlaneously lower fracture toughness. To counteract the formation of the brittle M_6C phase, elements like Ti, V and N with high affinity to C were added to the matrix powder in the work of Röttger and Winkelmann [64]. The elements should reacts with the free C released during the FTC dissoluton and form carbides. In this work Ti-TiN-Ti- and Ti-TiN-multilayers were deposited on the surface of the FTC HP to protect them against dissolution. The formation of the brittle phase was almost reduced. The adherence of the Ti -TiN-Ti-multilayer in comparison with the Ti-TiN to MM was better. It seems that more stable phases are formed at the interface Ti-TiN -Ti-multilayer - MM in comparsion with the interface Ti-TiN-multilayer - MM (figure B. 47).

Interfaces FTC HP - MM

Ti-TiN-Ti- and Ti-TiN-multilayers were deposited on the surface of the FTC HP to protect the HP against dissolution. The FTC HP tend to dissolve in the Fe-base materials due to their low thermodinamical stability. The formation of a η-phase at the interface MM - FTC was already mentioned in the work of Röttger [65]. There are two types of carbides which can be obtained, M_6C or $M_{12}C$ or M_6W_6C (M = Fe, Cr, Co, Mo) [66]. The formation of the η-phase results in loss of ductility. Futhermore, the surrounding MM is strenghened with carbid formation and solution hardening [67].

Interfaces FTC - Ti-TiN-Ti-multilayer - MM

In foreground of the EDX-investigations are the phase transformations at the interface FTC - Ti-TiN-Ti-multilayer - MM. From the results obtained with EDX-linescan we can assert,

that a higher amount of C diffused into the interface Ti-TiN-Ti-multilayer - MM, resulting in formation of a TiC phase according to the reaction Ti + XC → TiC. TiC can be described as an interstitial compound. The Ti atoms form a fcc lattice with octaedrical vacancies. Rather small atoms like N can occupie the vacancies, forming Ti(C,N) compounds. These compounds posses a high termodinamical stability in comparison to the respectively monocarbides [59] and provide a firmly bonding of the FTC HP in the MM.

5.5. Tribological properties of the new developed Fe-base MMC

In figure B. 53 wear results obtained with the ASTM G65 test are gathered. From the wear results it can asserted, that the sputtering coating on the surface improved the bonding behaviour between the MM and the hard HP and thereby influences also the wear resistance. The best wear resistance was obtained by the samples with coated AlZrO HP. Adding a coating on a AlZrO HP improved the wear resistance of about 50 %. The wear rate of the sample IC(Al-Zr-O)Ti_{180} is 105 mg/km and those of sample IC(Al-Zr-O)$Ti_{180}V_{180}$ 107 mg/km. The high wear resistance can be attributed to the high amount of Ti and V-rich oxides and carbides at the AlZrO - MM interface and to the firmly bonding of the AlZrO HP in the MM. Futhermore, also the measured hardness of the AlZrO HP was high (2200 HV0.05). Also the wear resistance of MMCs with coated SiC HP is high. The high hardness of the SiC HP (3500 HV0.05) and the formation of Ti-rich carbides at the SiC HP - MM is responsile for the high wear resistance of MMCs with coated SiC HP. The best wear resistance was obtained with the sample IC(Si-C)$Ti_{120}TiN_{60}Al_{60}Ti_{60}TiN_{60}$ with the wear rate 88 mg/km. The wear rates of other MMCs with coated SiC HP increase, the wear rate of the sample (Si-C)$Ti_{30}TiN_{120}TiC_{60}Ti_{3O}$ is 132 mg/km, the one of sample $Ti_{30}TiN_{120}TiC_{60}Ti_{3O}TiN_{120}$ 155 mg/km and of the sample (Si-C)$Ti_{30}TiN_{120}TiC_{60}$ is 157 mg/km. The differences in the wear resistance of the SiC-base samples can be attributed to the amount of diffusion zones and stable phases formed at the interface. The diffusion zones are brittle and rough abrasives can break them out. Adding a coating on the surface of the FTC HP did not improve the wear resistance. The wear rate of the MMC with uncoated FTC is the same as the wear rate of the IC(F-C)$Ti_{120}TiN_{60}$ sample (186 mg/km). The high wear resistance of the non-coated FTC HP can be attributed to the formation of the η-carbide at the interface FTC HP - MM. Coating the FTC HP leads to the

reduction of the η-carbide formation, hence the hard phase content decreases. However, fracture toughness increases, simultaneously. The lowest wear resistance can be obtained with the sample (Si-O)$Al_{60}Ti_{60}$ with wear rate of 318 mg/km. Also the wear resistance of other SiO_2 HP is low. The low wear resistance can be traced back to the low measured hardness of the SiO_2 (1200 HV0.05). The rough abrasives (SiC) can easily wear the SiO_2 HP.

5.6. Conclusions and outlook

Conclusions

This research topic is dealing with the development of novel Fe-base MMCs. Technically interesting (hardness, resistance, toughness) HPs like FTC, SiC, AlZrO and SiO_2 were embedded in a mixture of steel powders X220CrVMo13-4 and X200CrNiMo10-4-3-3 to increase the wear resistance of the novel Fe-base MMCs. On the surface of the HP a layer was deposited by means of magnetron sputtering process. In the case of thermal sensitive HP (SiC, FTC) the deposited layer can act like a diffusion barrier and prevents the reactions between the HP and the MM. On the other hand, the deposited coating acts like a promoter for a firmly embedding of the ionic bonded hard HP. Thereby, reactive materials can be deposited promoting the formation of thermal stable phases with the hard HP al well as with the MM.

In the first part the embedding of the AlZrO HP in the MM was investigated. The AlZrO HP are firmly embedded in the MM. The deposition of the V-Ti-multilayer on the surface of the AlZrO HP improved the bonding behaviour of the AlZrO HP in the MM significantly due to the formation of Ti and V- rich stable phases at the interface MM - AlZrO HP. In the MM micro cracking can be observed. The crack formation can be described by the transformation of the tetragonal ZrO_2 structure into the monolitic structure during cooling. Large tensile residual stresses are generated due to the transformation, promoting the crack propaganation in the MM.

On the surface of the SiC HP different multilayers were deposited to prevent the formation of the diffusion zones at the interface SiC HP - MM and to provide a firmly embedding of SiC HP in the MM. From the results obtained it can be asserted, that the deposition of the Ti-TiN-Al-Ti-TiN-multilayer on the surface of the SiC is not suitable. Since the melting temperature of the element Al is lower than the processing temperature of the MM, the liquid Al flows in the MM. Due to the missing layer, the SiC HP react with the MM, resulting in for-

mation of large Fe-Si-C-rich diffusion zones. Depositing the Ti-TiN-TiN-Ti-, Ti-TiN-TiC- and Ti-TiN-TiC-Ti-TiN-multilayers reduced the formation of diffusion zones significantly. Since the multilayers were not deposited completely on the surface of SiC HP, the formation of diffusion zones is not completely reduced. In the MM big cracks can be observed due to the difference in the coefficients of thermal expansion between the MM and the SiC HP.

On the surface of the FTC HP Ti-TiN- and Ti-TiN-Ti-multilayers were deposited to prevent the formation of the η-phase and to improve the embedding of the FTC HP in the MM. The formation of the η-phase was almost completely reduced. The FTC HP are firmly embedded into the MM due to the formation of Ti-rich phases at the interface FTC HP - MM, which possess a higher thermodinamical stability than the FTC HP. In the MM no crack and no pores can be observed. The SiO_2 HP were coated with Ti-, Ti-V-, Ti-Al-multilayers and V- and Ti-layers. In the MM big break outs and crack can be observed. The worse embedding behaviour can be attributed to the big difference of thermal expansion between MM and SiO_2 HP. The coated SiO_2 HP were firmly embedded in the MM due to the formation of stable phases at the interface SiO_2 HP - MM.

The tribological properties were investigated with the ASTM G65 test. The sputtered coating on the surace of the HP improved the embedding of the HP in the MM and thereby also the the wear resistance of the MMCs. The best wear resistance was obtained by the samples with coated AlZrO HP. The high wear resistance can be attributed to the formation of the Ti-and V rich oxides and carbides at the interface AlZrO HP - MM and the high measured hardness of the AlZrO HP. Also the wear resistance of the samples with coated SiC HP is high due to the firmly embedding of the SiC HP in the MM and the high measured hardness of the SiC HP. Coating the FTC HP with Ti-TiN- and Ti-TiN-Ti-multilayers did not significantly improved the wear resistance of the samples with coated FTC HP. The high wear resistance of the non-coated FTC HP can be attributed to the formation of the η-phase at the interface FTC HP - MM. Coating the FTC HP with a layer reduces the formation of the η-phase. Adding coated SiO_2 HP in the MM did not improve the wear resistance. The low wear resisistance of the MMCs with coated SiO_2 hard HP can be attributed to the low measured hardness of those HP.

Outlook

In this work a coating was deposited on the surface of the HP with the PVD process. Since the the coatings produced with the chemical vapor deposition (CVD) process have proven to be

superior in many applications, especially in high stress metal-forming applications where sliding friction wear-out and galling are pervasive, instead of the PVD process the CVD process should be used for depositing a hard coating on the surface of the HP. The CVD process creates a diffusion type bond between the coating and the substrate which is much stronger than the bond created with the PVD process.

Appendix A

Tables

Table A. 1.: Sputtering parameteres for monolayers and bilayers on HP

HP	Layer	Base pressure [Pa]	Process pressure [Pa]	Coating time [min]	Temperature interval [°C]
AlZrO	Ti	0.006	0.15	180	200-201
SiO_2	V	0.006	0.16	180	202-203
SiO_2	Ti	0.005	0.37	180	200-202
AlZrO	Ti	0.005	0.15	120	202-204
	V	0.005	0.16	120	201-202
SiO_2	Al	0.002	0.26	60	202-202
	Ti	0.002	0.25	120	202-202
SiO_2	V	0.005	0.16	120	200-202
	Ti	0.005	0.15	120	200-200
FTC	Ti	0.05	0.24	120	202-200
	TiN	0.05	0.32	60	432-450

Table A. 2.: Sputtering parameteres for multimayers on HP

HP	Layer	Base pressure [Pa]	Process pressure [Pa]	Coating time [min]	Temperature interval [°C]
FTC	Ti	0.05	0.25	120	202-205
	TiN	0.05	0.3	60	432-455
	Ti	0.05	0.32	60	202-203
SiC	Ti	0.005	0.27	120	202-203
	TiN	0.003	0.27	60	435-450
	Al	0.002	0.24	30	203
	Ti	0.002	0.24	60	201-202
	TiN	0.002	0.28	60	436-445
SiC	Ti	0,005	0.16	30	201-201
	TiN	0.005	0.19	120	431-436
	TiC	0.005	0.17	60	400-400
SiC	Ti	0.004	0.16	30	202-203
	TiN	0.005	0.18	120	435-436
	TiC	0.005	0.16	60	400-403
	Ti	0.005	0.16	60	200-100
SiC	Ti	0.008	0.16	30	201-202
	TiN	0.005	0.18	120	431-445
	TiC	0.005	0.16	60	400-422
	Ti	0.00009	0.17	30	201-204
	TiN	0.005	0.18	120	431-436

Table A. 3.: Properties of the SiC, ZTA, FTC, SiO_2 hard particles [68, 6]

HP	Lattice	Hardness [HV0.05]	ρ [g/cm^3]	α_{th} [K^{-1}]	E-modul [GPa]
SiC	α-hex	3500	3.2	$5.68 \cdot 10^{-6}$	480
FTC	hex	2260	16	$1.2\text{-}11.4 \cdot 10^{-6}$	430
SiO_2	trigonal	1200	2.2	$1.2\text{-}1.4 \cdot 10^{-6}$	111.4
ZTA	bbc/hex	1400-2000	5.5	$9.0 \cdot 10^{-6}$	220-360

Table A. 4.: Properties of Ti [33], TiN, TiC [68] and Al [53]

Material	Lattice	Hardness [HV0.05]	ρ [g/cm^3]	α_{th} [K^{-1}]	E-modul [GPa]
TiN	fcc	1800	5.21	$9.4 \cdot 10^{-6}$	590
TiC	fcc	3200	4.93	$7.42 \cdot 10^{-6}$	400
Ti	α-hex	330	4.51	$8.5 \cdot 10^{-6}$	110
Al	fcc	20 - 40	2.7	$23.6 \cdot 10^{-6}$	66.6

Table A. 5.: Chemical composition of the steel X200CrNiBMo10-4-3-3 in mass.-%

Alloying Elements	C	B	Si	Cr	Mo	V	Cu	Ni	Fe
Composition	2.0	3.5	1.8	10	3.5	0.1	1.2	4.0	rest

Table A. 6.: Chemical composition of the steel X220CrVMo13-4 in mass.-%

Alloying Elements	C	Si	Mn	S	Cr	Mo	V	Fe
Composition	2.25	0.29	0.32	0.001	12.34	0.98	3.94	rest

Table A. 7.: Aritmetic average values of hardness and E-moduls of the HP at constant load of 100 mN and 10 -% of penetration depth of 10 -%

Sample	Hardness [HV0.05]	Young's modulus [GPa]
(Si-O)$Al_{60}Ti_{180}$	1219.36	101.83
(Al-Zr-O)Ti_{180}	2085	302.764
(Si-O)$Ti_{120}V_{120}$	1112.11	95.075
(Si-O)V_{180}	1125	96.65
(Si-O)Ti_{180}	1372.6	104.15
(Al-Zr-O)Ti_{180} V_{180}	2332.9	354.40
(Si-C)$Ti_{120}TiN_{60}Al_{60}Ti_{60}TiN_{60}$	3204.53	491.824
(Si-C)$Ti_{120}TiN_{60}Al_{60}$ $Ti_{60}TiN_{60}$- diffusion zone	629.96	156.54
(Si-C)$Ti_{30}TiN_{120}TiC_{60}Ti_{30}$	3154.5	472.6
(Si-C)$Ti_{30}TiN_{120}TiC_{60}Ti_{30}$- diffusion zone	583.92	138.65
(Si-C)$Ti_{30}TiN_{120}TiC_{60}$	3373.9	462.36
(Si-C)$Ti_{30}TiN_{120}TiC_{60}$ - diffusion zone	551.61	135.2
(Si-C)$Ti_{30}TiN_{120}TiC_{60}Ti_{30}TiN_{120}$	3609.66	477.143
(Si-C)$Ti_{30}TiN_{120}TiC_{60}Ti_{30}TiN_{120}$ - diffusion zone	529.06	123.96
(F-C)$Ti_{120}TiN_{60}$	2065.26	400.42
(F-C)$Ti_{120}TiN_{60}Ti_{60}$	1988.13	471.2

Table A. 8.: EDX-measurements of the coatings of respectively hard particles in at.-%

Coating	Figure	N	C	O	Al	Zr	Si	Ti	V	Fe	Co	Cr	Mn	Mo	W	Ni
Ti - V	B. 12	-	28.63	36.87	24.57	4.31	-	1.23	4.39	-	-	-	-	-	-	-
Ti - V	B. 20	-	11.53	41.56	-	-	14.8	7.82	22.02	2.12	0.15	-	-	-	-	-
Ti - TiN - Ti	B. 22	-	43.16	26.95	-	-	-	5.42	-	-	-	-	-	24.47	-	
Ti	B. 27	-	-	42.25	39.4	7.09	-	0.97	6.57	-	1.52	-	-	-	-	-
Ti - V	B. 29	-	11.53	41.56	-	-	7.82	22.02	2.12	0.15	-	-	-	-	-	
Ti - TiN - TiC	B. 36	15.16	10.67	7.31	-	-	44.60	22.17	-	-	-	-	-	-	-	-
Ti - V	B. 42	-	4.39	38.5	-	-	35.00	1.71	1.09	16.03	-	2.5	-	0.68	-	-
V	B. 43	-	-	48.61	-	-	39.98	-	1.69	8.13	-	1.59	-	-	-	-
Ti - Al	B. 44	-	4.33	39.30	2.08	-	37.02	1.09	-	15.71	-	1.47	-	-	-	-
Al	B. 44	-	3.99	30.46	34.02	-	0.91	-	-	3.78	-	23.19	-	3.64	-	-
Ti - TiN	B. 51	-	13.35	-	-	-	-	-	-	31.01	-	7.21	0.15	-	-	-
Ti- TiN - Ti	B. 48	-	8.08	13.29	-	-	-	2	-	17.94	-	2.31	-	-	53.87	2.52
TiN particle	B. 18	33.93	-	-	-	-	-	12.0	-	5.42	-	-	-	-	60.65	-
Interface AlZrO - MM	B. 29	-	-	40.3	40.31	7.94	-	-	7.61	-	1.83	-	-	-	-	-
Interface SiO_2 - MM	B. 41	-	5.43	21.26	8.23	-	23.02	-	-	34.15	-	4.19	0.23	1.15	-	-

Table A. 9.: Values for entalphies, entropies and free bonding entalpies of the carbides in kJ and at different temperatures [52]

Compound	$-\Delta H_{298}$ 25 °C	S_{298} 25 °C	$-\Delta G_{300}$ 27 °C	$-\Delta G_{500}$ 227 °C	$-\Delta G_{1000}$ 727 °C	$-\Delta G_{1500}$ 1227 °C	$-\Delta G_{2000}$ 1727 °C
WC	37.7	41.8	37.3	36.4	35.6	34.8	33.5
VC	100.9	27.6	-	-	94.6	91.3	80.4
TiC	183.3	24.3	180.0	177.9	172.9	167.1	160.4
SiC	67.0	16.54	-	58.2	55.3	53.2	41.9

Table A. 10.: Values for entalphies, entropies and free bonding entalpies of the oxides in kJ and at different temperatures [52]

Compound	$-\Delta H_{298}$ 25 °C	S_{298} 25 °C	$-\Delta G_{300}$ 27 °C	$-\Delta G_{500}$ 227 °C	$-\Delta G_{1000}$ 727 °C	$-\Delta G_{1500}$ 1227 °C	$-\Delta G_{2000}$ 1727 °C
Al_2O_3	1678.2	51.1	1584.0	1520.8	1362.4	1146.9	-
SiO_2	910.9	41.5	-	-	716.9	640.0	538.5
V_2O_5	1219.4	98.4	1147.0	1099.7	982.0	864.4	-
TiO_2	944.1	50.2	862.1	827.3	739.5	652.7	564.8
ZrO_2	1101.3	50.7	1042.2	1003.7	909.9	818.2	729.5

Appendix B

Pictures

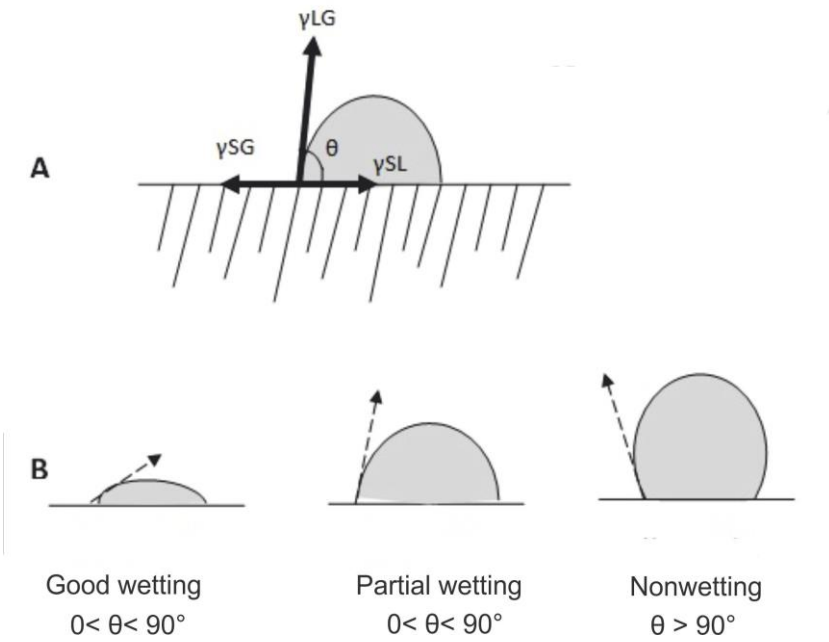

Figure B. 1.: A: Shematic of a liquid drop showing the quantities in the Youngs equation; B: Wetting behaviour according to different contact angles [69]

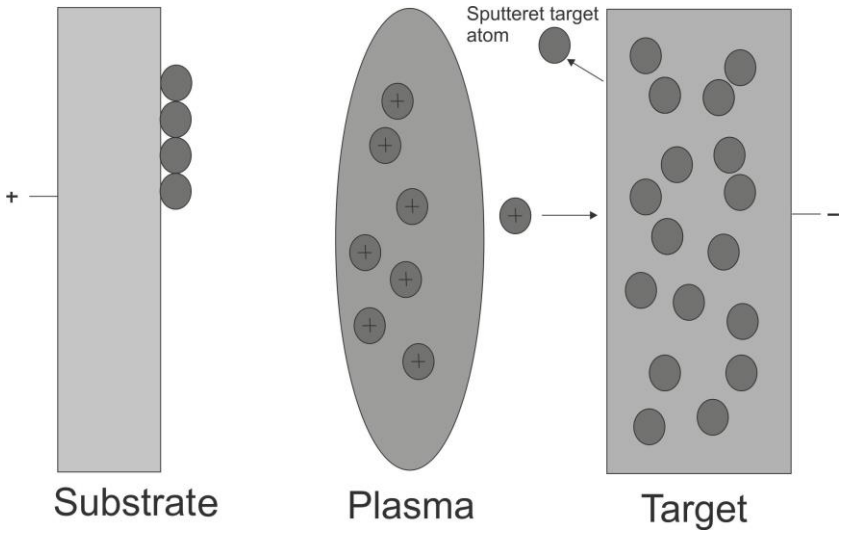

Figure B. 2.: The basic component of a sputering process; Ionized argon bombardes a target, releasing atoms which form a layer on a substrate [33]

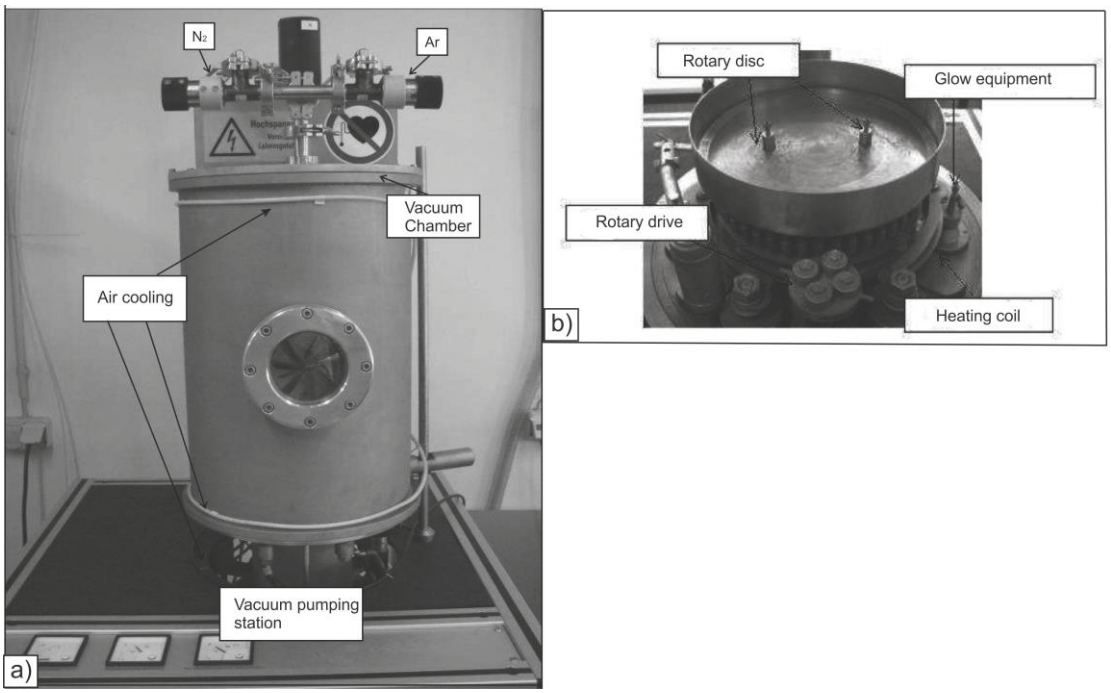

Figure B. 3.: PVD coating device: a) The applied direct current (DC) magnreton sputtering device B30 and b) rotary disc in a vacuum chamber [3]

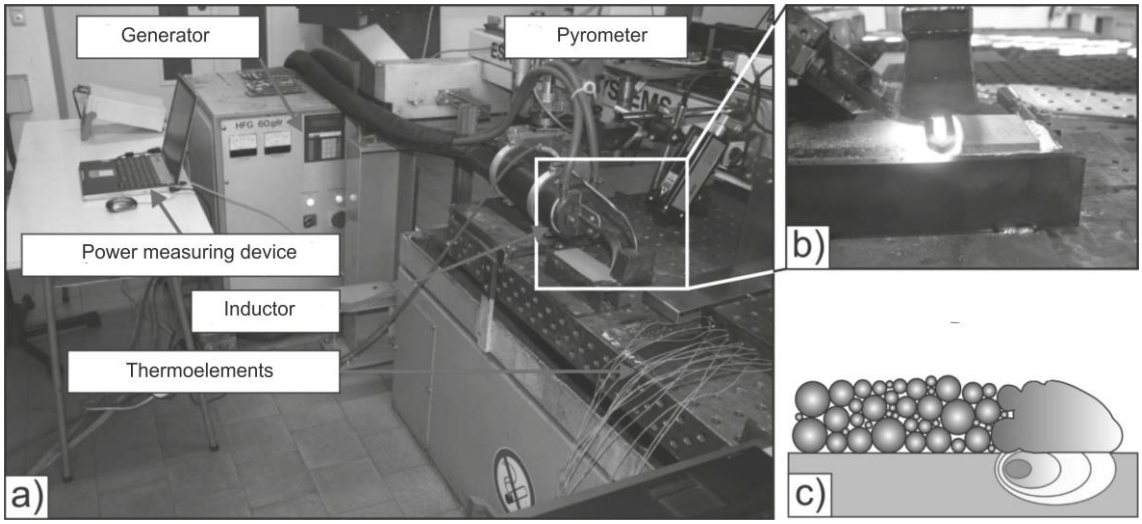

Figure B. 4.: a) InduClad setup b) Heat development in substrat with eddy currents c) Heat conduction trought the powder bulk [65]

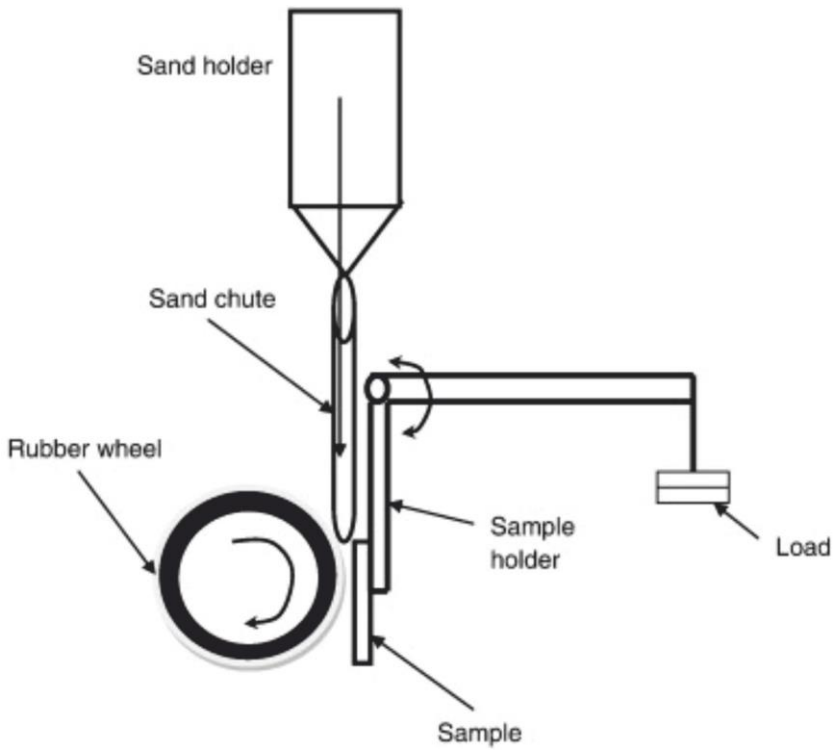

Figure B. 5.: Rubber wheel equipment according to ASTM G65 [70]

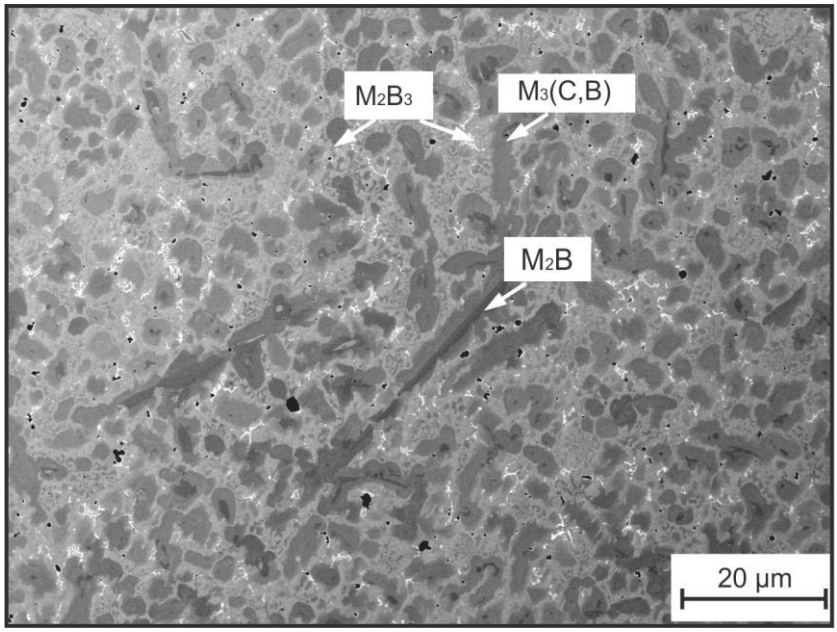

Figure B. 6.: Microstructure of the steel X200CrNiBMo10-4-3-3 in InduClad state

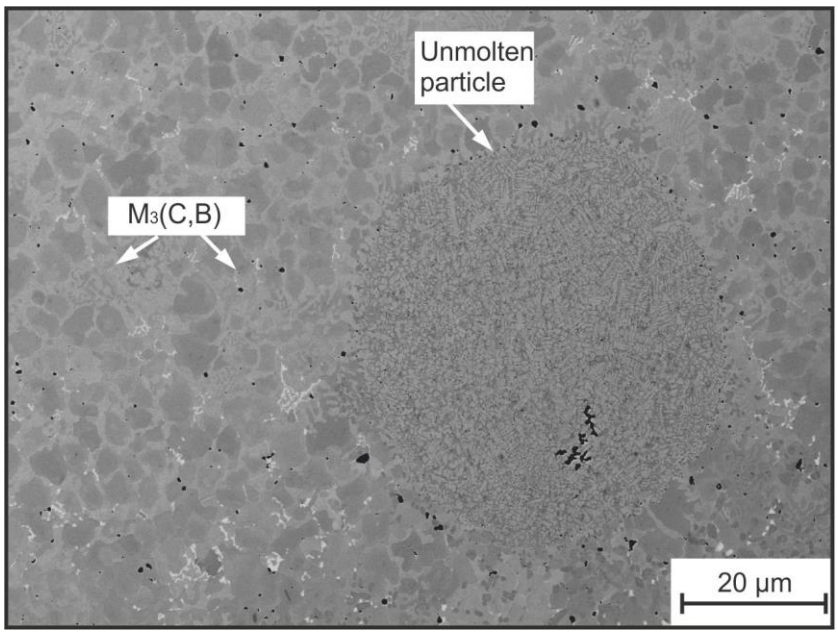

Figure B. 7.: Microstructure of an unmolten particle from the steel X220CrVMo13-4 in a steel matrix X200CuNiBMo10-4-3-3 in InduClad state

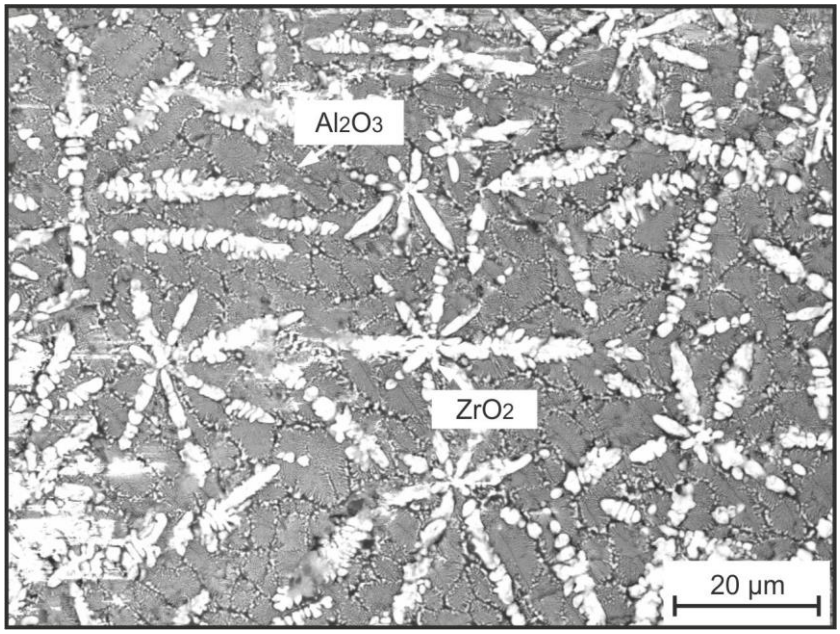

Figure B. 8.: Microstructure of the eutectic structure of an AlZrO particle. The bright phase represents ZrO_2, the dark phase Al_2O_3

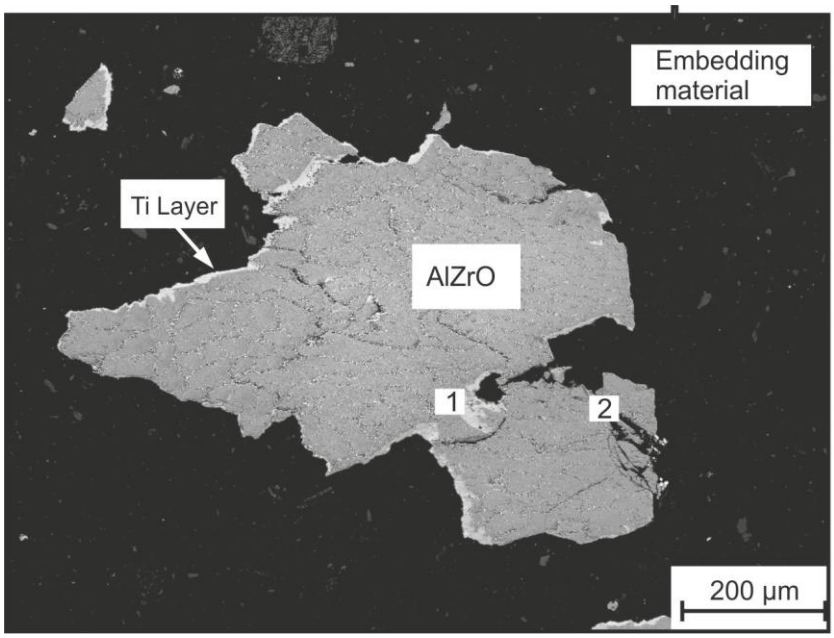

Figure B. 9.: Microstructure of a Ti-coated AlZrO particle with Ti (1) and microcracks (2) on the surface (sample (Al-Zr-O)Ti_{180})

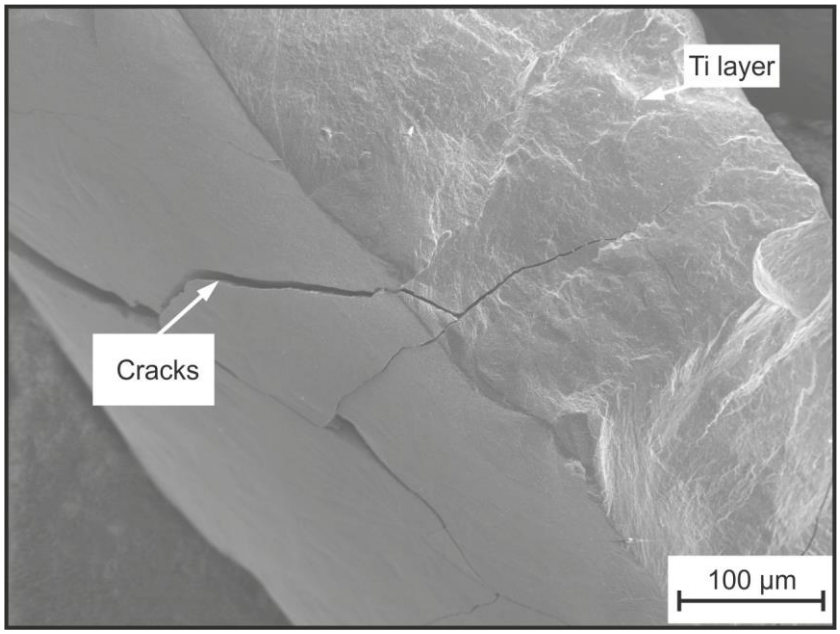

Figure B. 10.: Microstructure of a dense Ti-layer on the surface of the AlZrO HP

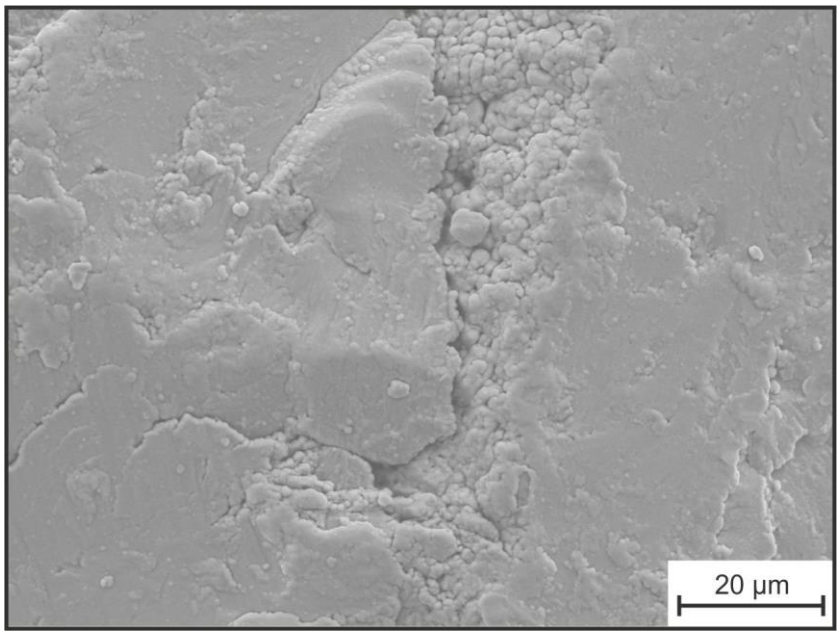

Figure B. 11.: Microstructure of a dense Ti-V-multilayer on the surface of the AlZrO HP

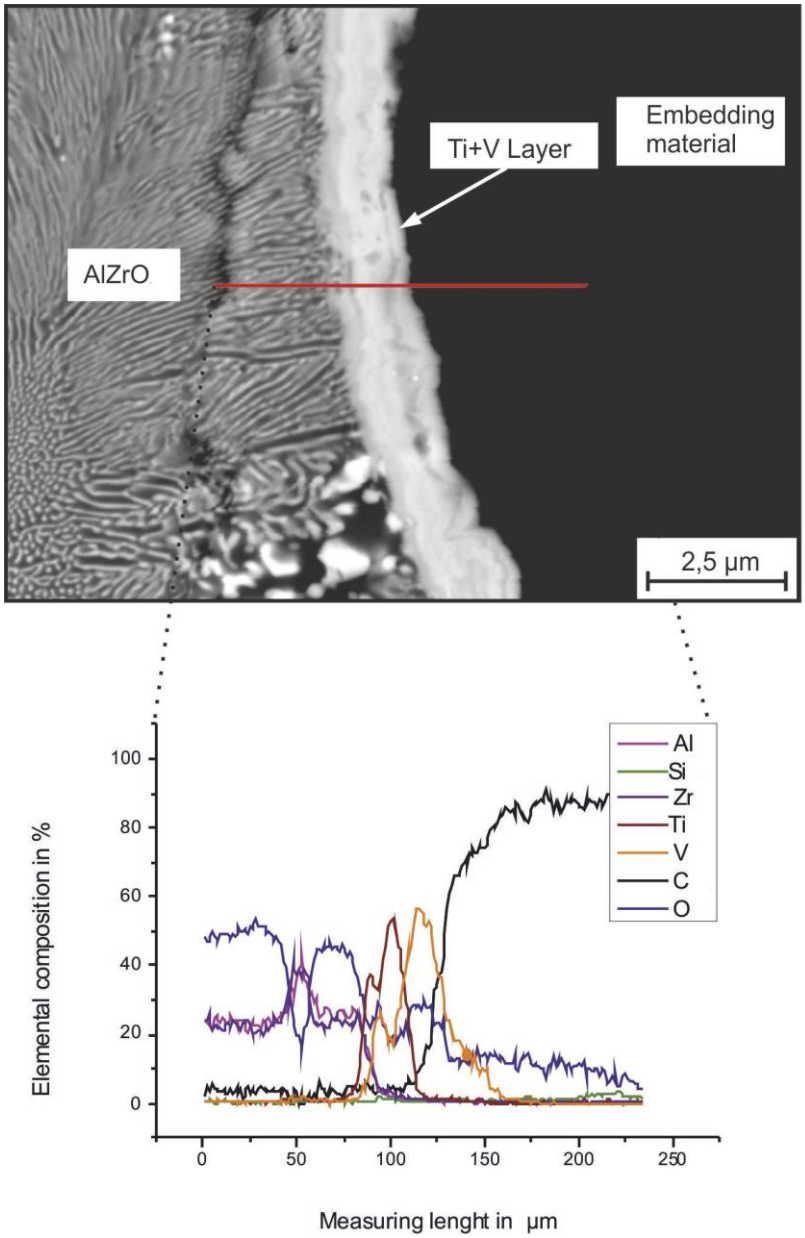

Figure B. 12.: EDX-linescan at the interfaces AlZrO HP - Ti-V-multilayer - embedding material, sample (Al-Zr-O)$Ti_{180}V_{180}$

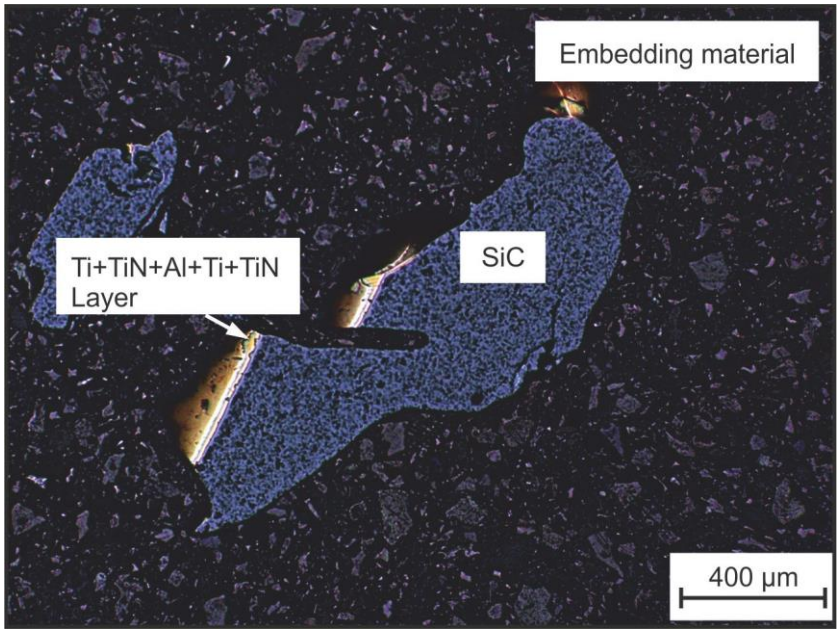

Figure B. 13.: Microstructure of a Ti-TiN-Al-Ti-TiN-coated SiC HP (sample (Si-C)$Ti_{120}TiN_{60}Al_{60}Ti_{60}TiN_{60}$)

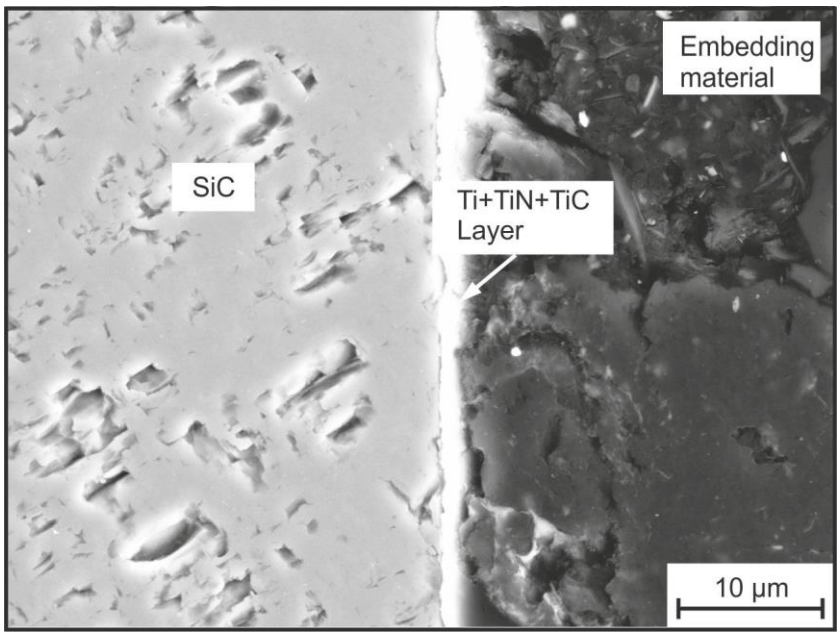

Figure B. 14.: Microstructure of a Ti-TiN-TiN-coated SiC HP (sample (Si-C)$Ti_{30}TiN_{120}TiC_{60}$)

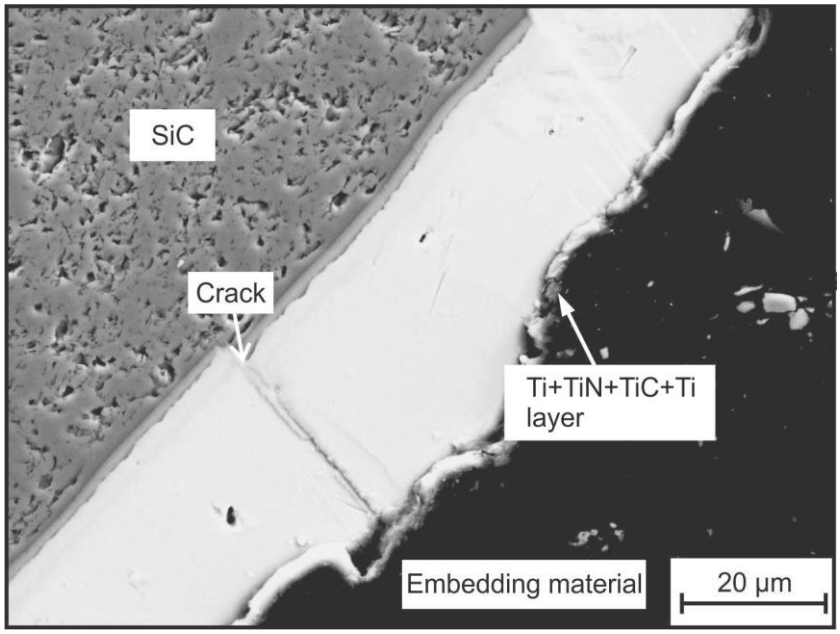

Figure B. 15.: Microstructure of the Ti-TiN-TiN-Ti-coated SiC particle (sample (Si-C)$Ti_{30}TiN_{120}TiC_{60}Ti_{30}$)

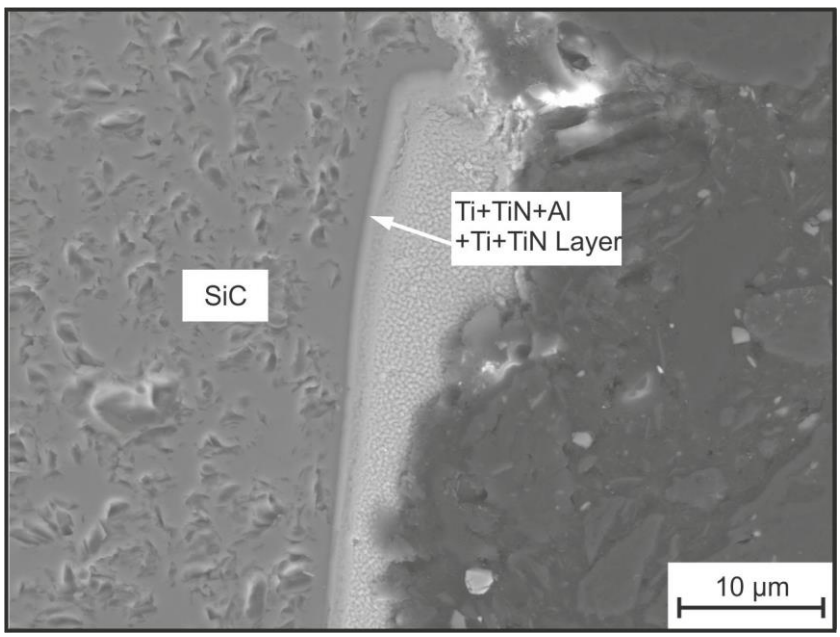

Figure B. 16.: Microstructure of the Ti-TiN-Al-Ti-TiN-coated SiC particle, a wider view due the fracture of the embedding material (sample (Si-C)$Ti_{120}TiN_{60}Al_{60}Ti_{60}TiN_{60}$)

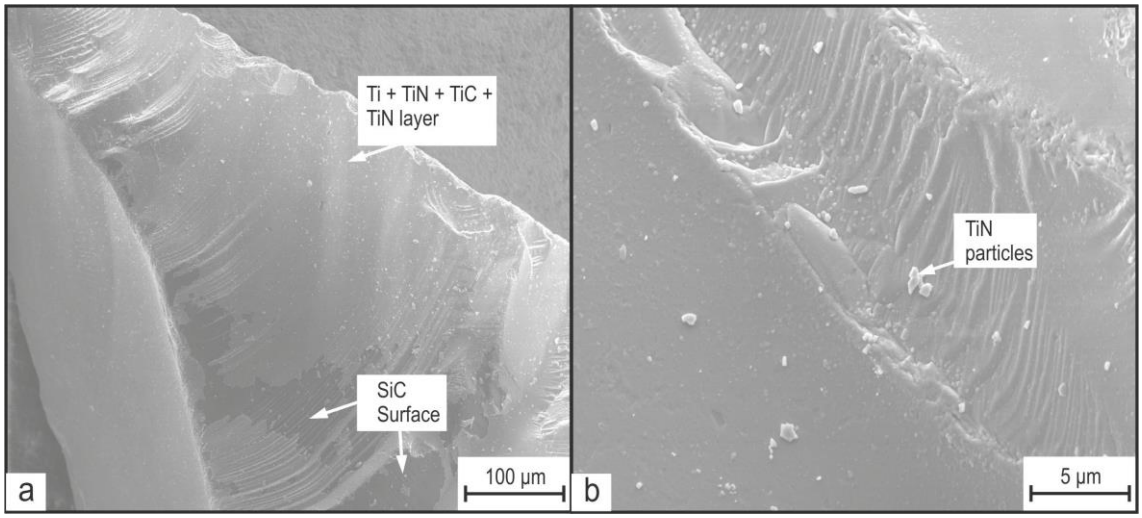

Figure B. 17.: a) Microstructure of the Ti-TiC-TiN-Ti-TiN-coated SiC particle b) Microstructure of the Ti-TiC-TiN-Ti-TiN-multilayer

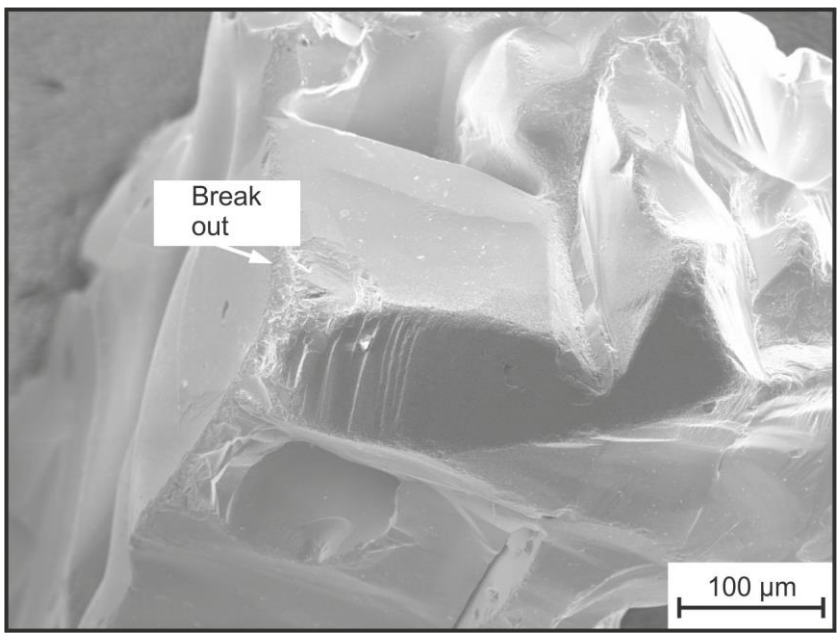

Figure B. 18.: Microstructure of a Ti-TiN-Al-Ti-TiN-coating on a surface of a SiC HP

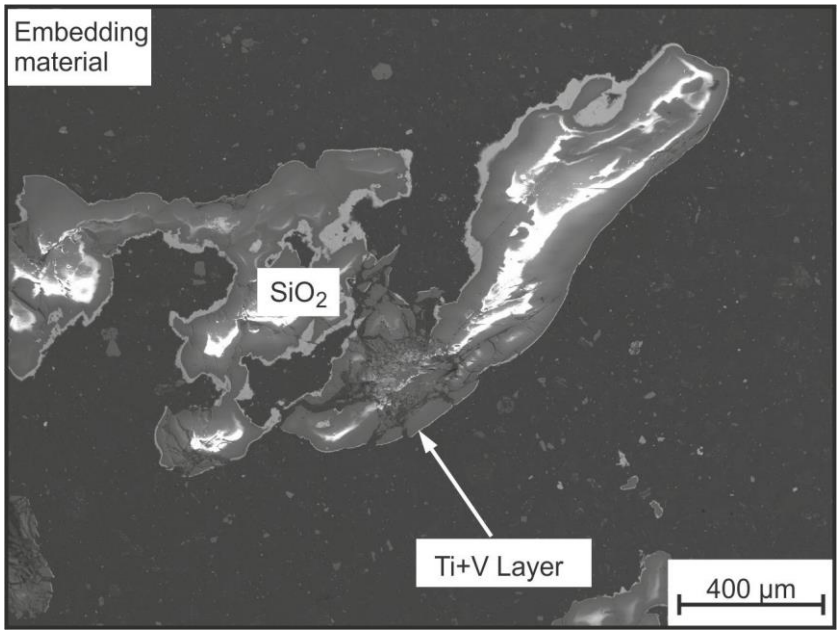

Figure B. 19.: Microstructure of a Ti-V-coated SiO_2 HP, (sample $(Si\text{-}O)_2V_{120}Ti_{120}$)

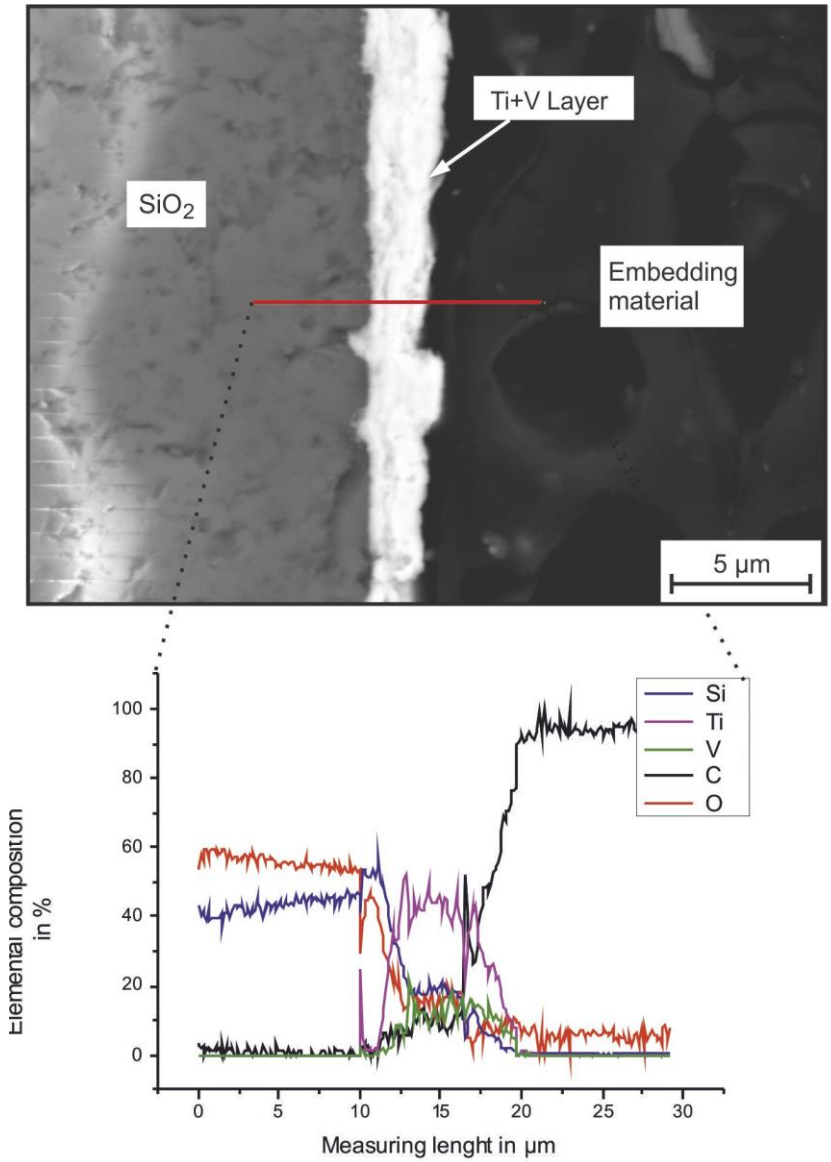

Figure B. 20.: Linescan at the interfaces SiO_2 - Ti-V-multilayer - embedding material, (sample $(Si\text{-}O)_2V_{120}Ti_{120}$)

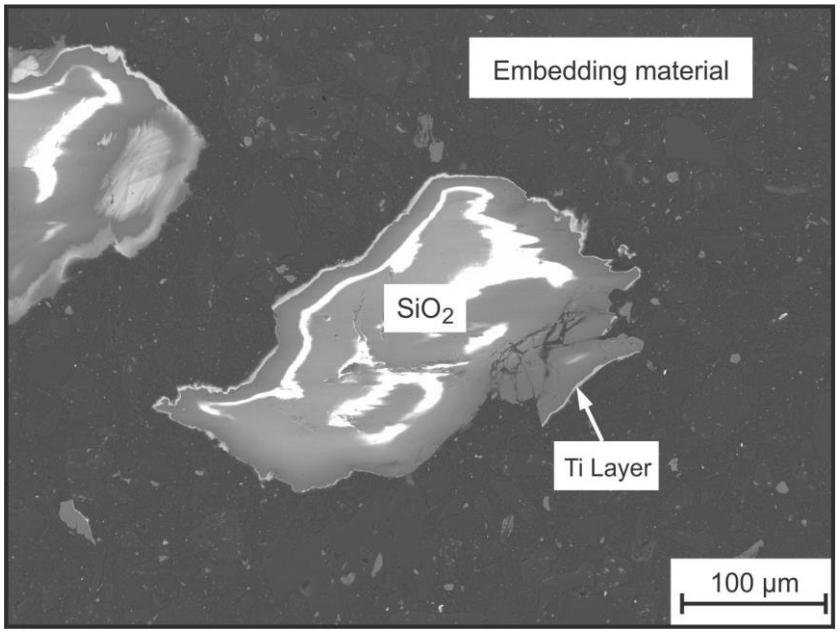

Figure B. 21.: Microstructure of a Ti-coated SiO_2 HP, (sample (Si-O_2)Ti_{180})

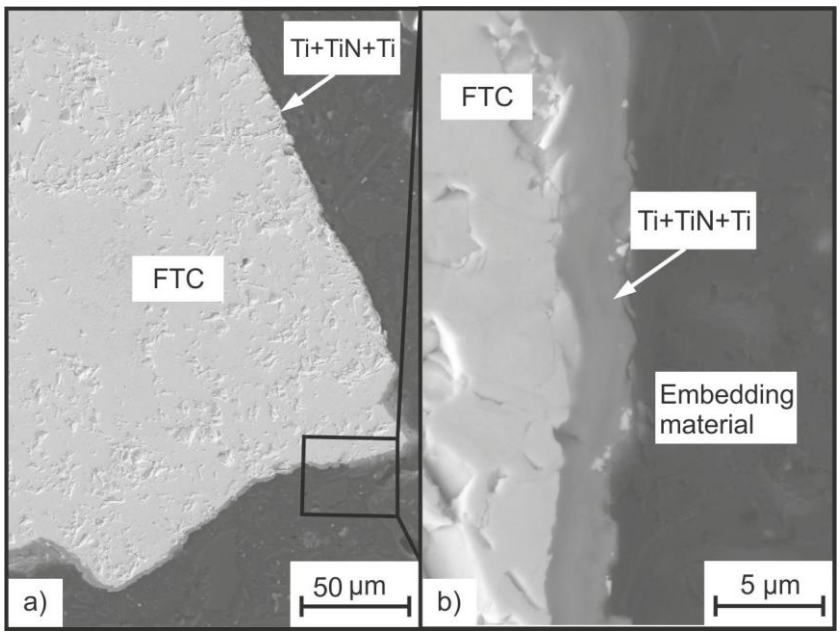

Figure B. 22.: a) Microstructure of a Ti-TiN-Ti-coated FTC HP (sample IC(F-C)$Ti_{120}TiN_{60}Ti_{60}$)
b) Microstructure of the Ti-TiN-Ti-multilayer at higher magnification

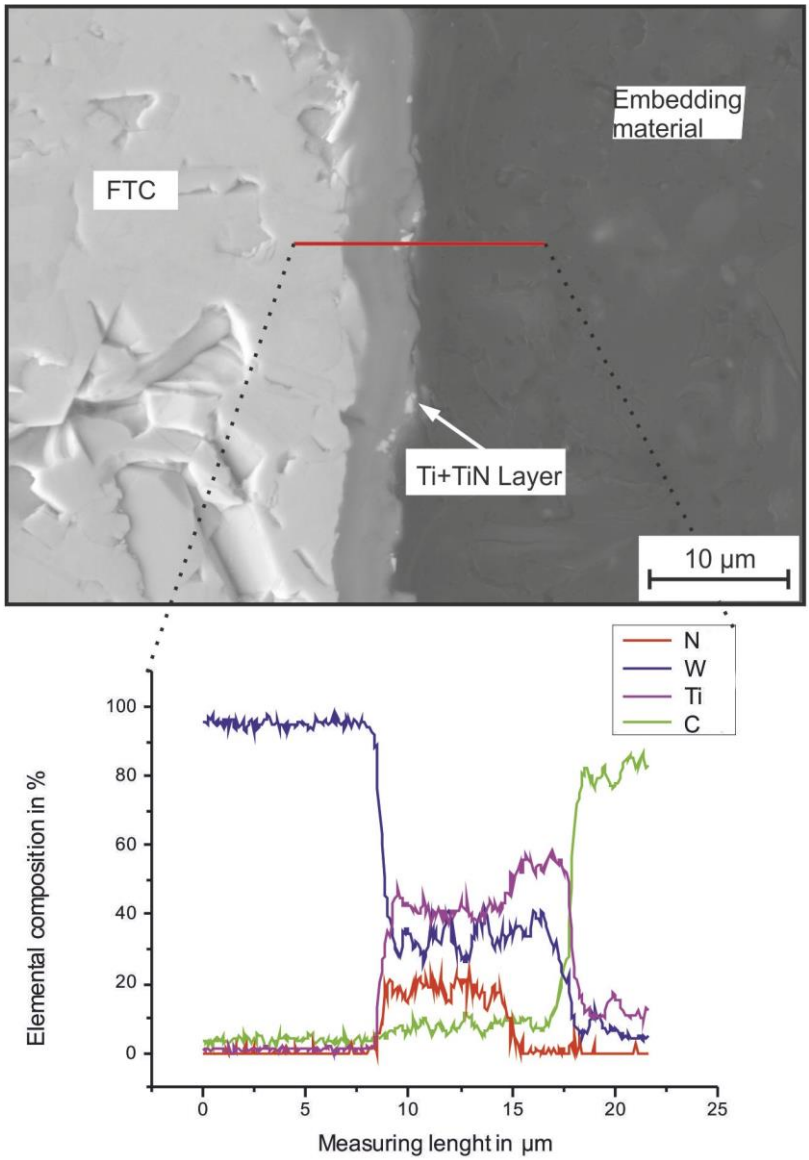

Figure B. 23.: EDX - linescan at the interfaces FTC - Ti-TiN-Ti-multilayer - embedding material, (sample IC(F-C)$Ti_{120}TiN_{60}Ti_{60}$)

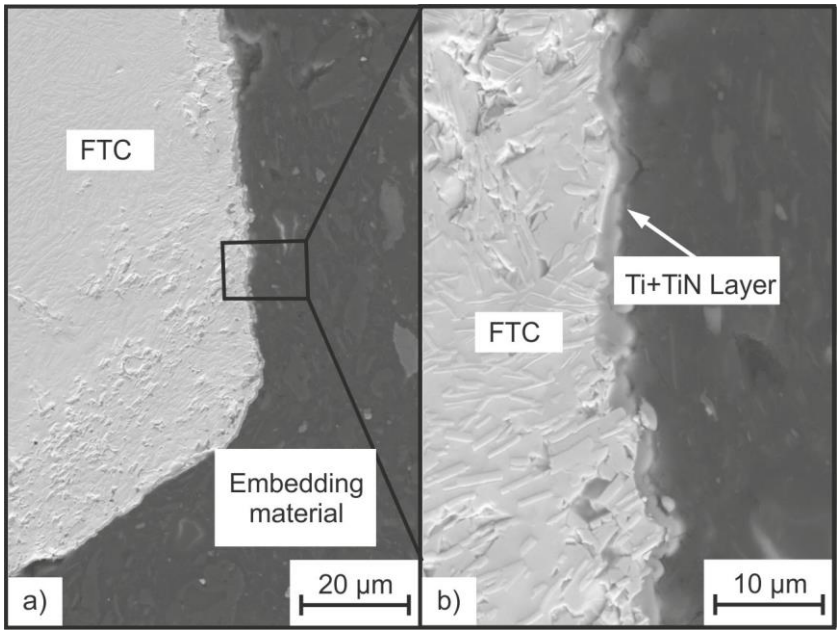

Figure B. 24.: a) Microstructure of a Ti-TiN-coated FTC HP (sample (F-C)$Ti_{120}TiN_{60}$) b) Microstructure of the Ti-TiN-multilayer at higher magnificantion

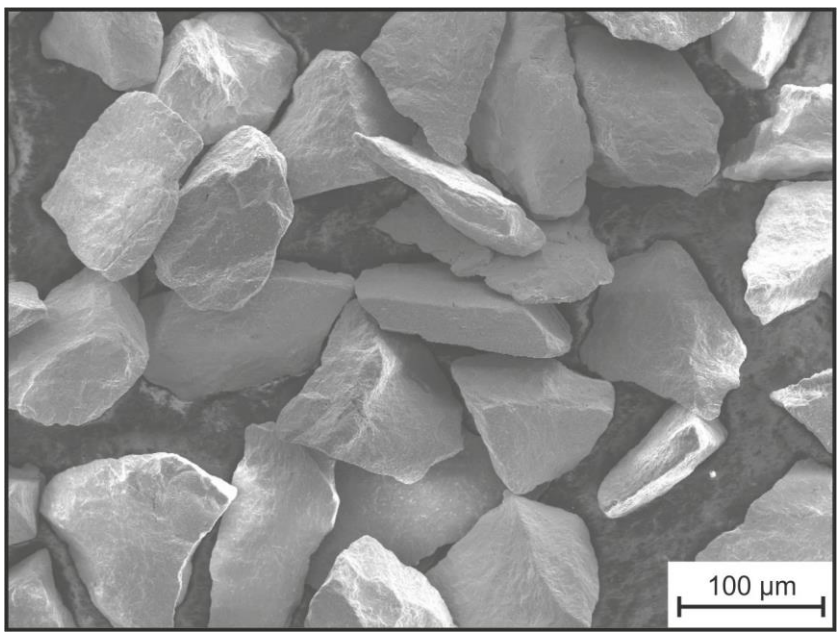

Figure B. 25.: Microstructure of the Ti-TiN-TiN-coated FTC HP

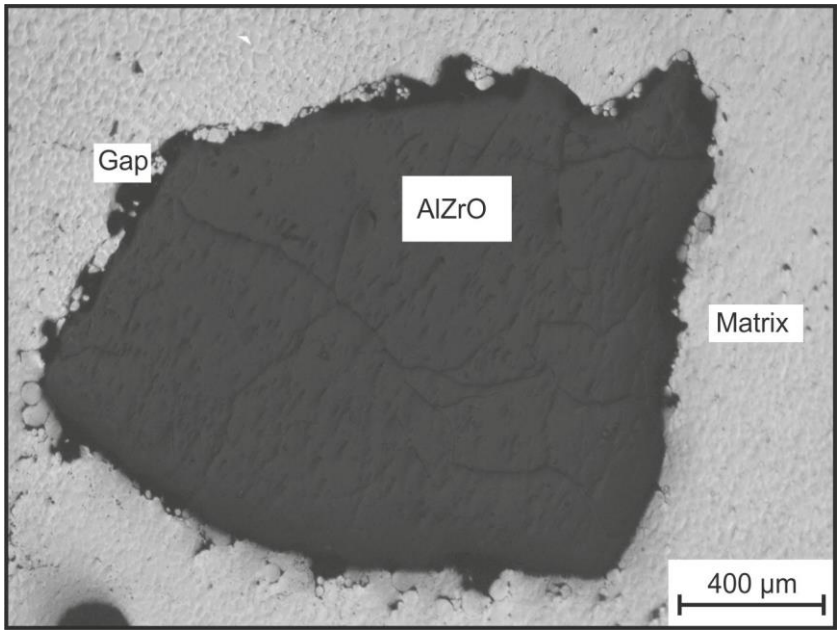

Figure B. 26.: Microstructure of the sample IC(Al-Zr-O)Ti_{180} with with gaps at the interface AlZrO HP - MM

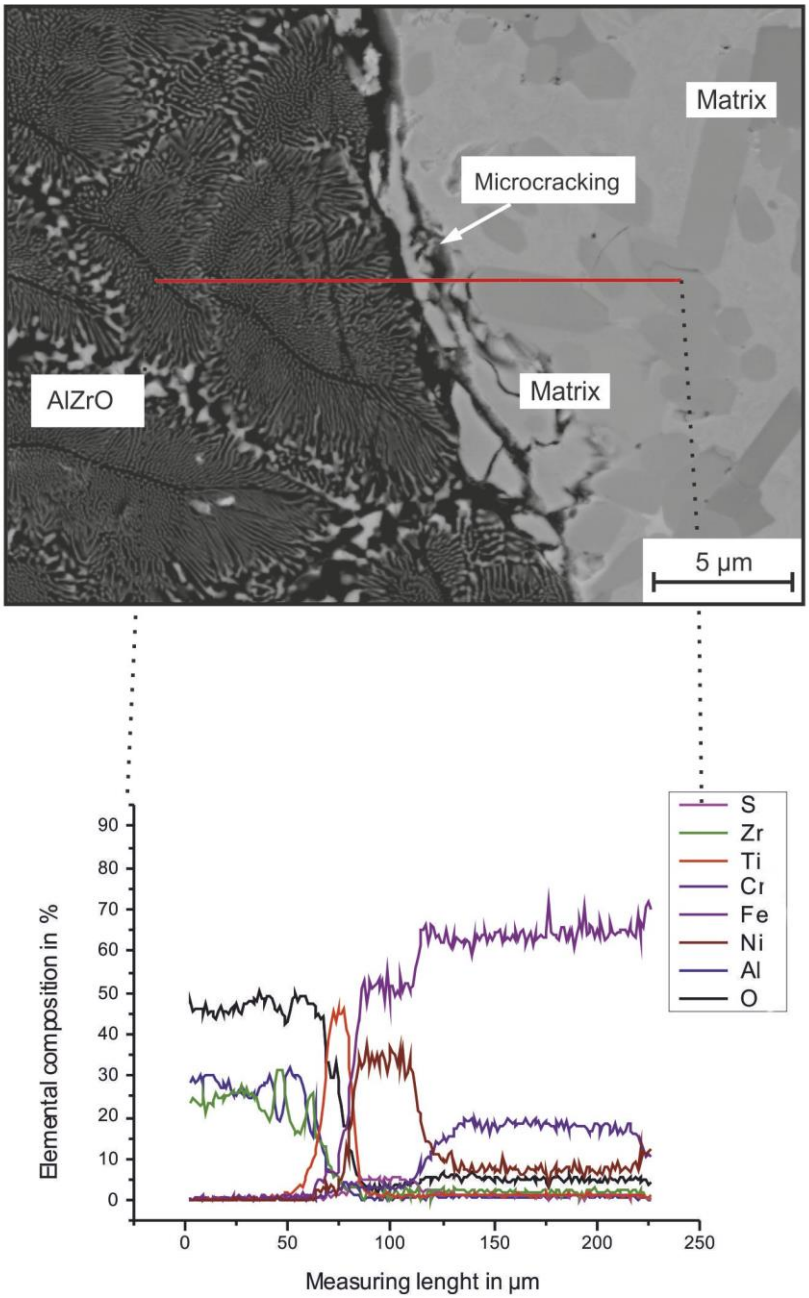

Figure B. 27.: EDX-linescan at the interfaces AlZrO - Ti-layer - MM, (sample IC(Al-Zr-O)Ti_{180})

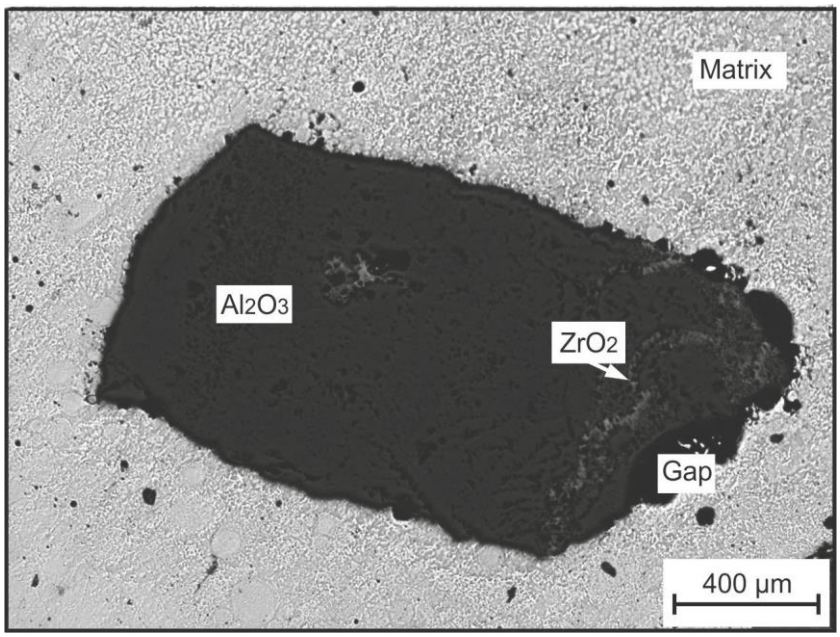

Figure B. 28.: Microstructure of a IC(Al-Zr-O)$Ti_{120}V_{120}$ sample with gaps at the interface AlZrO HP - MM

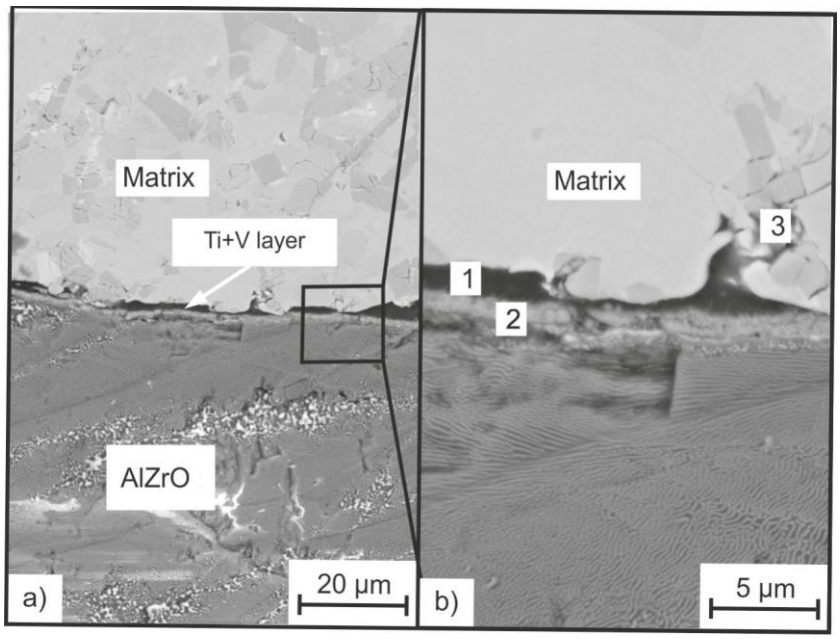

Figure B. 29.: a) Microstructure of a Ti-V-coated AlZrO HP (sample IC(Al-Zr-O)$Ti_{120}V_{120}$) b) Gap (1), Ti-V-multilayer (2) and microcracking(3) at the interface AlZrO HP - MM

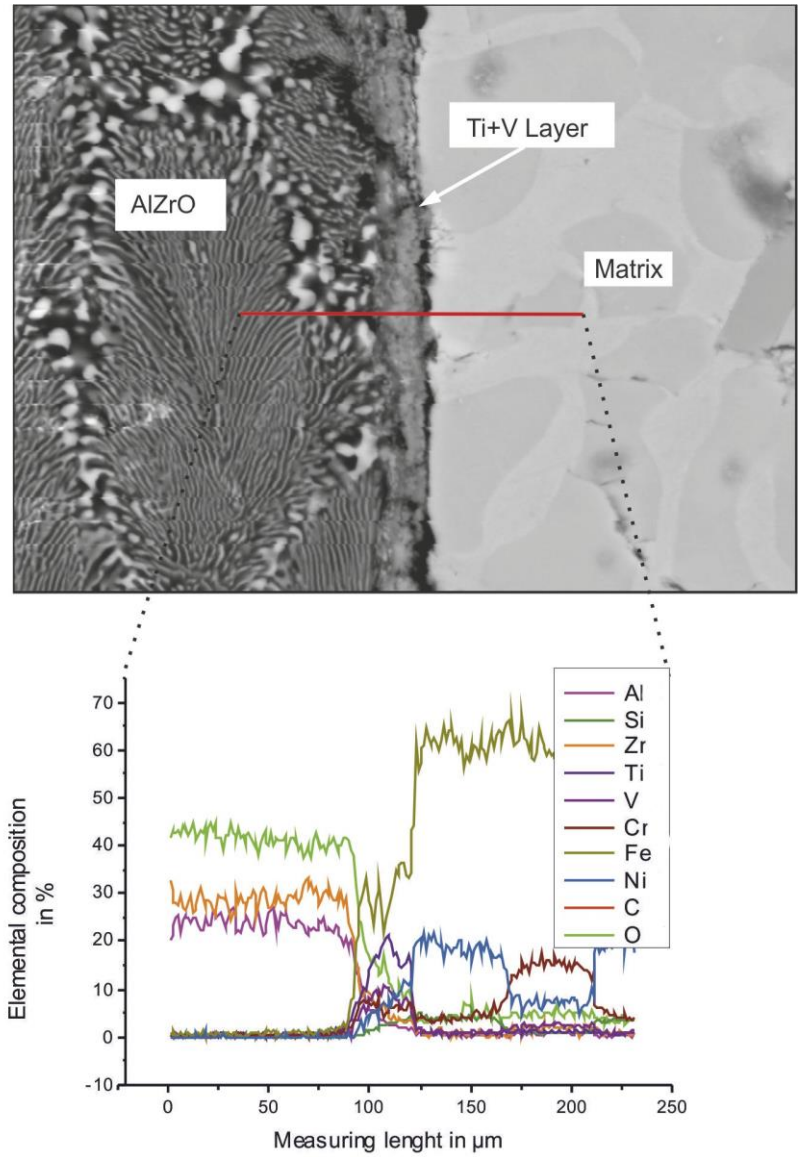

Figure B. 30.: Linescan at the interface AlZrO HP - Ti-V-multilayer - MM, (sample IC(Al-Zr-O)$Ti_{120}V_{120}$)

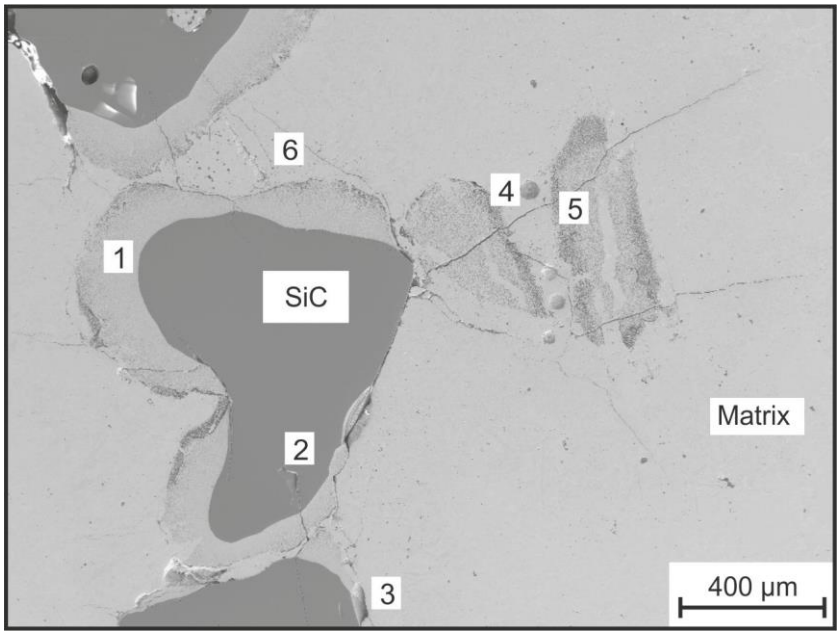

Figure B. 31.: Microstructure of a IC(Si-C)$Ti_{120}TiN_{120}Al_{60}Ti_{60}TiN_{60}$ sample with craks (6) and pores (4) in the MM, diffusions zone with Fe-rich silicides and graphite (1) and coarse phases (5) at the interface SiC HP - MM, gaps in the SiC HP (2) and gaps at the interface SiC HP - MM (3) (sample IC(Si-C)$Ti_{120}TiN_{120}Al_{60}Ti_{60}TiN_{60}$)

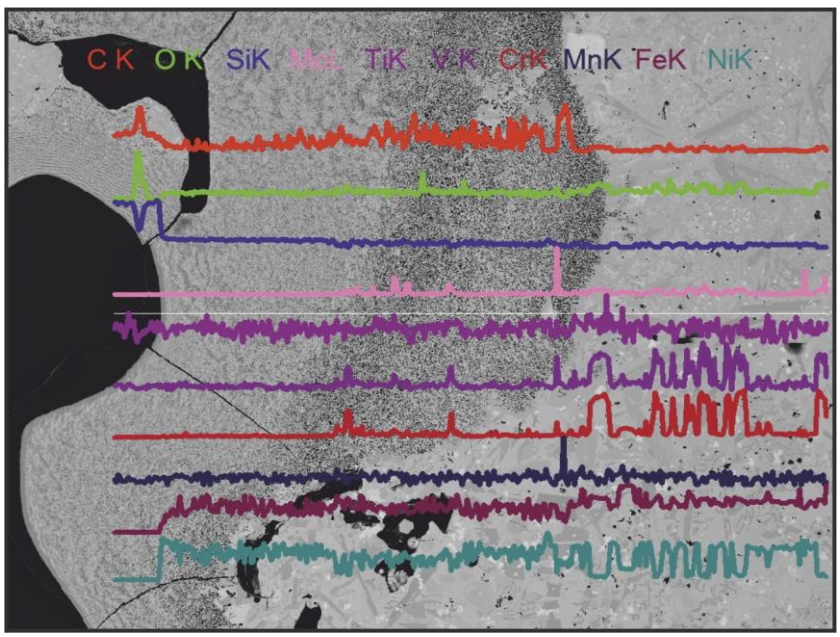

Figure B. 32.: EDX- linescan at the diffusion zone, sample (IC(Si-C)$Ti_{120}TiN_{120}Al_{60}Ti_{60}TiN_{60}$)

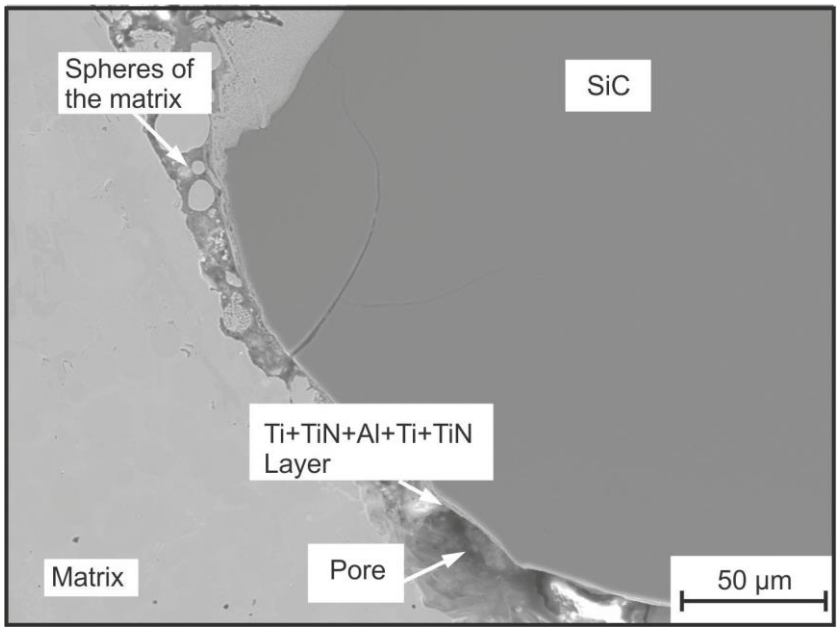

Figure B. 33.: Spheres of MM and pores at the interace SiC HP - MM, sample (IC(Si-C)$Ti_{120}TiN_{120}Al_{60}Ti_{60}TiN_{60}$)

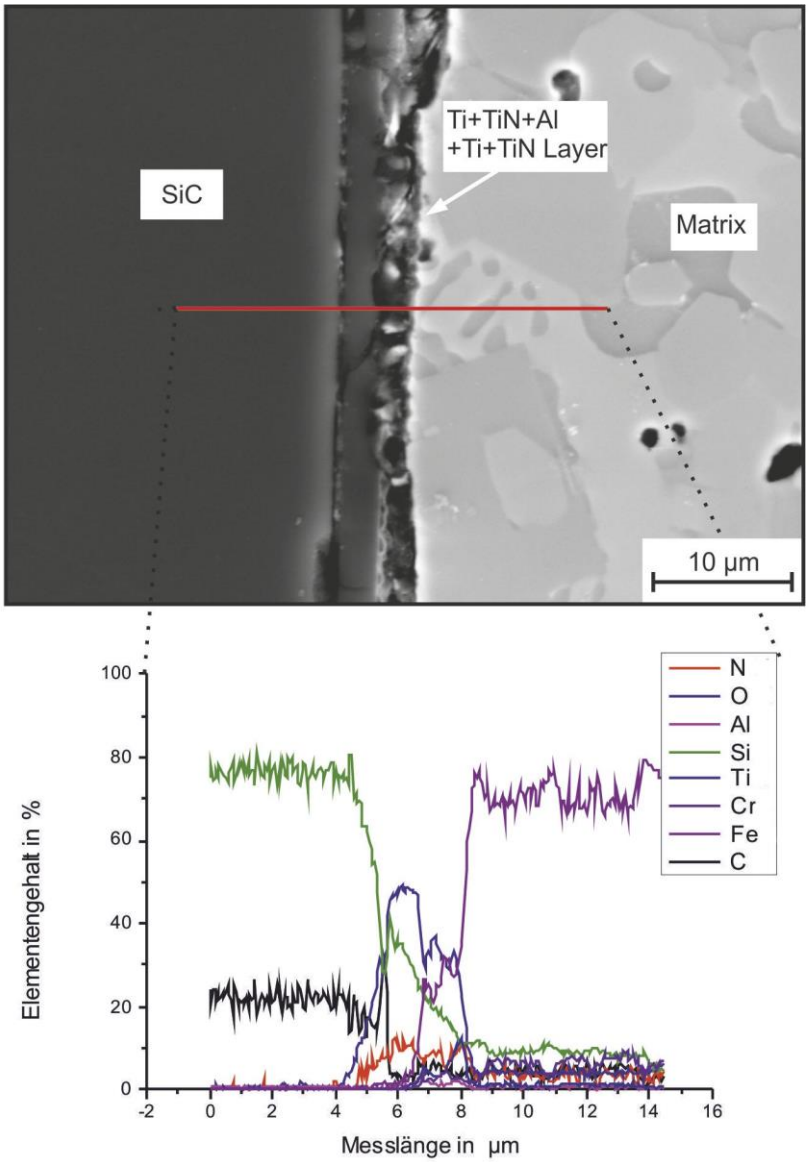

Figure B. 34.: Linescan at the interface SiC HP - Ti-TiN-Al-Ti-TiN-multilayer - MM, sample IC(Si-C)$Ti_{120}TiN_{120}Al_{60}Ti_{60}TiN_{60}$

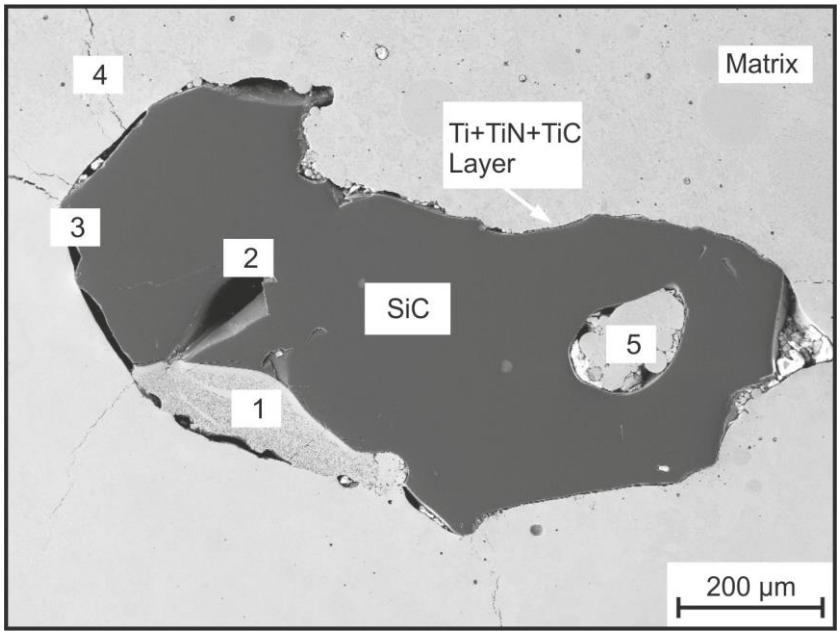

Figure B. 35.: Microstructure of a IC(Si-C)$Ti_{30}TiN_{120}TiC_{60}$ sample with cracks in the MM (4), gaps in the SiC HP (2), diffusion zone at the interface SiC HP - MM (1), gaps at the interfac SiC HP - MM (3) and matrix material in a gap on the SiC HP (5)

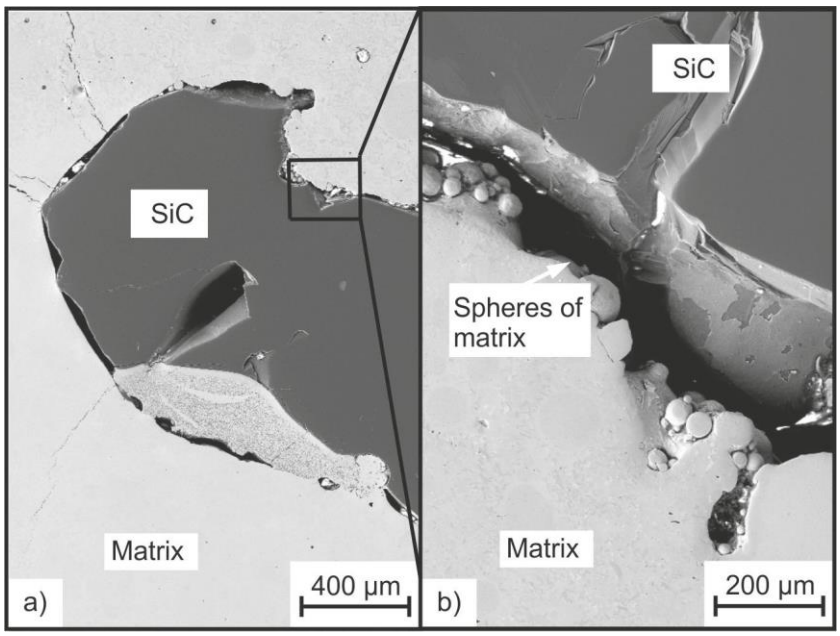

Figure B. 36.: a) Microstructure of the sample IC(Si-C)$Ti_{30}TiN_{120}TiC_{60}$, b) Microstructure of the spheres of the MM at the interface SiC HP - MM

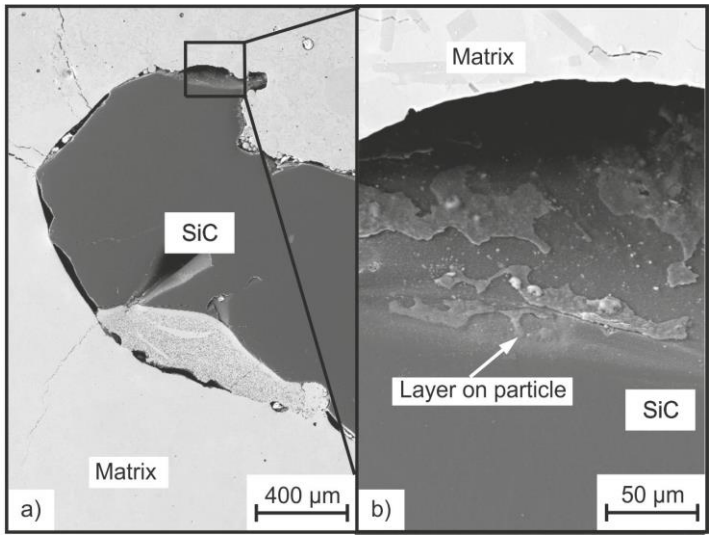

Figure B. 37.: a) Microstructure of the sample IC(Si-C)$Ti_{30}TiN_{120}TiC_{60}$, b) Microstructure of Ti-TiN-TiC-multilayer deposited in gap at the interface SiC HP - MM

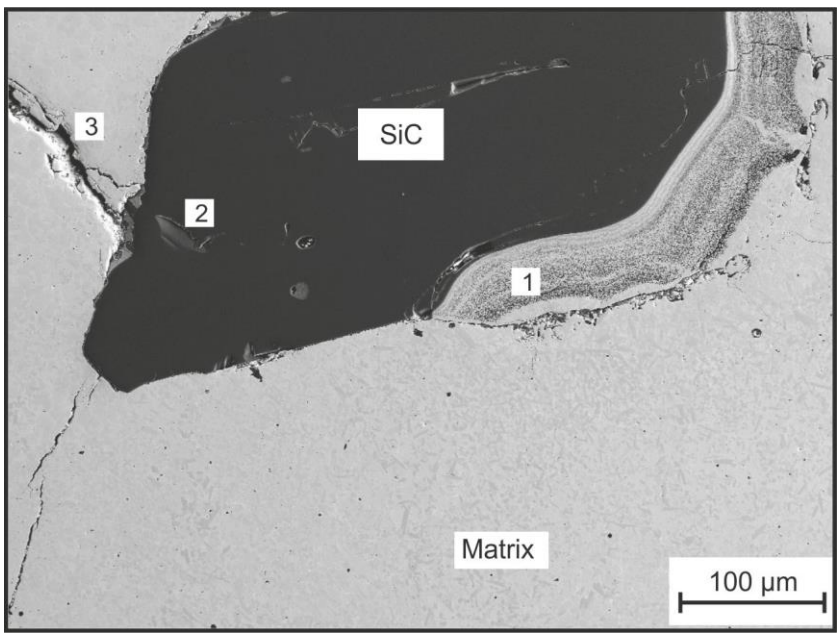

Figure B. 38.: Microstructure of the IC(Si-C)$Ti_{30}TiN_{120}TiC_{60}Ti_{30}$ sample with cracks in the MM (3), diffusion zone at the interface SiC HP - MM (1) and gaps in the SiC HP (2)

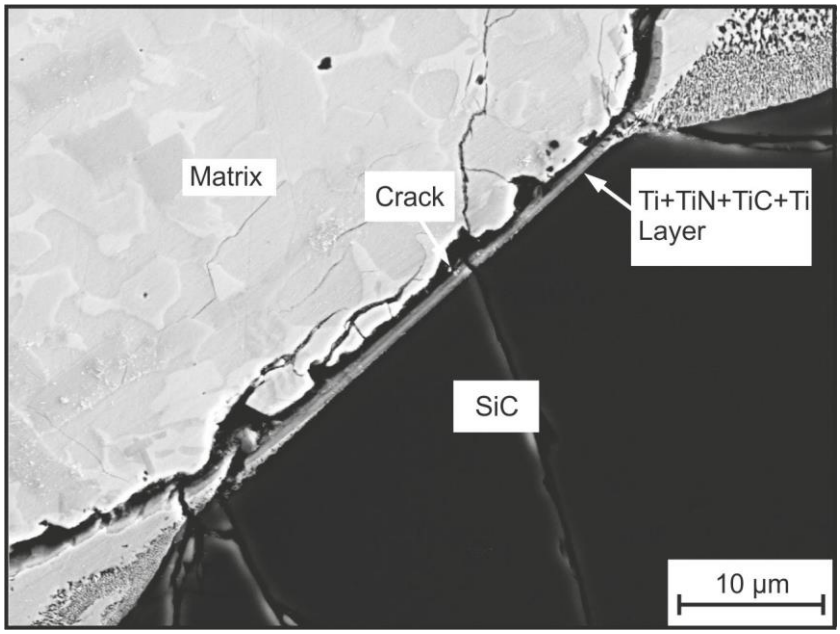

Figure B. 39.: Microstructure of the Ti-TiN-TiC-Ti-multilayer, (sample IC(Si-C)$Ti_{30}TiN_{120}TiC_{60}Ti_{30}$)

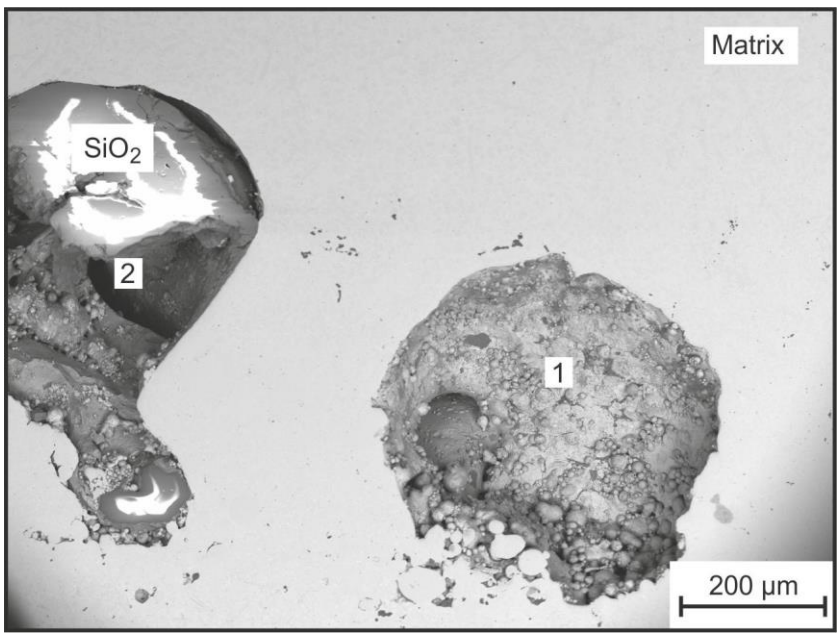

Figure B. 40.: Microstructure of the sample IC(Si-O)$Ti_{120}V_{120}$ with SiO_2 HP break outs (1), gaps at the interface SiO_2 - MM

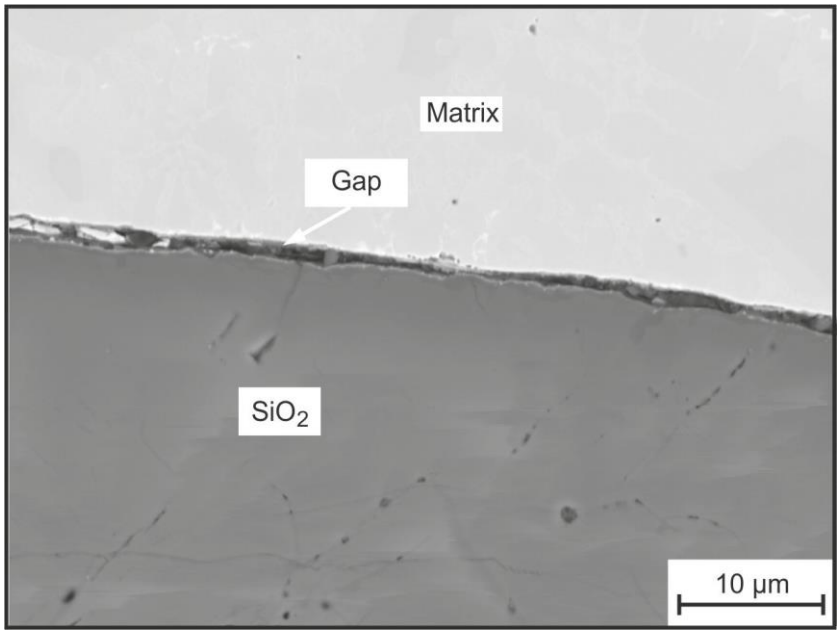

Figure B. 41.: Gap at the SiO_2 - MM interface, sample IC(Si-O)$Ti_{120}V_{120}$

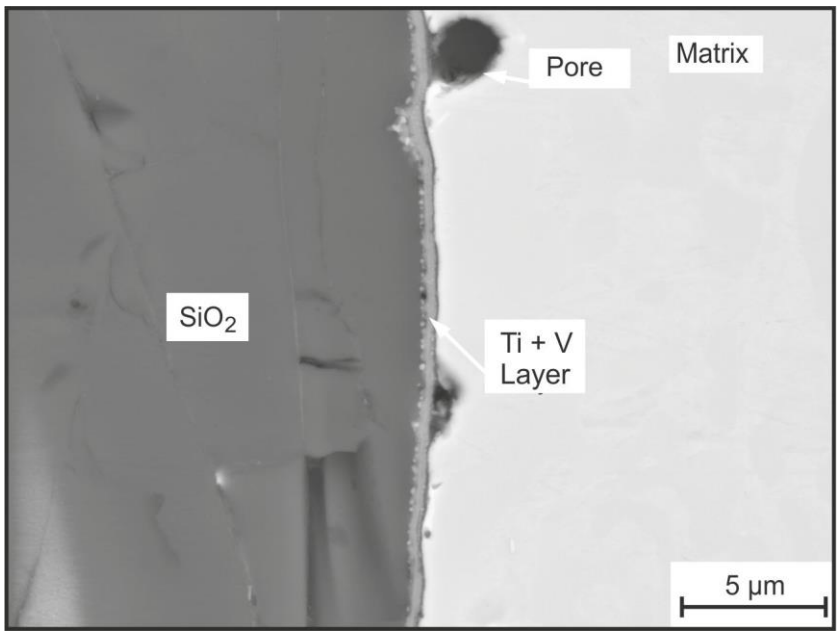

Figure B. 42.: Microstructure of the Ti-V-multilayer, sample IC(Si-O)$Ti_{120}V_{120}$

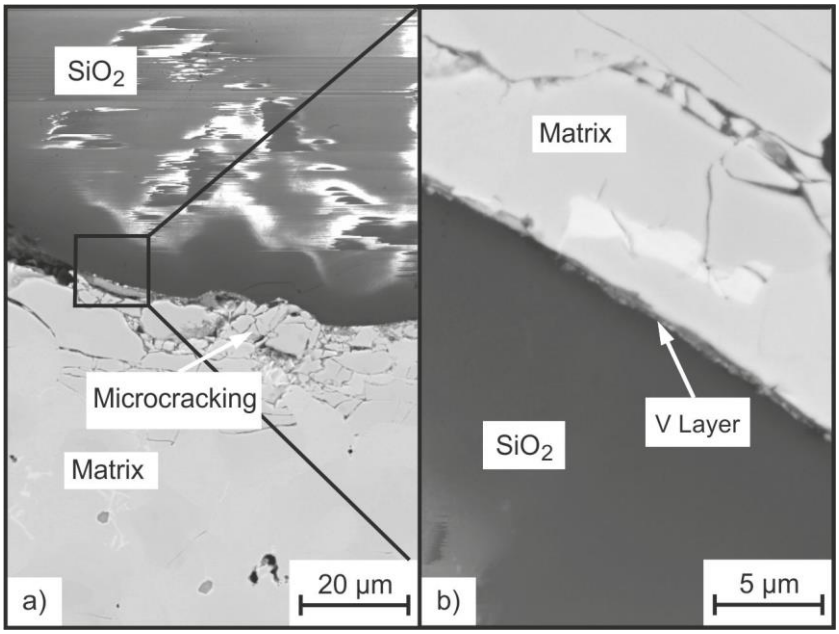

Figure B. 43.: a) Microstructure of the sample (Si-O)V_{180} with microcracking in the MM b) Microstructure of the V-layer at the interface MM - SiO_2

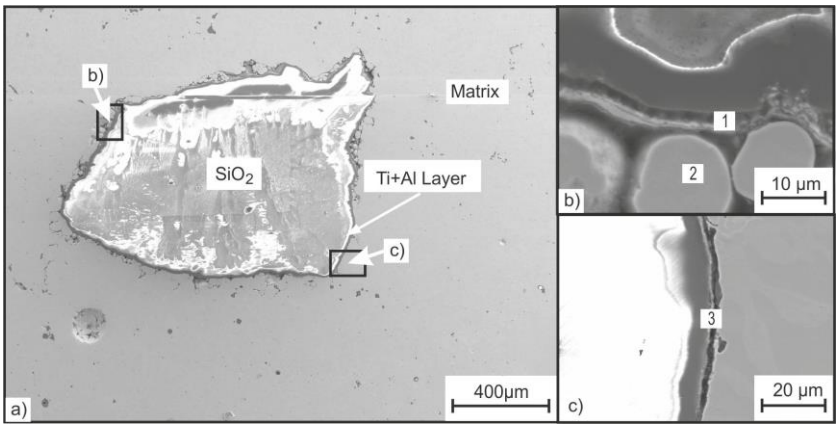

Figure B. 44.: (a) Microstructure of the sample IC(Si-O)$Al_{60}Ti_{120}$ b) Microstructure of the spheres of matrix material (2) and the Ti-Al-multilayer (1) at the interface SiO_2 - MM c) Microstructure of the Al layer (3)

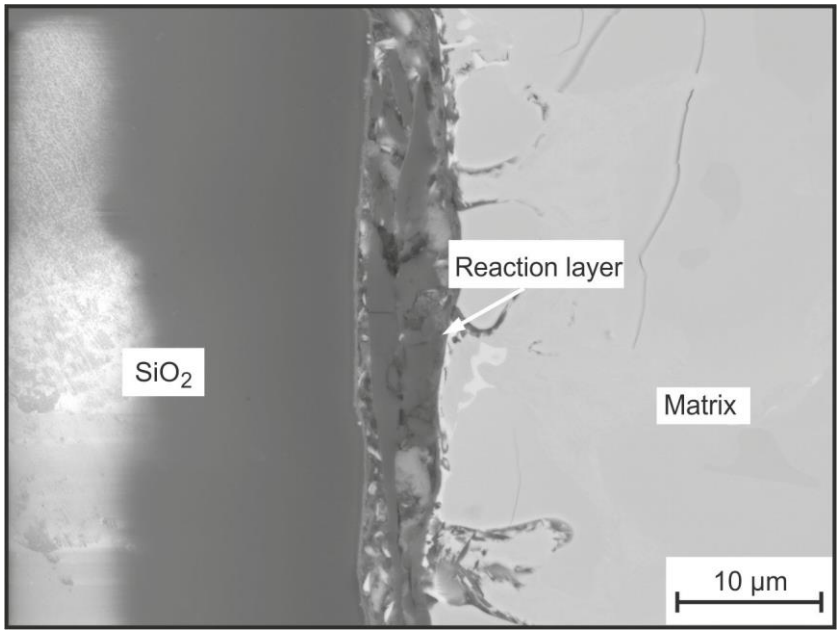

Figure B. 45.: Microstructure of the reaction layer at the interface SiO_2 - MM, sample IC(Si-O)$Al_{60}Ti_{120}$

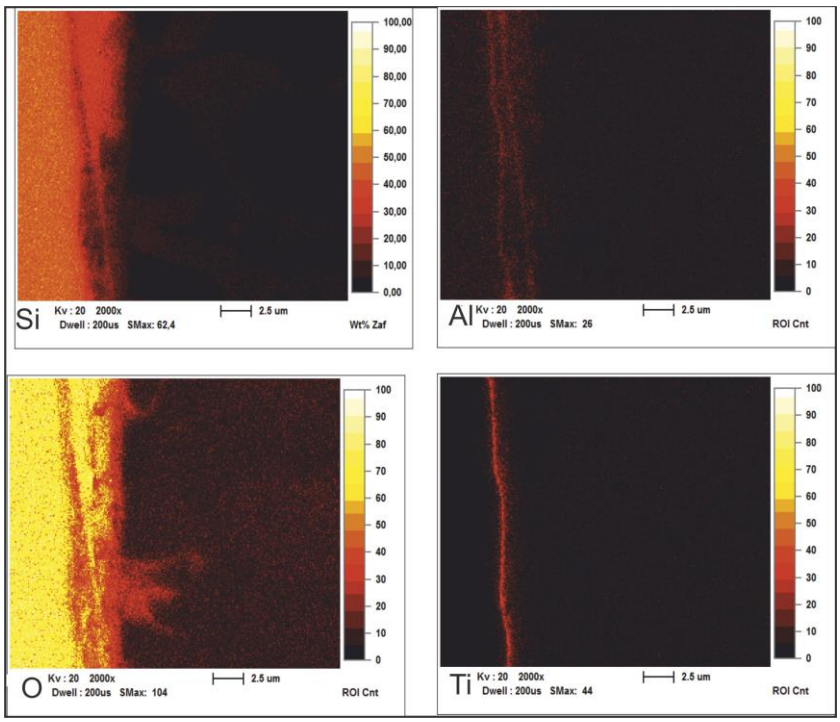

Figure B. 46.: Distribution of elements for the B. 45 picture mit ZAF-correction in mass .-%, sample (Si-O)$Al_{60}Ti_{120}$

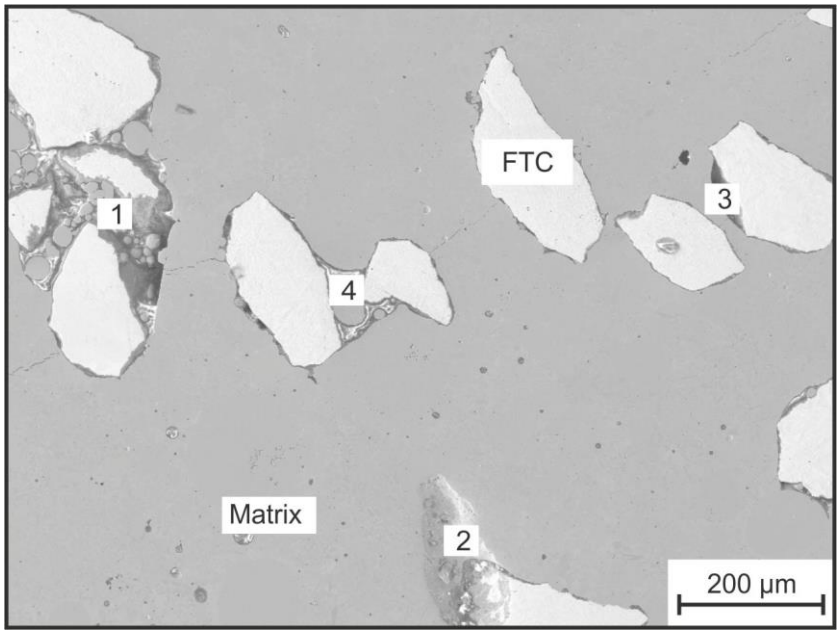

Figure B. 47.: Microstructure of the samples (F-C)$Ti_{120}TiN_{60}Ti_{60}$ with gaps (3) and spheres of the MM (1) at the MM - FTC interface (1), diffusion zone at the MM - FTC interface (2) and Ti-TiN-Ti-multilayer on the surface of MM (4)

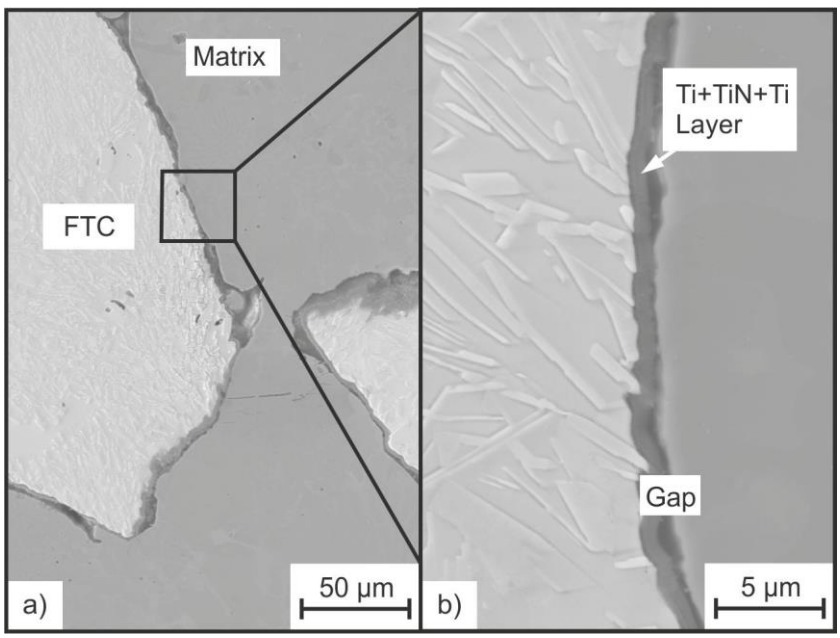

Figure B. 48.: Microstructure of the sample (F-C)$Ti_{120}TiN_{60}Ti_{60}$ b) Microstructure of the Ti-TiN-Ti-multilayer at the interface FTC HP - MM

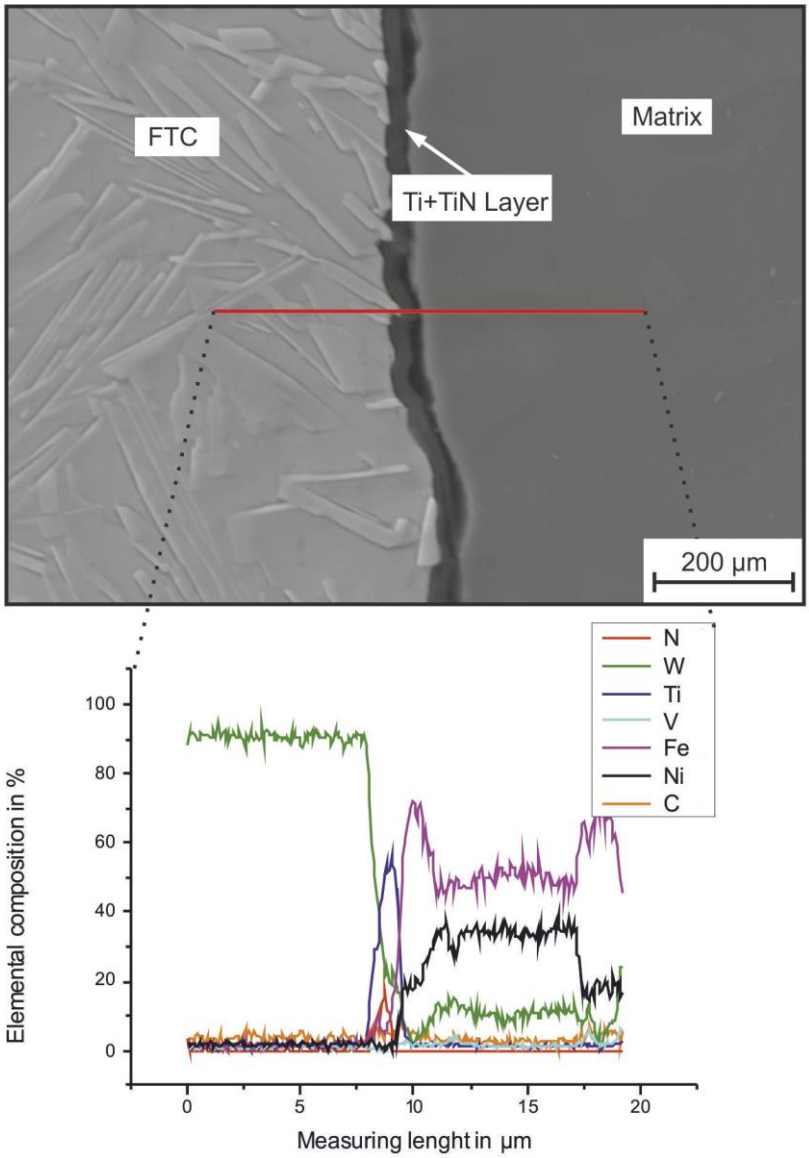

Figure B. 49.: Linescan at the interface FTC - Ti-TiN-Ti-multilayer - MM, sample (F-C)$Ti_{120}TiN_{60}Ti_{60}$

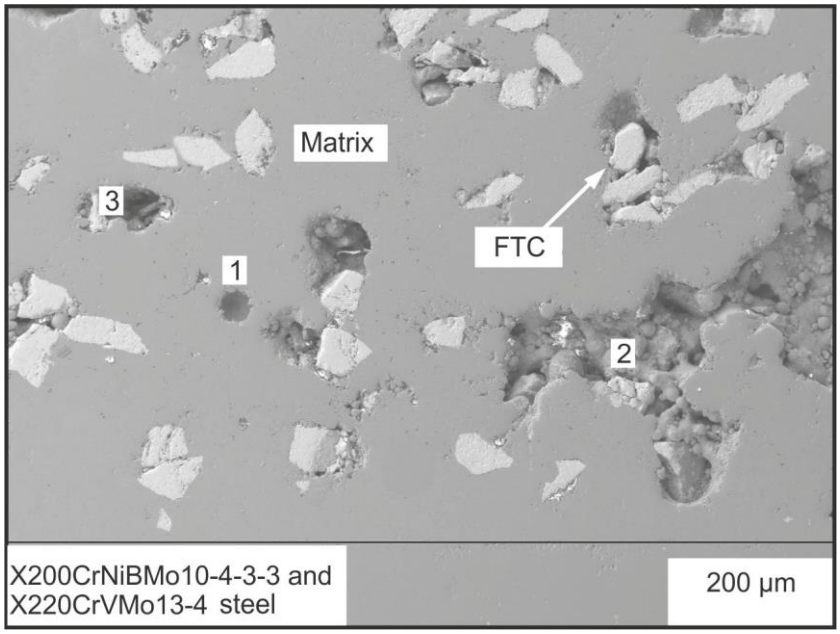

Figure B. 50.: Microstructure of the samples IC(F-C)$Ti_{120}TiN_{60}$ with HP break outs (1) and pores (2) in the MM

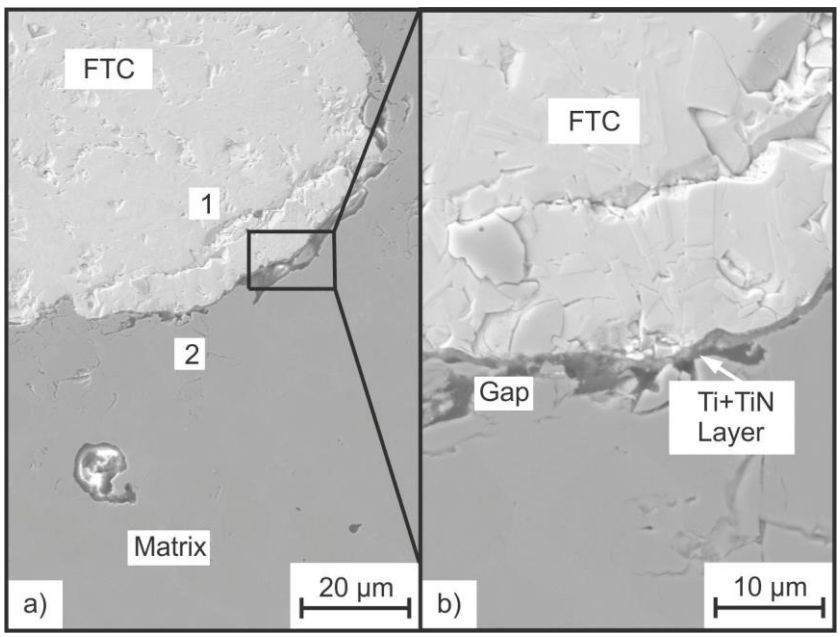

Figure B. 51.: a) Microstructure of the sample IC(F-C)$Ti_{120}TiN_{60}$ b) Microstructire of the Ti-TiN-multilayer at the interface FTC HP - MM

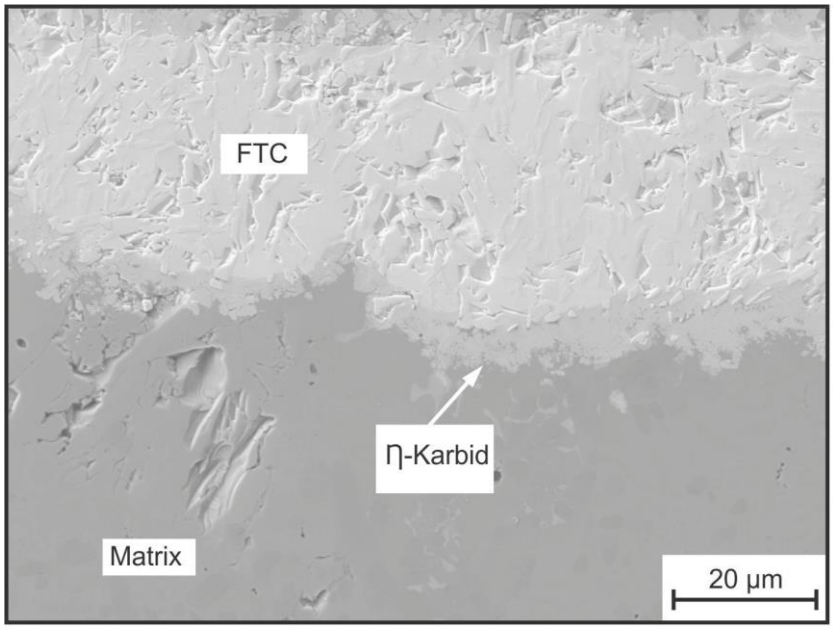

Figure B. 52.: Microstructure of the η-phase at the FTC - MM interface, sample IC(F-C)$Ti_{120}TiN_{60}$

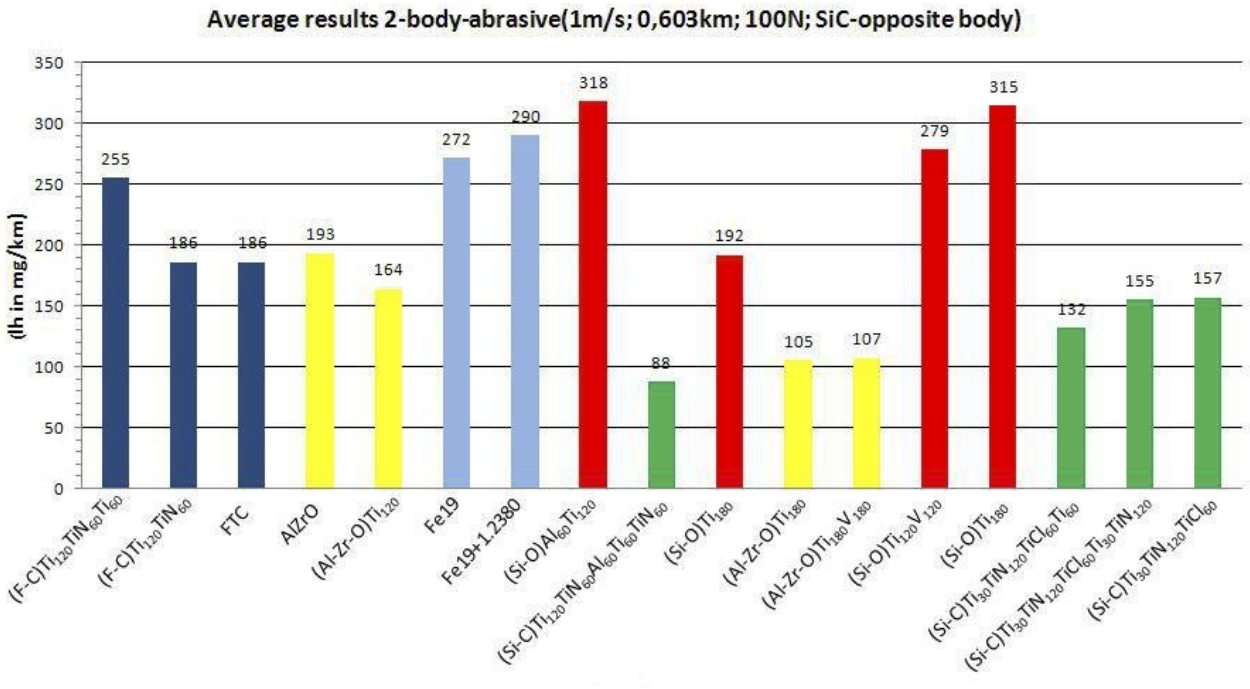

Figure B. 53.: A comparison between the wear rates according to ASTM 65

Literature

[1] S.Prabhu and B.K.Vinayagam. Nano surface generation of grinding process using carbon nano tubes. Materials Processing Technology 36 (2010) 6, page 747-760.

[2] F.Wendel. Wissenschaftliches Praktikum:Verschleiß. (2010).

[3] A.Röttger. Entwicklung neuer Schictverbunde auf Fe-basis gegen Abrasion. Dissertation. (2010).

[4] F. Bochmann; S. Gabriel; J.U Hahn; A. Hartwig; V. Mittenzwei, and M. Rocker. Hartmetallarbeitsplätze: Exposition und Bewertung (2008).

[5] A.Röttger; S.L.Weber; W.Theisen; B.Rajasekaran, and R.Vaßen. High Velocity Oxy Fuel Spraying of Cold Work Tool Steels- A Novel Approach to Thick Coatings for Wear Protection Applications. Advanced Engineering Materials 11 (2009) 12, page 1015-1022.

[6] R.Winkelmann; J.Smenda; W.Rank; W.Theisen; A.Röttger, and S.Weber. Induclad - verfahrens-und werkstoffechnische Grundlagen einer neuen Beschichtungstechnologie. (2010).

[7] F. Schreiber. Verschleißschutz durch Einsatz von Wolfram- Schmelzcarbid. (2002), page 12-17.

[8] H.Berns. “Hartlegierungen und Hartverbundwerkstoffe”. Springer-verlag Berlin Heildelberg (1998).

[9] A.Packeisen and W.Theisen. Spanende Bearbeitungen von Hartlegierungen - Drehen und Schleifen; Teil I: Gefüge und Eigenschaften von Hartlegierungen. 30 (1999), page 151-158.

[10] W.Theisen. “Gefüge hartstoffhaltiger Fe-basis Werstoffe”. Lehrstuhl Werkstofftechnik, Institut für Werkstoffe, Ruhr Universität Bochum.

[11] R.B.Grundlach and D.V.Doane. “ASM handbook: Properties and selection: Iron, Steels and high performance Alloys section: Cast irons”. ASM international (2005).

[12] R.Singh. Materail selection and design: Cast Iron Metallurgy. (2009), page 58-61.

[13] H. Holleck. Material selection for hard coating. American Vacuum society 6 (1986), page 2661-2669.

[14] S.Ulrich; H.Holleck; M. Stüber; H.Leiste; He.J, and C.Ziebert. “Nanocrystalline Metastable Hard coatings”. (2009).

[15] H.Berns and B.Wewers. Development of an abrasion resistant steel composite with in situ TiC particles. Wear 251 (2001) 11-12, page 1386-1395.

[16] S.Weber and A.Saltykova. Wear resistance of in situ MMC produced by supersolidus liquid phase sintering(SLPS). Wear 267 (2009) 11, page 1791-1797.

[17] S.Weber. Gezielte Ausnutzung des Stofftransports zur Herstellung neuartiger PM-Hartverbundwerkstoffes auf Eisenbasis. Dissertation. (2005).

[18] H.Berns; W.Theisen; F.Castro, and B.Wewers. Verschleißwiderstand von pulvermetallurgische in-situ gefertigten Stahl/TiC-Verbundwerstoffen. Mat.-wiss. u. Werkstofftech. 31 (2000) 8, page 776-770.

[19] H.Berns; W.Theisen; F.Castro, and B.Wewers. In situ Bindung von TiC in Fe-matrices bei pulvermetallurgischem Fertigung. In sonderbände der Praktischen Metallographie 31 (2000), page 291-196.

[20] A.Saltykova. Verschleißbeständige in situ MMC durch Sintern mit flüssiger Phase. Dissertation. (2010), page 291-196.

[21] H.Moll. Werstoffeche Betrachtung des Pulverbeschichtens durch Walzen.Dissertation. (2009).

[22] P.Schütte. Untersuchung pulvermetallurgischer Schichten und ihrer Entwicklung im Radial-Axial Ringwalzprocess. Diplomaar. (2008).

[23] A.Röttger; S.L.Weber; W.Theisen; B.Rajasekaran, and R.Vaßen. HVOF Spraying of Fe-Based MMC Coatings with In Situ Formation of Hard Particles by Hot Isostatic Pressing. Thermal Spray Technology 28 (2011) 2, page 344-354.

[24] L.Juffus and D.Roy. “Welding:Principles and Applications”. Cengage Delmar Learning, 5 edition (1988).

[25] GH Induction Atmosphere Group. What is Induction Heating?

[26] R.M.Nascimento; A.E.Martinelli, and A.J.A Buschinelli. Recent advances in metal-ceramic brazing. Cerâmica 49 (2003) 213.

[27] R. Arroyave and T.W Eagar. Metal substrate effects on the thermochemistry of active brazing interfaces. Pergamon (2003) 51, page 4871-4880.

[28] A.P.Tomsia. Ceramic/metal joining for structures and materials. Journal de physique 3 (1993), page 1317-1319.

[29] D.M.Mattox. “Physical Vapor Deposition (PVD) Processing”. Elviser (2010).

[30] D.G.Constantin; M. Apreutesei; R.Arvinte; A.Marin; O.CAndrei, and D.Munteanu. Magnetron sputterung technologie used for coatings deposition; Tehnologies applications. 30 (2011) 1(31), page 29-33.

[31] www.tf.uni kiel.de/matwis/amat/elmat$_e$n/kap$_6$/backbone/r6$_{41}$.html.P hysicalP rocessesf o

[32] H.S.Nalwa, editor. “Handbook of thin film materails”. Academic press (2002).

[33] M.Pritschow. Titannitrid- und Titan-Schichten für die Nano-Elektromechanic. Dissertation. (2007).

[34] L.Safi. Recent aspects concerning DC reactive magnetron sputtering of thin films: A review. Surface and Coating Technologie (200) 127, page 203-219.

[35] R.C.J Schieperes G.de.With; J.A. van Beek, and F.J.J van Loo. Journal of the Eurepean Ceramic Society. 11 (1993), page 211-218.

[36] H.S. Sarabjit; N.Jit, and A.K Tyagi. An overwiew of metal matrix composite: Processing and SiC based mechanical properties. Journal of Engineering Research and Studies 2 (2011), page 1989-2000.

[37] G.L Harris. “Properties of Silicon Carbide”. Institution of Engineering and Technology (1995).

[38] R.Radiel. “Handbook of ceramic hard particles”, volume 1. WILEY-VCH (2007).

[39] Dr.-Ing.F.Schreiber. Verschleißschutz durch Einsatz von Wolfram - Schmelzcarbid. (2002).

[40] www.thomasnet.com/articles/metals-metal-products/ziconia alumina. Zirconia Toughened Alumina.

[41] J.B.Wachtman. “Handbook of ceramic hard materials”, volume 2. Wiley GmbH (2000).

[42] U.Stüttgen. Untersuchungen zur lagerbedingten Änderung des Hafverbundes zwischen Titan und verschiedenen Keramiken mit und ohne Bonder. Dissertation.

[43] F.Binder. Titancarbid-Ein technisches Hartstoff. Chemie Ingenieur Technik 51 (1979) 5, page 1989-2000.

[44] L.A.Rocha; E.Ariza; A.M.Costa; F.J.Olivera, and R.F.Silva. Electrochemical Behaviour of Ti/ Al_2O_3 Interfaces Produced by Diffusion bonding. Material research 6 (2003) 4, page 439-444.

[45] DIN EN ISO 4957. Werkzeugstähle. (2010).

[46] DIN EN ISO 14577. Metallische Werstoffe-Instrumentierte Eindringprüfung zur Bestimmung der Härte und anderen Werstoffparametern - Teil 4: Prüfverfahren für metallische und nicht metallische Schichten. (2007).

[47] R.A.Haefer. “Oberflächen-und Dünnschicht-Technolgie Teil I - Beschichtungen von Oberflächen”. Springer - Verlag Berlin/Heilderberg/New York/London/Paris/Tokyo (1987).

[48] U.Wiklund; P. Medenqvist, and S.Hogmark. Multilayer cracking resistance in bending. 97 1-3, page 773-771.

[49] S.Ma; J.Xing; H.Fu; J.Zwang, and Zwang J. Effects of cromium concentration on microstructure and properties of Fe-3.5 alloy. Material Science and Engineering 527 (2010) 26, page 6800-6808.

[50] C.Lin; R.B.Chen, and R.K.S. A wettability of Cu/Sn/Ti active braze alloys on alumina. Material Science 251 (2001), page 2145-2150.

[51] J.J.Swab. “Properties of yttria-tetragonal zirconia polycrystal (Y-TZP) materials after longterm exposure to elevated temperatures”. U.S.Army materials technology laboratory Watertown, Massachutts (1989).

[52] W.F.Gale and T.C. Totemeier. Smithells Metal Reference Book. (2004).

[53] F.Ostermann. Anwendunstechnologie Aluminium. Springer verlag, Berlin/Heidelberg/New York (2007), page 421-426.

[54] B.E.Jacobson; R.F.Bunshah, and R.Nimmagadda. Transmission electron microscopy of TiC and VC-TiC deposites prepared by activated reactive evaporation. Thin solid films 54 (1978), page 107-18.

[55] V.N.Eremenko and A.L.Tretyachenko. The isothermal section of the system Ti-V-C at 1450 °C. Powder Metalurgy and Metal Ceramic (1964) 6, page 464-469.

[56] V.M.Cherkashenko; A.Vezhov; M.P Butsman; A.L.Ivanovski; E.Z.Kurmaev; B.V MItrofanov, and V.A. Gubanov. Study of electronic structure of ternary carbide alloys $Ti_xV_{1-x}C_y$ by means of x-ray spectroscopy and x-ray photoelectron spectroscopy. Journal of Structural Chemistry (1984) 5, page 714-720.

[57] B.S.Terry and O.S.Chinyyamakobvu. “Assessment of the reactions of SiC powders with iron-based alloys”. (1993).

[58] S.Grobelny. Charakterisierung der Grenzfläche zwischen SiC und Stahlmatrix in Fe-Basis-MMC. Studienarbeit. (2010).

[59] H.Holleck. “Binäre und Ternäre Carbide und Nitride der Übergangsmetalle und ihre Phasenumziehungen”. Institut für Material-und Festkörperforschung (1981).

[60] J.Kim and S.Kang. Phase stability of $Ti(C_{1-x}N_x$ solid solutions using ab-into calculation. Powder Metalurgy and Metal Ceramic.

[61] R.Kieffer and P.Ettmayer. Neue Entwicklungen auf dem Gebiet der Hartstoffe und Hartmetalle. 46 (1974), page 843-852.

[62] G.Neumann; R.Kieffer, and P.Ettmayer. Über das System TiC-TiN-TiO. 103 (1972), page 1130-1137.

[63] S.Roberts and P.J.Dobson. Evidence for reaction at the Al-SiO_2 interface. Journal of Physic D:Applied Physic 14 (1980) 3, page 17-22.

[64] W.Theisen; R.Winkelmann; A.Pelz, and B.Reichmann. Auftragenschweissen von Wolframkarbid in Fe-Basis-Legierungen. 7. Fachtagung Verschleißschutz von Bauteilen durch Auftragschweißen, Mai 2008, Halle.

[65] R.Winkelmann; W.Theisen; A.Röttger, and S.Weber. Verschleißbeständige Auftragungen mittels InsuClad:Tagungsband zum 13. Werkstofftechnischen Kolloquium. Werkstoffe und Werkstofftechnische Anwendungen.

[66] Z.Yao; J.J.Stiglich, and T.S.Sudarshan. Nano-grained Tungsten Carbide-Cobalt (WC/Co).

[67] A.Wank; G.Reisel; S.Steinhauser, and M.Woezel. Influence of thermal spraying method on the properties of tungsten carbide coating.

[68] C.Friedrich; G.Berg; E.Broszeit, and C.Berger. Datensammlung zu Hartstoffeigenschaften. Materialwissenschaft und Werstofftechnik 28 (1997) 2.

[69] C.Türkmen. Contemporary Approach to dental Ceris: Filling Materials for the Caries. (2012), page 333-361.

[70] O.P.Oladijo; N.Sacks; L.A.Cornish, and A.M.Venter. Effect of substrate on the body abrasion wear of HVOF WC-17 Wt.-% Co coatings. International Journal of Refractonary Metals and Hard Metals 35 (2012), page 288-294.